Geological Quarterly, 2023, 67: 46
DOI: http://dx.doi.org/10.7306/gq.1716

Sorption in an ammonioalunite-ammoniojarosite solid solution: results for the 1, 2, 4, 7, 11, 12 and 13 group elements and LREEs

Łukasz KRUSZEWSKI[1, *], Beata MARCINIAK-MALISZEWSKA[2] and Jakub KOTOWSKI[2]

[1] Polish Academy of Sciences, Institute of Geological Sciences, Twarda 51/55, 00-818 Warszawa, Poland; ORCID 0000-0001-6332-9944

[2] Institute of Geochemistry, Mineralogy and Petrology, Faculty of Geology, University of Warsaw, Zwirki i Wigury 93, 02-089 Warszawa, Poland; ORCID 0000-0001-9147-6639 [B.M.-M.], 0000-0002-3542-3519 [J.K.]

Kruszewski, Ł., Marciniak-Maliszewska, B., Kotowski, J., 2023. Sorption in an ammonioalunite-ammoniojarosite solid solution: results for the 1, 2, 4, 7, 11, 12 and 13 group elements and LREEs. Geological Quarterly, 67: 41; https://doi.org/10.7306/gq.1716

Associate Editor: Tomasz Bajda

This paper collates selected analytical results from a 1-year sorption experiments conducted on natural samples of an ammonioalunite-ammoniojarosite solid solution (AAJ) of known initial composition. These include Electron Microprobe (EPMA) and Powder X-Ray Diffraction (PXRD) results for baths subjected to $Li_2SO_4·H_2O$, KI, Rb_2CO_3 (0.33–0.62 wt.% Rb_2O in the AAJ, CsCl (0.24–1.07 wt.% Cs_2O), $Ca(OH)_2$ (ettringite formation), $Sr(NO_3)_2$ (0.31–10.25 wt.% SrO), $ZrO(NO_3)_2·2H_2O$, $MnSO_4·H_2O$, $CuSO_4·5H_2O$ (up to 1.05 wt.% CuO), $ZnCl_2$, $Ga(NO_3)_3·9H_2O$ (5.86–21.44 wt.% Ga_2O_3), $ZrCl_4$ (up to 17.56 wt.% ZrO_2 in AAJ, i.e., up to 0.27 apfu Zr, $InCl_3$ (0.85-17.04 wt.% In_2O_3, i.e., possibly up to 0.42 apfu), KH_2AsO_4 (up to 45.93 wt.% As_2O_5, recast to 1.64 apfu As), K_2SeO_3 (up to 44.86 wt.% SeO_2, recast to 1.55 apfu Se), $LaCl_3·7H_2O$ (0.17–0.22 wt.% La_2O_3), $CeCl_3·7H_2O$ (0.38–1.74 wt.% Ce_2O_3), and $PrCl_3·6H_2O$ (1.66–4.10 wt.% Pr_2O_3). Zn, Mn, and I only rarely show accumulation. $(NH_4)Fe_3(AsO_4)_2[(OH)_4(H_2O)_2]$ and $(NH_4)Fe_3[(AsO_4)(SO_4)][(OH)_5(H_2O)]$ are occasionally the dominant hypothetical end-members in the As experiment. In the KI case the resulting material is 1.6 times more enriched in K than the base used. Special attention is paid to Zr, with PXRD and EPMA results not ideally coincident with a trial Scanning Electron Microscopy-Electron Backscatter Diffraction study suggesting deposition of tetragonal $ZrSiO_4$ (synthetic zircon).

Key words: alunite group, sorption, gallium, indium, zirconium, strontium, hypothetical end-members.

INTRODUCTION

The alunite supergroup is a relatively large group of minerals (herein referred to as ASM), with general chemistry given as $AB_3(TO_4)_2(OH)_6$, where *A* = K, Na, H_3O, NH_4, Ca, Sr, Ba, Pb, REE (and, more rarely, Ag, Bi; H_2O); *B* = Al^{3+} and Fe^{3+} (and, more rarely, Cu, Zn, V^{3+}, Ga^{3+}, Ge^{4+}), *T* = S, P, As (and to a lesser extent Si, Se, Mo, W, with possible protonation). The current nomenclature of the ASM was introduced by Jambor (1999) and then updated by Bayliss et al. (2010). The ASM are divided into the alunite group (sulphates(VI), 16 approved members), the beudantite group (orthoarsenate(V)- and orthophosphate(V)-sulphates(VI), 11 approved members including a single valid unnamed mineral, and at least a single unnamed member), the dussertite group (orthoarsenates(V) and monohydroxoorthoarsenates(V), with 12 approved members), and the plumbogummite group with 10 orthophosphates(V), 7 phosphate-hydroxophosphates, one arsenate, and one unapproved vanadate. As many as 60 ASM representatives are thus currently known (Mindat, 2022). Within this group there are sulphates of the alunite group. The above formula, as shown, e.g., by Drouet et al. (2004), is far from universal, as some of the hydroxyl sites may be largely substituted by H_2O. Water occurrence, along with likely oxonium (H_3O^+), was also confirmed by Parafiniuk and Kruszewski (2010) – for the precursor material also studied here – who also reported non-accidental enrichment in Cl at the *X* (nominally: OH) site. Hydration in alunites is related to protonation of the OH groups which, in turn, is a way of compensation of non-ideal occupancy of the *A* and *B*-sites and of the related non-stoichiometry. The latter phenomenon is especially frequent in synthetic alunite-type compounds (e.g., Kydon et al., 1968; Drouet et al. 2004; Rudolph and Schmidt, 2011). The *B*-site occupancy may be as low as 82% (Rudolph and Schmidt, 2011).

Numerous solid solutions are known among the ASM, including K-Na-H_3O (Brophy and Sheridan, 1965; Drouet and Navrotsky, 2003), K-H_3O (Brown, 1970), Fe-Al and NaFe-Na-Al (Drouet et al., 2003, 2004), and NH_4Al-NH_4Fe (Parafiniuk and Kruszewski, 2010).

* Corresponding author: e-mail: lkruszewski@twarda.pan.pl

Received: January 19, 2023; accepted: September 29, 2023; first published online: December 21, 2023

SUBSTITUTIONS IN ALUNITES – STATE OF THE ART

There are many papers dealing with different issues related, in general, to the guest-host geochemistry of the ASM. The use of jarosite in element utilization was discussed by Asokan et al. (2006), who noted elevated amounts of zinc, lead, manganese, chromium, copper and cadmium in material formed abundantly during zinc ore-extraction. Synthesis of exchanged analogues of the ASM, their thermochemical behavior, labile character of the alunite-type structure, and non-stoichiometry issues were largely addressed in Dutrizac and Kaiman (1976) and Drouet et al. (2004). Jones (2017) studied the jarosite-to-alunite transition during relatively low-temperature synthesis. Solid solutions and end-members were also studied in relation to the confirmed occurrence of jarosite on Mars (Liu et al., 2017). Dutrizac and Jambor (2000), in a review paper devoted to hydrometallurgical applications of the ASM, summarized records of a number of natural and synthetic compounds of the alunite-type stoichiometry and structure known at that time. One year later, a similar comparison, also highlighting the ASM as storage materials of toxic elements, was made by Kolitsch and Pring (2001). These authors pointed to the known potential residence of Rb^{+}, Tl^{+}, Ag^{+}, Pb^{2+}, Ca^{2+}, Sr^{2+}, Ba^{2+}, Hg^{2+}, Bi^{3+} and $LREE^{3+}$ as major, and Th^{4+}, U^{4+} and Zr^{4+} as minor, elements at the *A*-site. They also noted the possibility of Cu, Zn, Co, Ni, Mg, Mn (divalent), Cr, Ga, In, V (tervalent), Ge (tetravalent), and even Sb, Nb, and Ta (pentavalent) and W (hexavalent) of enter the *B*-site; and the tetravalent Si and C, pentavalent As and P, and hexavalent Se and Cr as residents to be encountered, in varying amounts, at the *X*-site. Considering the *A*-site dominance, the known, natural end-members include dorallcharite (the Tl-dominant analog of jarosite), argentojarosite (Ag), Pb, plumbojarosite (Pb), huangite (the Ca equivalent of alunite), and walthierite (the Ba analogue of alunite), all belonging to the alunite group, while the Bi-, REE-, and Th-dominant compositions concern the separate plumbogummite group species: florencite-(Ce), $CeAl_3(PO_4)_2(OH)_6$ and its La-, Nd-, and Sm-dominant analogues, arsenoflorencite-(Ce), $CeAl_3(AsO_4)_2(OH)_6$ and its La- and Nd-dominant analogues, zaúrite, $BiFe_3(PO_4)_2(OH)_6$, its Al-dominant analogue waylandite, and eylettersite, $Th_{0.75}Al_3(PO_4)_2(OH)_6$. Copper- and zinc-dominant end-members are beaverite-(Cu) and its Al-analogue osarizawaite, and beaverite-(Zn), all of the alunite group. Gallium is found as essential in galloplumbogummite, $Pb(Ga,Al)_{3-x}Ge_xH_{1-x}(PO_4)_2(OH)_6$. A number of additional Pb- (beudantite, corkite, hidalgoite, hinsdalite) and Sr- (kemmlitzite, svanbergite, and the recently discovered oberwolfachite) -dominant members are collected in the beudantite group, which also has the Ba-dominant weilerite as a member. The dussertite group is represented by Ba-rich dussertite, Sr-rich arsenogoyazite, Pb-dominant philipsbornite and segnitite, and others. Examples from the plumbogummite group include the Sr-bearing benauite and goyazite, Ca-bearing crandallite and UM2006-23-PO:AlBiCaFeH, Ba-rich gorceixite, and Pb-rich kintoreite and plumbogummite. The only approved V-dominant ASM is springcreekite. Approval of tomsquarryite, $NaMgAl_3(PO_4)_2(OH,F)_6{\cdot}8H_2O$ (trigonal, R-3m) in 2022 expanded our knowledge of the already advanced complexity of the ASM structural type.

Many papers devoted to the synthesis, crystallography (in part), and sorption capacity of mostly synthetic analogs of the ASM. The chemical systems analyzed include boron (Kavak, 2008), scandium (Kolitsch, 2015), vanadium (Zhao et al., 2016; Wang et al., 2021), chromium(III) (Lengauer et al., 2013; Reyes et al., 2016), chromium(VI) (Drouet et al., 2003; Kolitsch, 2015), manganese (Teixeira and Tavares, 1986), copper (Dijkhuis, 2009), nickel and cobalt (Dutrizac and Chen, 2004; in relation to Ni-laterite materials: Nheta and Makhata, 2013; White and Gillaspie, 2013), zinc (Grey et al., 2009; Arabyarmohammadi et al., 2016), gallium (Rudolph and Schmidt, 2011, who noted 1000 ppm Ga contents in jarosite; Kydon et al., 1968; Kamoun et al., 1989), arsenic (Paktunc and Dutrizac, 2003; Asta et al., 2010; Sunyer i Borrell, 2013; Murray et al., 2014; Hudson-Edwards, 2019), rubidium (Ivarson et al., 1981; Kolitsch, 2015), selenium(VI) (Strawn et al., 2002; Franzblau et al., 2014), molybdenum (natural samples: Luddington, 1995; Žáček et al., 2008), tungsten (Frost et al., 2011), silver (Kolitsch, 2015), cadmium (Dutrizac et al., 1996), indium (Dutrizac and Mingmin, 1993; Kolitsch, 2015), antimony (Hudson-Edwards, 2019), cesium (Fairchild, 1933; Dutrizac and Jambor, 1987, although this paper concerns the use of alunite crystallization as a K-Cs separation tool), mercury (Dutrizac and Chen, 1981), thallium (Dutrizac et al., 2005), and lead (Akar et al., 2013; Murray et al., 2014 – a paper related to bioremediation; Dutrizac, 1991; Figueira and Pereira da Silva, 2011). A number of papers discuss Acid-Mine-Drainage-related As and Pb immobilization in the ASM (e.g., Asta et al., 2010). Less is known regarding Sr in the alunite group, mentioned by Hikov (2013) and May et al. (1963). Unsuccessful REE-end-member synthesis was described by Dutrizac (2003), who later studied the REE-ASM system also (Dutrizac, 2004). Natural enrichment of alunite and jarosite in gallium, known from argillization and high-sulphidation zones, was discussed, e.g., by Rytuba et al. (2003). The latter authors noted up to 339 ppm Ga in alunite. The behaviour of the group-2 elements, including radium, was analyzed by Dutrizac and Chen (2008), while that of halogens was studied by Dutrizac and Chen (2009). Halogen incorporation in jarosite-type compounds is a link between jarosite geochemistry/crystallochemistry and the mineralogy of Mars, due to simultaneous occurrence of jarosite and halogen-rich soils on the planet – a field explored by Zhao et al. (2014).

The geochemical sorption potential of the ASM-type materials is not only due to the structural lability and crystal-chemical flexibility of the structure type. Adsorption phenomena are also important, e.g., for Al, Cd, Cu and Zn, as shown by the computer simulations of Hudson-Edwards and Wright (2011). The adsorption is possible due to the negative charge of the ASM surface (Wang et al., 2021).

Studying the sorption capacity of the ASM-type materials is important not only due to them being potential sinks, but also in relation to leaching. Post-hydrometallurgical jarositic waste studied by Hage and Schuiling (2000), with 6.0 wt.% Zn, 0.42 wt.% Cu, 0.10 wt.% Mn, 0.2 wt.% As, 203 ppm Cd and traces of Co, B (0.06 wt.%), Ni, Cr, Pb, Ba and Sb, were shown to retain ~83% Cu, ~80% As, ~67% B, ~28% Zn and ~10% Mn, but with 50% more B (and K and Ti), ~33% more Ba, ~34% more Pb, and 25% more Sb in a leachate produced. A similar study was by Asokan et al. (2006), with jarosite holding 8.2 wt.% Zn, 1.93 wt.% Pb and 0.20 wt.% Mn.

GOALS

Most of the papers devoted to guest elements in the ASM are devoted to chemically pure, synthetic compounds. In this paper we explore the sorption capabilities of a natural representative of the ammonioalunite-ammoniojarosite series of known chemistry. Due to the large amount of experimental data, the present paper describes only part of the results, for selected elements.

MATERIALS

Samples of ammonium-dominant members of the alunite supergroup were collected in fieldwork during Ph.D. studies of Ł.K. (e.g., Parafiniuk and Kruszewski, 2010), from a fumarolic sulphate crust in the burning "Dębieńsko" mine waste heap at Czerwionka-Leszczyny (Lower Silesian Coal Basin, S Poland). They constitute a solid solution with ammonioalunite (here abbreviated as Ama) and ammoniojarosite (Amj) as the main end-members. The material is herein referred as to AAJ. The average composition of the whole-series material, for which a complete solid solution was confirmed, is (n = 24, wt.%): 3.71 $(NH_4)_2O$, 0.80 K_2O, 0.35 Na_2O, 0.07 CaO, 0.10 MgO, 0.006 MnO, 16.37 Al_2O_3, 24.06 Fe_2O_3, 34.69 SO_3, 0.95 SiO_2, 0.81 Cl and 17.77 H_2O (the latter calculated by difference). This corresponds to the empirical formula:

$$[(NH_4)_{0.85}K_{0.08}Na_{0.05}Mg_{0.01}Ca_{0.01}]_{1.00}(Al_{1.43}Fe_{1.34})_{3.00}$$
$$[(SO_4)_{1.93}(SiO_4)_{0.07}]_{2.00}[(OH)_{5.76}Cl_{0.10}(H_2O)_{0.14}]_{6.00}$$

(basis: B = 3 apfu; molecular water by difference, after attributing OH amount based on charge balance, after subtracting Cl). As oxonium presence was not reliably confirmed, it will be omitted in the following empirical formulae. The ammonioalunite-dominant material has the following composition, and related empirical formula (n = 12): 4.12 $(NH_4)_2O$, 0.60 K_2O, 0.29 Na_2O, 0.08 CaO, 0.12 MgO, 0.005 MnO, 25.85 Al_2O_3, 10.70 Fe_2O_3, 36.04 SO_3, 1.74 SiO_2, 1.05 Cl and 19.35 H_2O;

$$[(NH_4)_{0.88}K_{0.06}Na_{0.04}Mg_{0.01}Ca_{0.01}]_{1.00}(Al_{2.12}Fe_{0.56})_{3.00}$$
$$[(SO_4)_{1.88}(SiO_4)_{0.14}]_{2.00}[(OH)_{5.58}Cl_{0.12}(H_2O)_{0.30}]_{6.00}$$

Data for the ammoniojarosite-dominant part is as follows (n = 12): 3.30 $(NH_4)_2O$, 1.00 K_2O, 0.41 Na_2O, 0.06 CaO, 0.08 MgO, 0.006 MnO, 6.89 Al_2O_3, 37.42 Fe_2O_3, 33.33 SO_3, 0.15 SiO_2, 0.57 Cl, and 16.18 H_2O;

$$[(NH_4)_{0.80}K_{0.11}Na_{0.06}Mg_{0.01}Ca_{0.01}]_{1.00}(Fe_{2.24}Al_{0.55})_{3.00}$$
$$[(SO_4)_{1.99}(SiO_4)_{0.01}]_{2.00}[(OH)_{6.09}Cl_{0.08}]_{6.17}.$$

Trace elements determined in the AAJ occur in amounts below 0.1 wt.% and include V (58–190 ppm), Cr (85–140 ppm), Mn (up to 66 ppm), Co (3.3–6.8 ppm), Ni (7.4–21 ppm), Cu (6.2–17 ppm), Zn (19–34 ppm), Sr (42–420 ppm), Ba (1.7–16 ppm) and Pb (9.4–340 ppm). Titanium and phosphorus were not previously measured; some TiO_2 inclusions (crystals up to ~20 μm in length) were rarely found within the material studied. Free silica (probably as a chalcedony-like substance deposited as a residue from acidic semi-volatile solutions, parental for the AAJ, interacting with the shale/clinker substrate) and tschermigite, $(NH_4)Al(SO_4)_2{\cdot}12H_2O$, were found in some voids, too. Trace Ti and P were not previously measured in this material. The extent of the chemical variation in the AAJ is shown in heat (density) triangular plots in the Appendix Figures SF1 (A-site representation; *Triplot* software used) and SF2 (X-site representation). These figures show the datapoints plotted close to but not at the NH_4^+ edge, and an extension towards both H_2O- and Cl-rich compositions can also be seen. The AAJ fragments were put into plastic containers and filled with aqueous solutions (50 ml) of the following chemicals (concentrations reported in parentheses): $Li_2SO_4{\cdot}H_2O$ (1.21%), KI (1.19%), Rb_2CO_3 (1.23%), CsCl (1.24%; group 1), $Ca(OH)_2$ (amount corresponding to 1.2%), $Sr(NO_3)_2$ (1.22%; group 2), $ZrCl_4$ (1.20%; group 4), $MnSO_4{\cdot}H_2O$ (1.19%; group 7), $CuSO_4{\cdot}5H_2O$ (1.35%; group 11), $ZnCl_2$ (1.35%; group 12), $Ga(NO_3)_3{\cdot}9H_2O$ (1.24%), $InCl_3$ (0.59%; group 13), KH_2AsO_4 (0.99%), K_2SeO_3 (1.08%), $LaCl_3{\cdot}7H_2O$ (1.26%), $CeCl_3{\cdot}7H_2O$ (1.28%), $PrCl_3{\cdot}6H_2O$ (1.65%) and $TaCl_5$ (0.49%). The AAJ samples were kept in these solutions for 1 year, in stable and dark conditions, then removed, thoroughly flushed with redistilled waters, and prepared as thin sections. Many other experiments, involving further chemicals, were also run, but their results will be described elsewhere, as explained below. The water used in the experiment was redistilled.

RESEARCH METHODS

Powder X-ray diffraction (PXRD) was used to determine the mineralogical composition of the samples. Samples were crushed and ground in an agate mortar. The PXRD analyzes were conducted using a *Bruker AXS D8 ADVANCE* diffractometer at the Clay Minerals Laboratory, Institute of Geological Sciences, Polish Academy of Sciences, Kraków. The apparatus was equipped with a superfast *LPSD VÅNTEC-1* detector and used non-monochromatized, K -filtered CoK radiation. The following parameters describe the analysis conditions: Bragg-Brentano geometry, 3–8° 2 range, 0.02° 2 step, 1s per step counting time. Two evaluation softwares, EVA (v. 4.2) coupled with the Crystallography Open Database (COD), and an older EVA version communicating with the PD Database (PDF) were used for phase identification. The evaluation of the alunite-type compounds was based on the following standards: (1) COD, 9014708, alunite; 9010441, jarosite; (2) PDF, 017-0753, ammoniojarosite; 042-1430, ammonioalunite; 042-1332, synthetic ammonioalunite; 036-0427, hydronian jarosite; and 022-0827, synthetic jarosite. *TOPAS* (v. 3.0) software with implemented Rietveld method was used for the qualitative phase analysis. The approach used was tested via attendance at the Reynolds Cup 2018 competition (Ł.K.) and details of it may be found. The description hereafter proposes some hypothetical end members of the alunite supergroup, hereafter referred to as HEMs. In the Rietveld refinements, the following main model structures were used: (1) ammoniojarosite, a = 7.3177 Å, c = 17.534 Å (Basciano and Peterson, 2007); (2) alunite, a = 6.9749 Å, c = 17.315 Å (Zema et al., 2012).

The composition of the resultant AAJ was studied using an Electron Probe Micro-Analyzer (EPMA), model *Cameca SX100*, located at the Laboratory of Electron Microscopy, Microanalysis and X-Ray Diffraction, Institute of Geochemistry, Mineralogy and Petrology, Faculty of Geology, University of Warsaw. To confirm the association of the particular low-intensity elements with the AAJ, wavelength-dispersive (WDS) scans were done, preceded by control analyses within which the peak-to-background ratios were controlled. All EPMA measurements used identical conditions (10 nA and 15 kV current; beam size of 3 μm due to somewhat unstable nature of the AAJ samples related to their H_2O, OH^-, NH_4^+, S, and Cl content of the AAJ) to ensure meaningful comparison between the particular exchanged AAJ. Neither manganese, zinc nor iodine could be initially detected: the first two elements were measured even though they could not be seen, and their contents, if any, were always below their detection limits (in wt.%: S 0.07–0.09, Ta 0.21–0.25, As 0.06–0.07, P 0.04–0.05, Zr 0.14–0.17, Se 0.11–0.17, Si 0.03–0.04, Ti 0.03, Fe 0.15–0.18, In 0.12, Ga 0.24, Al 0.04, Ce 0.07–0.08, La 0.06–0.07, Pr 0.60, Zn 0.31–0.43, Cu 0.20–0.21, Mn 0.11–0.14, Sr 0.12–0.16, Ca 0.04–0.05, Mg 0.03, Cs 0.09–0.01, Rb 0.08, K 0.05, Na 0.05–0.08, and Cl 0.02). To confirm/disprove their sorption, and to obtain some high-quality microphotographs of the experi-

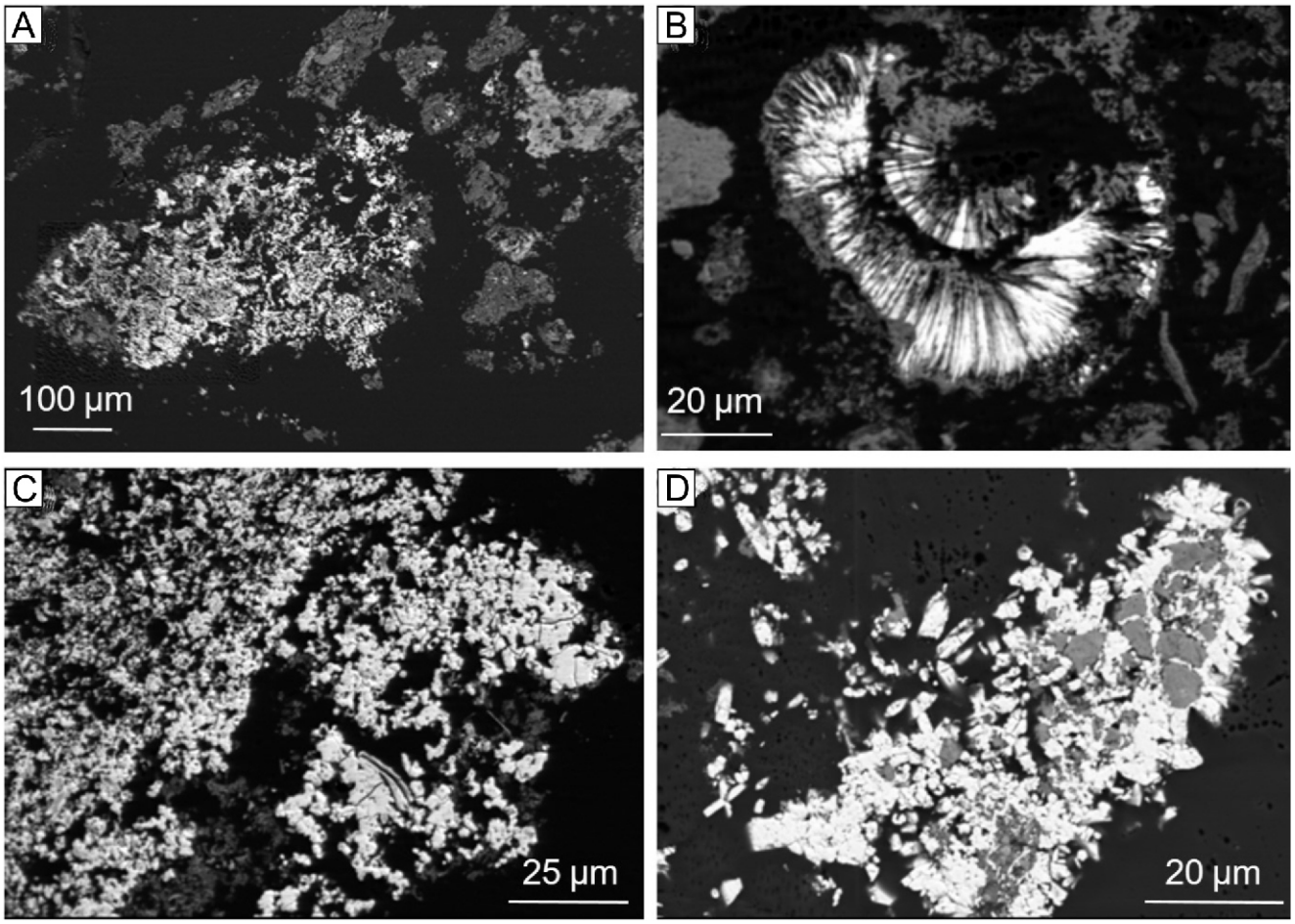

Fig. 1. Selected Backscatter-Electron Images (from EPMA) of some of the exchanged AAJ

A – arsenic-exchanged AAJ with different As contents revealed by varying electron density contrast; **B** – fan-shaped complex aggregate of intergrown BSE-bright Fe chloride and arsenate-bearing exchanged AAJ; **C** – selenium-exchanged AAJ with variable Se(IV) content; **D** – BSE-bright newly formed $SrSO_4$ crystals among BSE-darker Sr-exchanged AAJ; A and B – KH_2AsO_4 experiment; C – K_2SeO_3 experiment; D – $Sr(NO_3)_2$ experiment; the BSE-darkest aggregates mainly comprise aluminosilicate and quartz impurities of the original AAJ sample

ments' products, a *ZEISS Sigma VP* scanning electron microscope located at the Nano Fun National Multidisciplinary Laboratory of Functional Nanomaterials (Faculty of Geology, University of Warsaw) was used. The microscope is equipped with two Bruker 6|10 XFlash EDS (energy-dispersive X-ray spectrometers) that have higher-quality detector crystals allowing for the detection of light elements at lower detection limits.

The Zr-rich sample was, in addition, analysed with Electron Backscatter Diffraction (EBSD) for confirmation of Zr sorption by the AAJ. For this purpose, the sample was analyzed using a *ZEISS Auriga 60* field emission scanning electron microscope (FE-SEM) equipped with Bruker e-Flash HR+ EBSD spectrometer localized at the CryoSEM Laboratory (part of the National Multidisciplinary Laboratory of Functional Nanomaterials), Faculty of Geology, University of Warsaw. The following conditions were applied: 20 keV, 15 nA current, working distance of 27.885 mm; EBSD parameters: 70° sample tilt, 1.425° detector tilt, detector distance of 15.8 mm and PC = (0.824, 0.334) calibration values, 400 px area size (10 averaged patterns, number of points equal to 30, detector distance variation range of 20–30 mm).

For the purpose of statistical analysis, the compositional results were transformed with the logratio procedure (e.g., Kynčlová et al., 2017) and introduced to the *PAST* software (Hammer et al., 2001). Mean-and-whisker plots and triangular plots were drawn. The univariate analysis consisted of the normality test (i.e., ordination associations measurement) for which Kendall rank correlation (KRC) was applied. This method reports correlation coefficients as the t parameter. Multivariate analysis included PCA (Principal Component Analysis) and cluster analysis. Due to the large amount of tabulated data, it is contained exclusively within the Appendix Tables.

RESULTS

Representative SEM images of the resulting compounds are shown in Figure 1. Figures 2–5 juxtapose selected element-correlation diagrams. Unit cell parameters derived from Rietveld refinements of the treated AAJ samples are given in Appendix Table ST1. Along with the most intense reflections, at *d* ~3.02 Å (attributable to ammonioalunite, herein referred to as Ama) and 3.07 Å (ascribable to ammoniojarosite, herein referred to as Amj), other reflections fittable to PDF-database standards of alunite (Alu, *d* ~3.00*n* to 3.03 Å) and jarosite (Jar, *d* ~3.03 to 3.09 Å) were observed in some diffractograms.

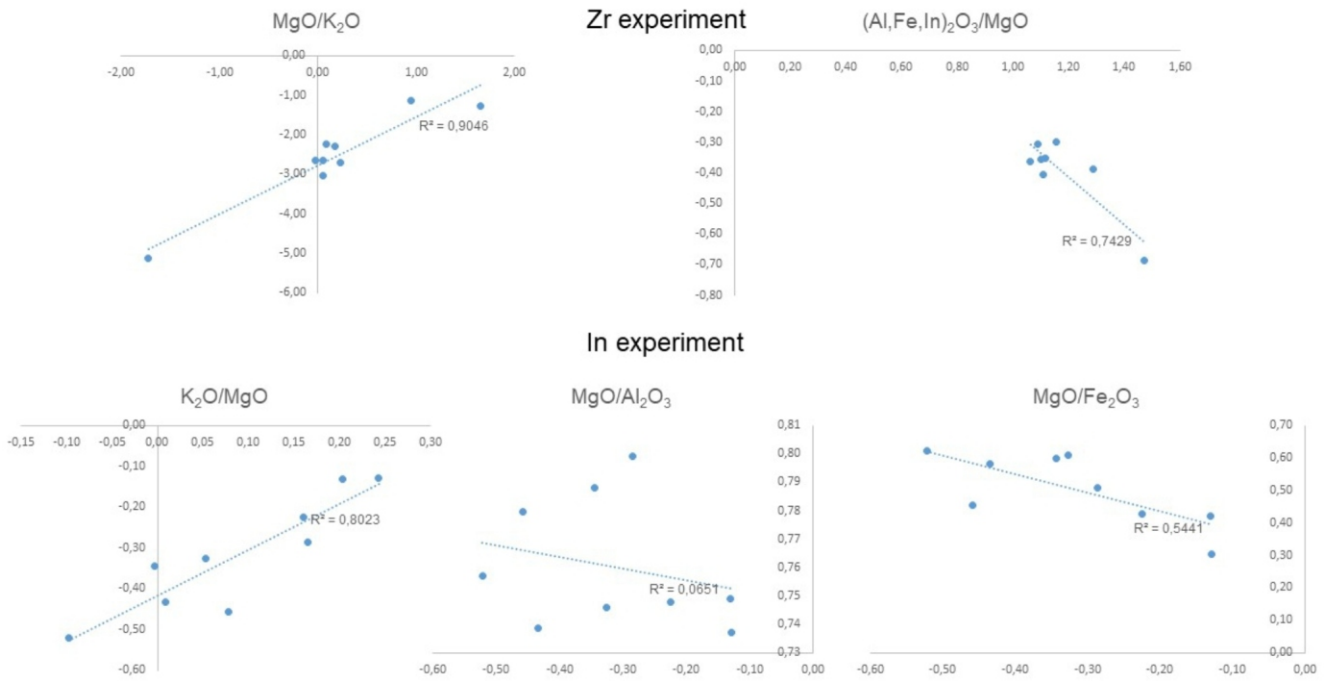

Fig. 2. Correlation of Mg and other elements from selected experiments (logratioed data used)

LITHIUM EXPERIMENT

The average (geometric mean, GM) content of the non-NH_4 *A*-site components corresponds to total 0.15 atoms per formula unit (apfu). There is thus no difference in the occupancy as compared to the unreacted AAJ. As such, and considering the formula below, we do not suspect any larger (i.e., 0.01 apfu) amounts of Li entering the AAJ.

The Ama reflections are much stronger than the Amj ones, though the latter are evident and quite well separated. A weak reflection at d = 3.232 Å could, possibly, be attributed to LiCl crystallized via exchange, especially that the AAJ composition within this experiment (Appendix Table ST2) is low in Cl:

$$[(NH_4)_{0.85}K_{0.07}Na_{0.05}Mg_{0.02}Ca_{0.01}]_{1.00}(Al_{2.49}Fe_{0.51}T_{i0.01})_{3.01}$$
$$[(SO_4)_{1.44}(SiO_4)_{0.38}(PO_4)_{0.04}]_{1.86}\{[(OH)_{5.49}Cl_{0.06}]_{5.55}(H_2O)_{0.45}\}$$

(n = 7). As such, this material bears even more K than the unreacted ammonioalunite. It corresponds to $Ama_{69}Amj_{14}Alu_6Naa_4Jar_1Hua_1Mgh_1(Caj+Mfh)_4$ mean end-member composition, where Ama is ammonioalunite, Amj – ammoniojarosite, Alu – alunite, Naa – natroalunite, Jar – jarosite, Hua – huangite, Mgh – "magnesiohuangite" HEM, Caj – "calciojarosite" HEM, and Mfh – "magnesioferrihuangite" HEM. P- and Si-dominant members are omitted here for clarity. The empirical formula assumes no Li substitution. As compared to the mean empirical formula of the base AAJ, the product is 1.8 times enriched in K. This, however, is due to original differences in the K content within the base. The *A*-site content is shown, for comparison, in Appendix Figure SF3. The plot does not differ much from that for the Al-rich base.

POTASSIUM IODIDE EXPERIMENT

Initially, no iodine could be seen in any of the many EDS spectra collected. Only with the use of the Sigma SEM was trace iodine detected in a single area, where evidently BSE-brighter (backscattered electrons imaging), tiny, rounded to somewhat undulose crystals/aggregates were found. The amount of iodine was too low to be detected (Appendix Figure SF4). However, as iodine-bearing ASM are unknown to the authors, a further, more detailed study of its assumed substitution is planned.

The averaged total content of the non-NH4 *A*-site components in the KI-treated sample equals 0.10 apfu (AppendixTable ST3). The difference in the occupancy from the unreacted AAJ is thus –40%. Iodine could not be detected in the thin section of the AAJ subject to the KI experiment; numerous EDS spectra did not show any trace of the element. The major line of chlorine, however, was always present, although with low intensity.

The Ama reflections are much stronger than the Amj ones, the latter being almost unrecognizable. The composition of the product is given in AppendixTable ST3. The iodide anion was not found entering the *X*-site, as shown by the empirical formula:

$$[(NH_4)_{0.89}K_{0.06}Na_{0.03}Mg_{0.01}Ca_{0.01}]_{1.00}(Al_{2.49}Fe_{0.51}Ti_{0.01})_{3.01}$$
$$[(SO_4)_{1.38}(SiO_4)_{0.23}(PO_4)_{0.02}]_{1.63}[(OH)_{6.27}Cl_{0.05}]_{6.32}$$

(n = 9). Normalized to T = 2 apfu, the formula takes the form:

$$[(NH_4)_{0.89}K_{0.06}Na_{0.03}Mg_{0.01}Ca_{0.01}]_{1.00}(Al_{2.49}Fe_{0.51}Ti_{0.01})_{3.01}$$
$$[(SO_4)_{1.69}(SiO_4)_{0.28}(PO_4)_{0.02}]_{1.99}\{[(OH)_{5.45}Cl_{0.05}]_{5.50}(H_2O)_{0.50}\}$$

End-member shares (with hypothetical P- and Si-dominant members omitted) may be expressed as $Ama_{74}Amj_{15}Alu_5Naa_2Jar_1(Mga+Hua+Caj+Mgj)_3$. The averaged total content of the non-NH_4 *A*-site components in the KI experiment equals 0.11 apfu. The difference in the occupancy from the unreacted AAJ is thus –27%. When compared to the base AAJ composition, the product is slightly depleted in K. Thus, potassium from KI does not seem to enter the structure. In spite of lacking I substitution the average Cl content is twice as low as in the non-exchanged AAJ. The *A*-site content is shown in Appendix Figure SF5. The plot is similar to that for the Li experiment, although the datapoints are more concentrated.

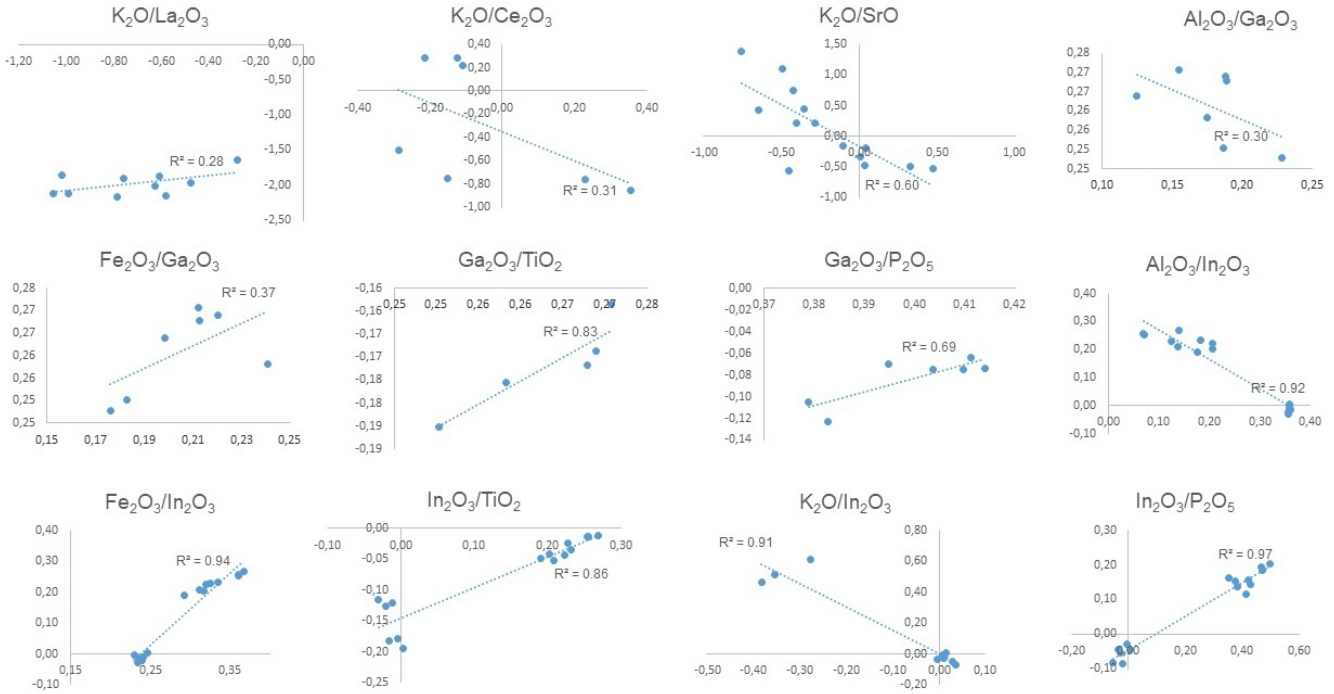

Fig. 3. Selected element correlation diagrams, La, Ce, Sr, Ga and In experiments (logratioed data used)

RUBIDIUM EXPERIMENT

Both the Si enrichment and small amount of Rb substituted in the AAJ made the visual identification of Rb lines difficult due to overlap of Rb L and Si K lines (Appendix Table ST4). However, in some areas analyzed, the Si Ká line is clearly broadened, with low intensity but evident "split" at ~1.70 keV (Appendix Fig. SF6). The Ama reflections, again, are much stronger than the Amj ones. The latter are diffuse and somewhat shoulder-like. The GM Rb_2O content is just 0.46 wt.%. The Rb content does not seem to be correlated with Al- or Fe-dominance. The composition of the rubidium-exchanged AAJ is given as

$$[(NH_4)_{0.87}K_{0.03}Na_{0.03}Mg_{0.04}\mathbf{Rb_{0.02}}Ca_{0.01}]_{1.00}$$
$$(Al_{1.90}Fe_{1.10}Ti_{0.01})_{3.01}[(SO_4)_{1.93}(PO_4)_{0.03}(SiO_4)_{0.02}]_{1.98}$$
$$[(OH)_{6.00}Cl_{0.06}]_{6.06}$$

(n = 12, with T-site occupancy normalized by stoichiometry; Appendix Table ST4). It corresponds to $Ama_{57}Amj_{33}Alu_2Naa_2Jar_1Mga_1Naj_1\mathbf{Rba_1Rbj_1}Mgj_1(Hua+Caj)_{<1}$ end-member representation (omitting P-and Si-dominant HEMs), where Rba stands for "rubidioalunite" HEM and Rbj for "rubidiojarosite" HEM. The A- site content is shown in Appendix Figure SF7. IT shows a similar image as in the KI and Li case. The normality test and Kendall statistical results are shown in Appendix Tables ST5 and ST6, respectively.

CESIUM EXPERIMENT

Cesium could clearly be seen in the EDS spectra at numerous spots, both in BSE-bright and relatively BSE-dark phases, especially using the Sigma system (Appendix Fig. SF8). The Cs-exchanged AAJ is observed as a single type of a low-Cs, siliceous phase, with Al only slightly prevailing over Fe, and with traces of Na, Mg, P and K (Appendix Table ST7). The Ama reflections are much stronger than the AMJ ones, which are very diffuse. In addition, a single sharp reflection is observed at d = 3.207 Å, attributed to CsCl. The WDS (LPET) scan shows an evident Cs-L line. The averaged total content of the A-site components in the KI experiment equals 0.15 apfu, discluding Cs, NH_4 and H_3O. The difference in the occupancy from the unreacted AAJ is thus +7%, and the GM Cs_2O content is 0.58 wt.%. The whole-series composition (Appendix Table ST5) is

$$[(NH_4)_{0.83}K_{0.08}Na_{0.04}\mathbf{Cs_{0.02}}Ca_{0.01}Mg_{0.01}Rb_{0.01}]_{1.00}$$
$$(Al_{1.83}Fe_{1.16}Ti_{0.01})_{3.00}[(SO_4)_{1.56}(SiO_4)_{0.40}(PO_4)_{0.04}]_{2.00}$$
$$\{[(OH)_{5.18}Cl_{0.04}]_{5.22}(H_2O)_{0.78}\}\ (n = 8)$$

It corresponds to an end-member composition $Ama_{52}Amj_{31}Alu_5Jar_4Naa_2Naj_2\mathbf{Csa_1Csj_1}Rbj_1(Rba+Mga+Mgj+Hua+Caj)_1$, where Csa stands for "cesioalunite" HEM and Csj for "cesiojarosite" HEM (P- and Si-dominant HEMs omitted). Rubidium stands for a chemical-derived impurity. A slightly less Cs-enriched, alunitic series (n = 3, i.e., analyses 1–3; GM of 0.26 wt.% Cs_2O) has the following composition:

$$[(NH_4)_{0.92}K_{0.05}Na_{0.02}\mathbf{Cs_{0.01}}]_{1.00}(Al_{2.61}Fe_{0.38}Ti_{0.01})_{3.00}[(SO_4)_{1.68}$$
$$(SiO_4)_{0.31}(PO_4)_{0.02}]_{2.01}\{[(OH)_{5.34}Cl_{0.04}]_{5.38}(H_2O)_{0.62}\}$$

(excess Si- at the T-site removed). This corresponds to $Ama_{80}Amj_{12}Alul_4Naa_2Jar_1\mathbf{Csa_1}(Mga+Naj+\mathbf{Csj}+Hua+Mgj+Caj)_{<1}$ end-member composition. The relatively Cs-enriched one (n = 5, analyses 4–8, 0.93 wt.% Cs_2O on average), jarositic material, is

$$[(NH_4)_{0.76}K_{0.11}Na_{0.05}\mathbf{Cs_{0.03}}Rb_{0.02}Mg_{0.02}Ca_{0.01}]_{1.00}$$
$$(Fe_{1.63}Al_{1.36}Ti_{0.01})_{3.00}[(SO_4)_{1.68}(SiO_4)_{0.27}(PO_4)_{0.06}]_{2.00}$$
$$\{[(OH)_{5.40}Cl_{0.05}]_{5.45}(H_2O)_{0.55}\}$$

(Si excess removed). As its corresponding end-member representation is $Amj_{42}Ama_{35}Jar_6Alu_5\mathbf{Csj_2Csa_1}Rba_1Rbj_1(Mga+Mgj+$

Caj+Hua)$_7$. In contrast to Cs, chlorine does not seem to be exchanged; its average content is twice as low as in the untreated AAJ. The *A*-site content is shown in Appendix Figure SF9. Compared to the Rb-experiment, some datapoints plot more towards the K(Na)-rich composition, in accordance with the presence of two slightly differing AAJ varieties. The normality test and Kendall statistical results are shown in Appendix Tables ST8 and ST9, respectively.

CALCIUM HYDROXIDE EXPERIMENT

The AAJ interacts with $Ca(OH)_2$ to form a synthetic equivalent of ettringite, $Ca_6Al_2(SO_4)_3(OH)_{12}\cdot 26H_2O$ (main reflections at 9.628 and 5.585 Å; a = 11.195(5) Å, c = 21.43(2) Å) with less evident admixture of a $Ca_3Al_2O_6$ compound (d = 2.699 Å with a coincidence issue; a = 15.25(1) Å), and synthetic analogues of letovicite, $(NH_4)_3H(SO_4)_2$ (d = 3.38 Å, split; a = 15.57(4) Å, b = 5.96(1) Å, c = 10.33(23) Å, = 103.75(61)°) and gypsum (a = 6.210(9)Å, b = 15.09(3)Å, c = 5.63(1)Å, =114.99(18)°). The presence of a synthetic analog of hibbingite, $Fe_2(OH)_3Cl$ (d = 2.366 Å), is less likely. Ama is present, too, especially manifested as still intense and relatively sharp reflections at 3.026 and 3.031 Å. The transformation process may take place according to the following reactions:

(1) $1.5(NH_4,K)Al_3(SO_4)_2(OH)_6 + 6Ca(OH)_2 + 26H_2O \rightarrow Ca_6Al_2(SO_4)_3(OH)_{12}\cdot 26H_2O + 1.5(NH_4,K)OH + 2.5Al(OH)_3$

(2) $(NH,KAl_3(SO_4)_2(OH)_6 + 3Ca(OH)_2 \rightarrow Ca_3Al_2O_6 + (NH_4,K)^+ + Al^{3+} + 2SO_4^{2} + 3H_2O$

(3) $4(NH_4,K)Fe_3(SO_4)_2(OH)_6 \rightarrow 4Fe_2(OH)_3Cl + (NH_4)_3H(SO_4)_2 + 4Fe(OH)_2 + 6SO_4^{2} + NH_3$

Alunite as a precursor to ettringite is well-known from cement studies, especially with reference to alunite expansive cement and to ettringite being known as "the best expansive cement" (Zhang, 2011). Ettringite formation from alunite and lime is mentioned in a paper of Kim et al. (2011) devoted to alunite calcination.

STRONTIUM EXPERIMENT

The main phase observed in the PXRD pattern and confirmed by EPMA is $SrSO_4$ (a synthetic equivalent of celestine). Among its crystals, very tiny (up to 2 μm in diameter) crystals of Sr-exchanged AAJ are observed. The brighter ones are Fe-dominant, with trace amounts of Cl and K. The darker ones represent an Al-dominant composition, with seemingly larger amounts of K and an admixture of Na. A representative EDS spectrum of Sr-exchanged AAJ is in shown in Appendix Figure SF10.

The averaged total content of the non-NH_4 *A*-site components in the KI experiment equals 0.16 apfu, excluding Sr. The GM-share of the latter is 0.06 apfu, and the GM SrO content is just 1.64 wt.%. The difference in the occupancy by comparison with the unreacted AAJ is thus +12.5%. The Ama reflections are very weak and very broad, while Amj reflections could not be detected. The Sr-dominant phase composition (Appendix Table ST6, with 10.25 wt.% SrO), is

$$(\mathbf{Sr_{0.45}}K_{0.03}Na_{0.02}Ca_{0.01}Mg_{0.01})_{0.52}(Al_{1.83}Fe_{1.16}Ti_{0.01})_{3.00}[(SO_4)_{2.09}(PO_4)_{0.02}]_{2.11}\{[(OH)_{5.71})Cl_{0.05}]_{5.76}(H_2O)_{0.24}\}$$

corresponding to the synthetic Sr analog of huangite (Ca species) and walthierite (Ba species). This composition leads to $\mathbf{Srh_{52}Sfh_{33}}Alu_4Naa_3Jar_2Naj_2Hua_1Mga_1Caj_1Mgj_1Goy_1Ben_{<1}$ end-member representation, where Srh stands for "strontiohuangite" and Sfh for "strontioferrihuangite" HEMs (P-dominant HEMs omitted). Medium-enriched species composition (n = 6, GM of 2.6 wt.% SrO) is

$$[(NH_4)_{0.84}\mathbf{Sr_{0.09}}K_{0.04}Na_{0.02}Mg_{0.01}]_{1.00}(Al_{1.75}Fe_{1.24}Ti_{0.01})_{3.00}[(SO_4)_{1.74}(SiO_4)_{0.15}(PO_4)_{0.02}]_{1.91}[(OH)_{5.95}Cl_{0.05}]_{6.00}.$$

A single analysis with 18.70 wt.% SrO was recalculated to

$$[(NH_4)_{0.78}\mathbf{Sr_{0.15}}K_{0.03}Na_{0.03}Ca_{0.01}]\acute{O}_{1.00}(Al_{1.59}Fe_{1.41}Ti_{0.01})_{3.00}[(SO_4)_{1.91}(PO_4)_{0.05}(SiO_4)_{0.04}]_{2.00}[(OH)_{6.01}Cl_{0.05}]_{6.06}$$

(medium-enriched AAJ) + $1.09SrSO_4$.

A mean end-member composition of the medium-enriched material is $Ama_{51}Amj_{37}\mathbf{Srh_3Sfh_2}Alu_2Jar_2Naa_2Naj_1(Mga+Mgj+Hua+Caj)_{<1}$. The low-Sr material has the following composition (n = 4, 0.53 wt.% SrO on average):

$$[(NH_4)_{0.85}K_{0.09}Na_{0.03}\mathbf{Sr_{0.02}}Mg_{0.01}]_{1.00}(Al_{2.25}Fe_{0.74}Ti_{0.01})_{3.00}[(SO_4)_{1.60}(SiO_4)_{0.37}(PO_4)_{0.03}]_{2.00}\{[(OH)_{5.22}Cl_{0.05}]_{5.27}(H_2O)_{0.73}\}.$$

This corresponds to $Ama_{69}Amj_{19}Alu_5Jar_2Naa_2Naj_1\mathbf{Srh_1}Mgh_1(Mgj+\mathbf{Sfh}+Hua+Caj)_{<1}$ end-member representation. The *A*-site content is shown in Appendix Figure SF11 drawn for the SrO-K_2O-*R* system (*R* standing for the remaining *A*-site-related oxides). The datapoints plot to two areas that illustrate the above findings. The normality test and Kendall statistical results are shown in Appendix Tables ST11 and ST12, respectively.

ZIRCONIUM EXPERIMENT

The BSE images of the AAJ subject to the Zr experiment are quite complex. The main, relatively BSE-dark, compact phase ("AAJ-Zr"; Appendix Table ST13), shows an EDS spectrum of AAJ (Al>Fe), with Zr superimposed. The thin section is rich in broken crusts of a Zr-rich Ca-bearing silicate that bears traces of Al, S, Mg, and yet lower amounts of Fe ("phase A"). Another phase that seems to represent a Zr-exchanged AAJ is strongly Al-dominant, with subordinate Si and Fe, and traces of Na, Mg, Cl and K ("AAJ-Zr-2"). Yet another, porous, phase was detected, that differs from the former in a clearly higher Si content, lower Zr levels, subordinate Fe (Al>Fe), evident K, and traces of Na, Mg and Cl ("phase B"). A darker variety of this phase additionally bears a small amount of P. A relatively BSE-dark phase is locally associated with these crusts; it is largely a Zr-Al-S-O phase, with slightly higher amounts of Si (S>Si), subordinate Fe, and trace Na, Mg, Cl, K and Ca. Representative EDS spectra of various Zr-exchanged AAJ and the Zr-Ca-silicate are given in Appendix Figure SF12.

The PXRD pattern shows Ama reflections that are much more intense than the Amj ones. The latter are barely recognizable. The most intense, split reflection, at 14.797 Å, belongs to an unspecified species. It likely fits to several other, weak, unattributed reflections at 10.453, 12.876, 8.458 and 9.718 Å. Neither of these reflections is attributable to tetragonal $ZrSiO_4$.

The zirconium experiment seems to bring the most interesting results, as Zr is not known to enter the *B*-site, while Ti, which has crystal-chemical behavior similar to that of Zr, is known to do so. The averaged total content of the *B*-site (Al+Fe+Ti) is 2.56

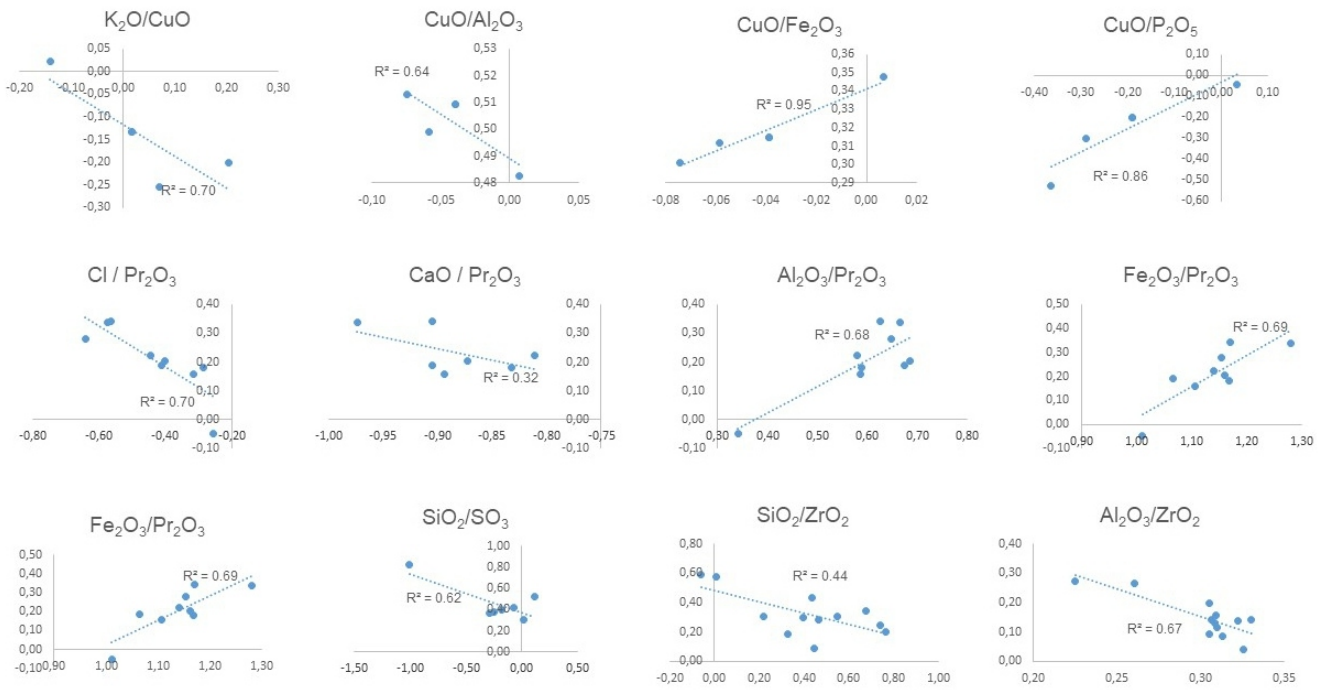

Fig. 4. Selected element correlation diagrams, Cu, Pr and Zr experiments (logratioed data used)

apfu (unnormalized data). Based on a *B* = 3 normalization, the average Zr sorption level is estimated at 5%. The GM ZrO_2 content equals 3.67 wt.%. Three phases were determined via EPMA, with a few likely representing various levels of ZrSi substitution. The Si-rich composition, corresponding to analyses 2–4 (Appendix Table ST7; GM ZrO_2 of 3.59 wt.%) is

$$[(NH_4)_{0.55}K_{0.26}Na_{0.09}Mg_{0.06}Ca_{0.04}]_{1.00}(Al_{2.48}Fe_{0.34}\mathbf{Zr_{0.15}}Ti_{0.04})_{3.01}[(SO_4)_{1.05}(SiO_4)_{0.91}(PO_4)_{0.04}]_{2.00}\{[(OH)_{4.38}Cl_{0.08}]_{4.46}(H_2O)_{1.54}\},$$

with Si excess removed. Analysis no. 1 recasts to

$$[(NH_4)_{0.69}K_{0.17}Na_{0.08}Mg_{0.03}Ca_{0.03}]_{1.00}(Al_{2.41}Fe_{0.44}\mathbf{Zr_{0.14}}Ti_{0.02})_{3.01}[(SO_4)_{1.33}(SiO_4)_{0.67}]_{2.00}\{[(OH)_{4.82}Cl_{0.09}]_{4.91}(H_2O)_{1.09}\},$$

after removal of Si excess at the *T*-site (by stoichiometry). Material with lower Si content has the following composition (analyses 5–10, *n*=6, average ZrO_2 content of 3.6 wt.%):

$$[(NH_4)_{0.88}K_{0.09}Na_{0.01}Ca_{0.01}Mg_{0.01}]_{1.00}(Al_{2.17}Fe_{0.66}\mathbf{Zr_{0.14}}Ti_{0.03})_{3.00}[(SO_4)_{1.56}(SiO_4)_{0.46}(PO_4)_{0.02}]_{2.04}\{[(OH)_{4.94}Cl_{0.07}]_{5.10}\{H_2O\}_{0.90}\}.$$

This phase is thus less aluminian and more ferric. The whole Zr-exchanged AAJ series composition is

$$[(NH_4)_{0.76}K_{0.15}Na_{0.04}Mg_{0.03}Ca_{0.02}]_{1.00}(Al_{2.28}Fe_{0.54}\mathbf{Zr_{0.14}}Ti_{0.03})_{2.99}[(SO_4)_{1.38}(SiO_4)_{0.59}(PO_4)_{0.03}]_{2.00}\{[(OH)_{4.91}Cl_{0.07}]_{4.98}(H_2O)_{1.02}\}.$$

The two last analyses of Appendix Table ST7 likely correspond to a phase of non-alunitic structure type. This phase could, possibly, correspond to the unattributed reflections in the PXRD pattern. Its composition may perhaps be approximated as

$$[(NH_4)_{0.94}K_{0.03}Ca_{0.03}]_{1.00}(Al_{0.94}Fe_{0.55}\mathbf{Zr_{0.51}})_{2.00}[(SO_4)_{0.99}(SiO_4)_{0.06}(PO_4)_{0.01}]_{1.06}\{[(OH)_{5.07}Cl_{0.07}]_{5.14}(H_2O)_{0.86}\}$$

(*B* = 2 basis). In a SiO_2-ZrO_2 correlation diagram (Fig. 4) the Si-rich composition shows a somewhat unclear negative trend with r^2 of 0.52. The corresponding parameter for ZrO_2-(Al_2O_3+Fe_2O_3+TiO_2) is as low as 0.21. However, for the moderately Si-enriched Zr-exchanged AAJ, r^2 equals 0.86 (negative trend), thus primarily confirming Zr entering the *B*-site. The SiO_2-SO_3 relation for the Si-high composition is described by a strong negative trend (r^2 = 0.90), while in the moderately siliceous material it is only 0.54 (also a negative trend). The ZrO_2-SO_3 correlation for the whole series shows an unclear negative trend (r^2 = 0.50). The (Al_2O_3+Fe_2O_3+TiO_2)-ZrO_2 diagram for the whole series shows a fairly clear negative trend, though r^2 is quite low at 0.56. As such, Zr seems to enter the AAJ structure as silicate and sulphate HEMs (ZrO_2-P_2O_5 diagrams do not suggest any trends). Thus, the proposed Zr-dominant silicate end-members are $(NH_4)Zr_3(SiO_4)_2[(OH)_5(H_2O)]$ (Azs) $KZr_3(SiO_4)_2[(OH)_5(H_2O)]$ (Pzs) $NaZr_3(SiO_4)_2[(OH)_5(H_2O)]$ (Szs), $Ca_{0.5}Zr_3(SiO_4)_2[(OH)_5(H_2O)]$ (Czs) and $Mg_{0.5}Zr_3(SiO_4)_2[(OH)_5(H_2O)]$ (Mzs). The corresponding sulphate HEMs could be $(NH_4)[Zr_{2.25}[]_{0.75}](SO_4)_2(OH)_6$ (Azu), $K[Zr_{2.25}[]_{0.75}](SO_4)_2(OH)_6$ (Pzu), $Na[Zr_{2.25}[]_{0.75}](SO_4)_2(OH)_6$ (Szu), $Ca_{0.5}[Zr_{2.25}[]_{0.75}](SO_4)_2(OH)_6$ (Czu), and $Mg_{0.5}[Zr_{2.25}[]_{0.75}](SO_4)_2(OH)_6$ (Mzu). The whole-series end-member representation would then take the form $Ama_{56}Amj_{14}Alu_{11}\mathbf{Azu_4}Naa_3Jar_2Mgh_2\mathbf{Azs_2}Naj_1\mathbf{Pzu_1}$(Hua+Mfh+**Pzs**+**Szu**+Caj+**Szs**+**Mzs**+**Czu**)$_2R_2$. The corresponding forms for the high-Si and moderately siliceous materials are $Ama_{47}Alu_{19}Amj_7Naa_7Mgh_4Jar_3\mathbf{Azu_3Azs_2}Naj_1Hua_1\mathbf{Pzu_1Pzs_1}Mfh_1$(**Szu**+**Mzu**+**Mzs**+Caj+**Czu**)$_{<1}R_3$ and $Amj_{62}Amj_{19}Alu_6\mathbf{Azu_4}Jar_2\mathbf{Azs_1}Mgh_1Naa_1$(**Pzu**+Mfh+Hua+Caj+Naj+**Pzs**+**Szs**+**Mzs**+**Szu**+**Mzu**+**Czu**)$_3R_1$. The ZrO_2/SiO_2 diagram for the Si-high material shows an unclear negative trend (r^2 = 0.52); for the moderately siliceous composition no trend is visible, unless two low-Si but high-Zr analyses are added, showing an unclear negative trend with r^2 of 0.54. The whole series does not show any clear trend (r^2 = 0.21). The Si-low, moderately Zr-enriched AAJ has a ZrO_2 content negatively correlated with (Fe,Al,Ti) oxides (r^2 = 0.86) that may be used as an argument for Zr entering the AAJ structure (even though the related r^2 for the whole ana-

lytical series is lower, at 0.56). Only the high-Si composition shows a very unclear positive trend for the Fe_2O_3/ZrO_2 relation (r^2 = 0.40). The Al_2O_3/ZrO_2 diagram shows very strong negative correlation (r^2 = 0.92) for the low-Si series with two high-Zr analyses added, while the related value for the whole series is 0.81, and for the low-Si series alone is only 0.40. The mean Cl content in the Zr-exchanged AAJ is, again, lower than in the base AAJ, although the difference here is smaller than in the former experiments. The *B*- and *T*-sites content is shown in Appendix Figures SF13 and SF14, respectively. The latter figure shows a possible S-rich and Si-rich composition of the Zr-exchanged AAJ. The normality test and Kendall statistical results are shown in Appendix Tables ST14 and ST15, respectively.

To the best knowledge of the authors, Zr substitution in alunite-supergroup minerals was not reported prior to our studies. Potential Zr substitution in the AAJ studied was thus analyzed in more detail. For this reason, the treated material was studied by EBSD. Initially, no phase could be indexed, most likely due to the very poor quality of the polished surface, as shown by *ARGUS*^{TM} imaging. Thus, the section was re-polished with nano-silica gel, which slightly improved the surface quality. Although this approach proved not to be enough, with an indexing error of 50%, the software used was able to attribute numerous areas of the sample to an alunite-type compound. Interestingly, some patterns attributed to tetragonal $ZrSiO_4$ were also present (Appendix Fig. SF15). The latter finding interferes with the above negative high-Si-Zr trend, but no reflections attributable to zircon were detected in the PXRD sample.

MANGANESE EXPERIMENT

Initially, manganese was not observed in the EDS spectra, and is thus lacking in the analytical set (Appendix Table ST16). A low-intense Mn K line was however detected in an evidently BSE-darker intra-grain zone, using the Sigma system (Appendix Fig. SF16), with an almost undetectable line in a BSE-brighter material. The Ama reflections, broad and multi-split, are much stronger than the Amj ones. The latter are very weak, diffuse, and shoulder-like. Manganese was not found substituted in the material studied. The whole-series formula, based on the EPMA data (n = 7, Appendix Table ST8) is

$$[(NH_4)_{0.91}K_{0.06}Na_{0.02}Mg_{0.01}]_{1.00}(Al_{2.42}Fe_{0.58}Ti_{0.01})_{3.01}[(SO_4)_{1.47}(SiO_4)_{0.27}(PO_4)_{0.03}]_{1.77}[(OH)_{5.87}Cl_{0.07}]_{5.94}.$$

The *T*-site-normalized (stoichiometry and proportion approach) form is

$$[(NH_4)_{0.91}K_{0.06}Na_{0.02}Mg_{0.01}]_{1.00}(Al_{2.42}Fe_{0.58}Ti_{0.01})_{3.01}[(SO_4)_{1.66}(SiO_4)_{0.31}(PO_4)_{0.03}]_{2.00}\{[(OH)_{5.33}Cl_{0.07}]_{5.40}(H_2O)_{0.60}\}.$$

This corresponds to $Ama_{72}Amj_{17}Alu_5Naa_2Jar_1$(Mgh+Hua+Mfh+Caj)$_3$ end-member composition (P-and Si-dominant HEMs omitted). Another trial of the analysis of Mn (and Zn) content using more sophisticated EPMA (with lower detection limits) is planned.

COPPER EXPERIMENT

The WDS (LPET) scan shows an evident Cu K line, as can be seen in Appendix Figure SF17. In the PXRD data, the Ama reflections are, as usual, much stronger than the Amj ones. The latter are very diffuse. The average summation of the *B*-site excluding copper is 2.99 apfu (Appendix Table ST17). The substitution level is calculated as 0.66 % of the *B*-site occupancy, with a mean of just 0.74 wt.% CuO. The composition of the product is

$$[(NH_4)_{0.90}K_{0.07}Mg_{0.01}Na_{0.01}]_{1.00}(Al_{2.59}Fe_{0.39}\mathbf{Cu_{0.02}}Ti_{0.01})_{3.01}[(SO_4)_{1.29}(SiO_4)_{0.33}(PO_4)_{0.03}]_{1.65}[(OH)_{5.99}Cl_{0.05}]_{6.04}$$

(n = 7). This corresponds to $Ama_{77}Amj_{12}Alu_6Jar_1Mgh_1Naa1$(Naj+Mfh+Hua+Caj+**Mbc**)$_{<1}R_2$, where Mbc corresponds to "magnesiobeaverite-(Cu)" HEM, or $Mg(Fe_2Cu)(SO_4)_2(OH)_6$ (P- and Si-rich HEMs omitted). As such, the Cu-dominant end-members stand for less than 0.5% of the end-member composition. Copper seems to enter the *B*-site via removal of Al (as in the In case – see below): the r^2 for a positive CuO/Fe_2O_3 trend is 0.52, and that for the CuO/Al_2O_3 trend is 0.83. The process of Cu entering seems to be related to P enrichment, as the r^2 in the P_2O_5/CuO diagram (positive trend) is 0.55. The *B*-site content is shown in Appendix Figure SF18; the aluminian character of the material is clearly seen. The normality test and Kendall statistical results are shown in Appendix Tables ST18 and ST19, respectively.

ZINC EXPERIMENT

Zinc, as manganese, was not found exchanged in the AAJ in amounts high enough to be measured by means of EPMA (Appendix Table ST20). A single EDS spectrum with some Zn seen was obtained. The small amount of material precluded obtaining PXRD pattern in this case. Zinc, as manganese, was not found to be substituting in the AAJ even though numerous attempts were made to localize any Zn anomalies. The composition of the material studied, n = 7, is

$$[(NH_4)_{0.88}K_{0.10}Ca_{0.01}Mg_{0.01}Na_{0.01}]_{1.01}(Al_{2.33}Fe_{0.66}Ti_{0.01})_{3.00}[(SO_4)_{1.37}(SiO_4)_{0.33}(PO_4)_{0.03})]_{1.73}\{[(OH)_{5.83}Cl_{0.06}]_{5.89}(H_2O)_{0.11}\}.$$

This corresponds to an $Ama_{67}Amj_{19}Alu_7Jar_2Naa_1Mgh_1Hua_1$(Mfh+Caj+Naj)$_{<1}R_2$ end-member composition (P- and Si-dominant HEMs omitted). The chlorine content is, again, smaller than in the base AAJ.

GALLIUM EXPERIMENT

The gallium experiment is interesting, e.g., due to the Amj reflections prevailing over the Ama ones. Both main reflections are quite broad. An additional, very broad reflection is observed as a feature centred at 2.943 Å. Yet another, very weak one, is present at 2.517 Å and may be attributable to a spinel-type phase. A representative EDS spectrum of Ga-exchanged AAJ is shown in Appendix Figure SF19. The geometric-average Ga_2O_3 content is relatively high, at 11.52 wt.%. The average total *B*-site occupancy, excluding gallium, is 1.74 apfu (Appendix Table ST21). This corresponds to a large sorption level of 42%. Gallium thus prevails over both Al and Fe, but not over their total, i.e., alunitic and jarositic end-members. The whole-series composition (n = 7) is

$$[(NH_4)_{0.96}K_{0.04}]_{1.00}(\mathbf{Ga_{1.26}}Al_{0.93}Fe_{0.80}Ti_{0.01})_{3.00}[(SO_4)_{1.95}(PO_4)_{0.05}]_{2.00}[(OH)_{5.91}Cl_{0.05}]_{5.96};$$

it corresponds to $\mathbf{Ags_{39}}Ama_{29}Amj_{25}\mathbf{Pgs_2}Alu_1Jar_1$(**Mgs**+Mgh+Mfh)$_1R_2$, where Ags is "ammonium gallium sulphate" HEM, or

$(NH_4)Ga_3(SO_4)_2(OH)_6$, Pgs is "potassium gallium sulphate" HEM, or $KGa_3(SO_4)_2(OH)_6$, and *R* stands for remaining phosphate-, titanium- and chlorine-dominant HEMs. Crystals with Al>Fe have the composition (*n* = 4, analyses 1–4):

$$[(NH_4)_{0.96}K_{0.04}]_{1.00}(\mathbf{Ga_{1.18}}Al_{1.11}Fe_{0.71}Ti_{0.01})_{3.01}[(SO_4)_{1.88}(PO_4)_{0.04}]_{1.92}[(OH)_{6.10}Cl_{0.06}]_{6.16}.$$

This corresponds to **Ags$_{37}$**Ama$_{34}$Amj$_{22}$Alu$_2$**Pgs$_2$**Jar$_1$(**Mgs**+Mgh+Mfh)$_{<1}R_2$. Crystals with Fe>Al (*n* = 3, analyses 5–7, after *T*-site normalization by stoichiometry), are more enriched in gallium:

$$[(NH_4)_{0.96}K_{0.04}]_{1.00}(\mathbf{Ga_{1.36}}Fe_{0.93}Al_{0.70}Ti_{0.01})_{3.01}[(SO_4)_{1.95}(PO_4)_{0.05}]_{2.10}[(OH)_{5.94}Cl_{0.05}]_{5.99},$$

corresponding to **Ags$_{44}$**Amj$_{29}$Ama$_{22}$**Pgs$_2$**Jar$_1$Alu$_1R_2$. Although this notion omits the P- and Si-dominant HEMs for clarity, gallium shows a quite strong correlation with P (r^2 = 0.65, positive trend), but an unclear negative correlation with Si (r^2 = 0.54). This is somewhat suggestive of coprecipitation with phosphate and silicate anions. Neither the Ga_2O_3/Fe_2O_3 nor Ga_2O_3/Al_2O_3 correlation diagrams give any evident trends. The *B*-site content is shown in Appendix Figure SF20. It illustrates the close-to-central location of the datapoint projection. The normality test and Kendall statistical results are shown in Appendix Tables ST22 and ST23, respectively.

INDIUM EXPERIMENT

The reflection ratioes of the AAJ in the indium experiment follow the most common rule, with Amj ones being very diffuse (though present, as shoulder-like features). An additional, very weak reflection is observed at 3.178 Å, possibly from a recrystallized $InCl_3$ or another chloride. EDS spectra of various In-exchanged products are juxtaposed in Appendix Figure SF21. Recasting of the results using the basis of *T* = 2 gives a large surplus *B*-site occupancy, with a geometric mean of 5.42 apfu. As such, the results were normalized to *B* = 3 apfu. Average In_2O_3 content is 4.05 wt.% (whole-data basis). The average indium sorption level is thus calculated to be ~8%. It follows that the whole-series composition (*n* = 15, Appendix Table ST24), is

$$[(NH_4)_{0.91}Ca_{0.04}K_{0.04}Mg_{0.01}]_{1.00}(Fe_{1.40}Al_{1.32}\mathbf{In_{0.25}}Ti_{0.03})_{3.00}[(SO_4)_{1.52}(PO_4)_{0.28}(SiO_4)_{0.19}]_{1.99}\{[(OH)_{5.31}Cl_{0.13}]_{5.44}(H_2O)_{0.56}\};$$

this corresponds to Ama$_{37}$Amj$_{34}$**Ais$_6$**Alu$_3$Caj$_2$Jar$_1$(Mgh+Mfh+Hua+**Pis**+**Mis**+**Cis**)$_2R_{15}$, where Ais stands for "ammonium indium sulphate" HEM, Pis is for "potassium indium sulphate" HEM, Mis for "magnesium indium sulphate" HEM, Cis for "calcium indium sulphate" HEM, and *R* for remaining phosphate-, titanium- and chlorine-dominant end-members. An In-rich composition (*n* = 6, GM of 13.07 wt.% In_2O_3), that is ammoniojarositic in terms of the major components, is

$$[(NH_4)_{0.91}Ca_{0.07}K_{0.02}Mg_{0.01}]_{1.00}(Fe_{2.12}Al_{0.42}\mathbf{In_{0.42}}Ti_{0.04})_{2.97}[(SO_4)_{1.45}(PO_4)_{0.45}(SiO_4)_{0.10}]_{2.00}\{[(OH)_{5.32}Cl_{0.16}]_{5.48}(H_2O)_{0.52}\},$$

corresponding to Amj$_{49}$Ama$_{10}$**Ais$_{10}$**Caj$_4$Jar$_1$**Cis$_1$**Hua$_1$(Mgj+**Mis**+Mgh)$_{<1}R_{24}$. In this case the sorption level increases to 14%. For the high-In series the average surplus *B*-site content (for the unnormalized data) is 4.96 ($_B$ = 7.96), that could in theory correspond to additional $(Fe_{3.70}In_{0.73}Al_{0.64}Ti_{0.08})_{5.15}$ atoms. These surplus atoms may be related to co-deposition of (semi)amorphous A_2O_3-type oxide(s) or (oxy-)hydroxides.

A high amount of P is not only reflected by a strong positive correlation of In and P, but also in the fact that the ideal formula of the high-In series can be written as $(NH_4)(Fe,Al,In)_3(SO_4)_{1.5}(PO_4)_{0.5}[(OH)_{5.5}(H_2O)_{0.5})]$ or $(NH_4)_2(Fe,Al,In)_6(SO_4)_3(PO_4)(OH)_9(H_2O)$. Similar formulae may be given for the whole In-exchanged AAJ series. The moderately In-enriched material shows the following formula:

$$[(NH_4)_{0.93}Ca_{0.06}K_{0.01}]_{1.00}(Fe_{1.87}Al_{0.73}\mathbf{In_{0.35}}Ti_{0.04})_{2.99}[(SO_4)_{1.52}(PO_4)_{0.43}(SiO_4)_{0.05}]_{2.00}\{[(OH)_{5.32}Cl_{0.22}]_{5.54}(H_2O)_{0.46}\}$$

(*n* = 3, 8.3 wt.% In_2O_3 on average), corresponding to Amj$_{45}$Ama$_{18}$**Ais$_9$**Caj$_3$**Cis$_1$**Hua$_1$Jar$_1R_{22}$. In this case, the *B*-unnormalized data recasts to a formula with a surplus of 3.30 apfu (*B*), possibly corresponding to additional $(Fe_{2.26}Al_{0.87}In_{0.43}Ti_{0.05})_{3.61}$ atoms. The indium-low series recasts to

$$[(NH_4)_{0.90}K_{0.08}Mg_{0.01}]_{1.00}(Al_{2.52}Fe_{0.45}\mathbf{In_{0.02}}Ti_{0.01})_{3.00}[(SO_4)_{1.60}(SiO_4)_{0.35}(PO_4)_{0.04}]_{1.99}\{[(OH)_{5.24}Cl_{0.05}]_{5.29}(H_2O)_{0.71}\},$$

or Ama$_{74}$Amj$_{13}$Alu$_7$Jar$_1$Mgh$_1$**Ais$_1$**Mfh$_1R_2$ (*n* = 6, mean of 0.87 wt.% In_2O_3). Here, the potential surplus *B*-site equals 0.68 apfu, that could correspond to $(Al_{0.69}Fe_{0.12})_{0.81}$ surplus atoms. A large content of phosphate-dominant end-members seems to be correlated with In enrichment, even though the charge of In is expected to follow that of Al and Fe, thus not requiring enlarging of negative charge. This may be due to the larger (compared to S) P expanding the structure, thus facilitating the relatively large In^{3+} substitution (Kolitsch, pers. *comm.*). Even though the analyses show large surplus Fe (with likely less pronounced excess of Al, In and Ti), correlation of In with Fe seems to be very strong, positive, and linear, with r^2 = 0.97. Indium seem to enter the structure with simultaneous removal of Al, as suggested by the negative In-Al trend (r^2 = 0.88). The K-In correlation forms a polynomial or parabolic trend, with r^2 = 0.78. The K-S correlation forms a similar trend (r^2 = 0.78); if, however, the trend line is of power type, the r^2 grows to 0.88. The related power trend in the In-Si diagram has an r^2 of 0.81.

The In experiment is interesting also due to clear Cl enrichment of the exchanged material. This is observed for both the In-rich and the moderately In-enriched material. Two projection areas and their varying shift towards the potential In-dominant compositions can be clearly seen in Appendix Figure SF22 addressing the *B*-site content. The normality test and Kendall statistical results are shown in Appendix Tables ST25 and ST26, respectively.

ARSENIC EXPERIMENT

EDS spectra showing variable As content in the reacted AAJ are shown in Appendix Figure SF23. The average (GM) As_2O_5 content of the whole series of the As-exchanged AAJ is 14.74 wt.%. The As experiment produced numerous As-exchanged phases:

- relatively BSE-bright, vermicular, porous aggregates of an As-rich ferric phase, with elevated amounts of S, minor Al, P, K and traces of Cl;
- BSE-darker cores of larger (up to ca. 50 µm in diameter) crystals and their aggregates, with much higher contents of O, S, Al and Fe, and with As as an important component; they bear minor amounts of K, P, Cl and traces of Na;

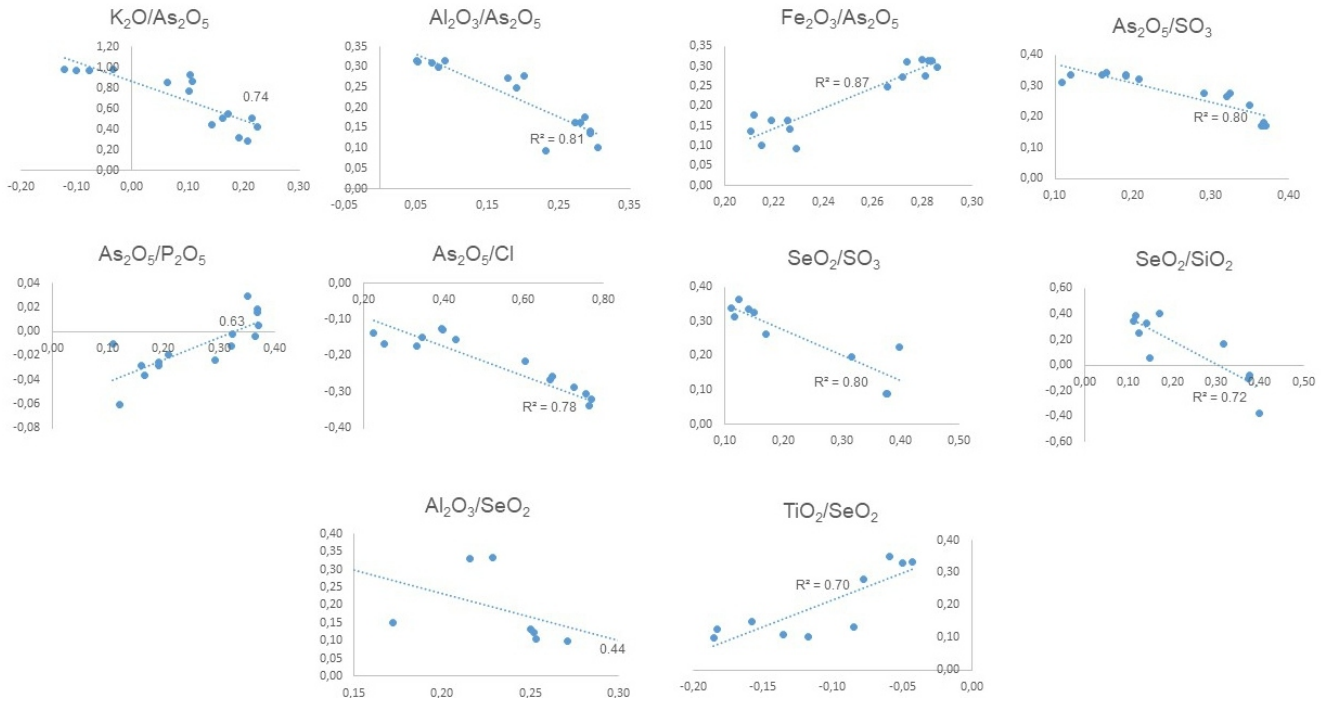

Fig. 5. Selected element correlation diagrams, As and Se experiments (logratioed data used)

- larger (up to ca. 400 μm in diameter) aggregates with BSE-brighter rims of a siliceous Al-Fe-rich arsenate-sulphate (As>S), with slightly elevated K and P contents, and low levels of Na, Cl, and Ti; and cores of a KMg(FeNa) aluminosilicate. A more pure Si-free phase corresponds to a low-K sulphate-arsenate of Al and Fe (Al>Fe) with a visible admixture of Cl;
- a relatively BSE-dark, microporous, siliceous arsenate-sulphate, characterized by much higher S and Al contents (Al>Fe), relatively K-rich, with subordinate amounts of Na, P, Cl, Ca and traces of Ti;
- slightly BSE-brighter crystals included in the former phase, that seem to represent the original AAJ probably intergrown with TiO_2, and SiO_2/aluminosilicate compounds, and
- large, low-vesicular aggregates of low-As, Si- and K-rich AAJ with subordinate Mg and trace Na and Cl; this phase has BSE-brighter zones which represent a more pure (low-Si) phase.

Some of these fine-grained phases may represent mutual intergrowths. When the facts above are summarized to encompass three levels of As substitution, the average As_2O_5 content is 43.15 wt.% in the As-high, 25.20 wt.% in the medium-high, and 5.4 wt.% in the As-low material.

The reflection ratios of the AAJ in the arsenic experiment follow the most common observation, with Amj-attributed ones being less intense than the Ama-ascribed ones. About six crystallochemical types of As-enriched substances were detected, listed in order of decreasing As substitution (Appendix Table ST27):

(1) As-richest, n = 4 (analyses 1–4 in the Appendix Table ST27):
$[(NH_4)_{0.80}K_{0.11}Na_{0.04}Ca_{0.03}Mg_{0.02}]_{1.00}(Fe_{2.65}Al_{0.32}Ti_{0.03})_{3.00}$ $[\mathbf{(AsO_4)_{1.62}}(SO_4)_{0.31}(PO_4)_{0.06}]_{2.00}\{[(OH)_{4.38}Cl_{0.04}]_{4.42}$ $(H_2O)_{1.58}\}_{6.00}$ (*T*-site normalized, with lacking Si to enter the *T*-sites); this corresponds to a high sorption level, at 81%;

(2) As-rich, corresponding to analysis no. 5:
$[(NH_4)_{0.66}K_{0.21}Na_{0.06}Mg_{0.05}Ca_{0.02}]_{1.00}(Fe_{2.63}Al_{0.34}Ti_{0.02})_{2.99}$ $[\mathbf{(AsO_4)}_{1.33}(SO_4)_{0.59}(PO_4)_{0.08}]_{2.00}\{[(OH)_{4.61}Cl_{0.04}]_{S4.65}$ $(H_2O)_{1.35})\}_{6.00}$; a still high sorption level of 66.5%;

(3) medium As-rich, n = 3:
$[(NH_4)_{0.71}K_{0.17}Na_{0.08}Ca_{0.03}Mg_{0.01}]_{1.00}(Fe_{1.89}Al_{1.09}Ti_{0.02})_{3.00}$ $[\mathbf{(AsO_4)_{1.00}}(SO_4)_{0.95}(PO_4)_{0.05}]_{2.00}\{[(OH)_{4.95}Cl_{0.05}]$ $(H_2O)_{0.99}]_{6.00}$ (*T*-site normalized, with Si removed due to excess negative charge); sorption level of 50%;

(4) As-low, n = 3:
$[(NH_4)_{0.81}K_{0.16}Na_{0.04}Ca_{0.01}]_{1.00}(Al_{2.33}Fe_{0.66}Ti_{0.01})_{3.00}[(SO_4)_{1.76}$ $\mathbf{(AsO_4)_{0.20}}(PO_4)_{0.04}]_{2.00}\{[(OH)_{5.75}Cl_{0.05}]_{5.80}$ $(H_2O)_{0.20}\}_{6.00}$; (*T*-site normalized, with Si removed); substitution level of just 10%;

(5) As-low, type 1, n = 3:
$[(NH_4)_{0.74}K_{0.18}Na_{0.04}Mg_{0.03}Ca_{0.01}]_{1.00}(Al_{2.37}Fe_{0.62}Ti_{0.01})_{3.00}$ $[(SO_4)_{1.68}\mathbf{(AsO_4)_{0.28}}(PO_4)_{0.05}]_{2.00}\{[(OH)_{5.66}Cl_{0.04}]_{5.70}$ $(H_2O)_{0.30}\}_{6.00}$ (*T*-site normalized, with Si removed); slightly higher substitution level, at 14%;

(6) As-low, type 2, a single analysis (no. 15):
$[(NH_4)_{0.63}K_{0.27}Na_{0.09}Ca_{0.01}]_{1.00}(Al_{1.85}Fe_{1.13}Ti_{0.02})_{3.00}$ $[(SiO_4)_{1.01}(SO_4)_{0.88}\mathbf{(AsO_4)_{0.08}}(PO_4)_{0.04}]_{2.00}$ $\{[(OH)_{3.79}Cl_{0.08}]$ $(H_2O)_{2.13}\}_{6.00}$ (*T*-site normalized, with Si removed); just 4% of the sorption level.

It is clearly seen that the As-rich and medium As-enriched compositions (first two types) are jarositic, while the As-low ones are alunitic. Indeed, the r^2 for the clearly positive trend in the As_2O_5/Fe_2O_3 diagram is high at 0.88. Simultaneously, a negative As_2O_5/Al_2O_3 correlation is observed (r^2 = 0.66). As undoubtedly substitutes S, as shown in the As_2O_5/SO_3 correlation diagram with a clear negative trend (r^2 = 0.82). No evident trends were found for SiO_2/SO_3, which argues for excluding the silicate anion from the above empirical formulae. The As_2O_5/TiO_2 correlation is unclear (supposed weak positive

trend, $r^2 = 0.44$). The strongest correlation, that is also difficult to explain without applying additional techniques like Single Crystal or Electron Diffraction, was found for the As_2O_5-Cl system ($r^2 = 0.91$, negative trend). The P_2O_5-Cl correlation is much less evident at $r^2 = 0.58$ (also a negative trend). K seems to be correlated with Cl, too (positive trend, $r^2 = 0.80$). The single As-rich material analysis with slightly lower As_2O_5 content, corresponding to analysis no. 5 in Appendix Table ST27, recasts to

$$[(NH_4,HO)_{0.66}K_{0.21}Na_{0.06}Mg_{0.05}Ca_{0.02}]_{1.00}(Fe_{2.63}Al_{0.34}Ti_{0.02})_{2.99}[(AsO_4)_{1.33}(SO_4)_{0.59}(PO_4)_{0.08}]_{2.00}\{[(OH)_{4.61}Cl_{0.04}]_{4.65}(H_2O)_{1.35}\}_{6.00}.$$

The end-member representation of the As-exchanged AAJ is variable. The type "(1)" composition clearly suggests the dominance of a $(NH_4)Fe_3(AsO_4)_2[(OH)_4(H_2O)_2]$ HEM. In the type "(2)", however, another HEM seems to be dominant, i.e., the $(NH_4)Fe_3[(AsO_4)(SO_4)][(OH)_5(H_2O)]$ HEM, somewhat resembling a stoichiometry typical for the beudantite group of the alunite supergroup. Indeed, the empirical formula of this second type is very close to the suggested HEM ideal composition. Changes in the *X*-site composition are necessary as a counterbalance to the variably elevated negative charge at the *T*-site. The related end-member composition for type "(1)" may be given as $Aaj_{58}Amj_{11}Aja_8Aaa_7Tpe_3Anj_3Ama_2Jar_2Tte_1Aal_1Mbe_1Naj_1R_2$, where Aaj is "As-substituted ammoniojarosite" HEM (with $T = 2$ As and $X = 4OH^- + 2H_2O$), Aja is a related "As-substituted jarosite" HEM, Aaa is an "As-substituted ammonioalunite" HEM, Anj is an "As-substituted natrojarosite" HEM, Aal is an "As-substituted alunite" HEM, and Mbe is a "magnesiobeudantite" HEM. The corresponding notation for the analysis #5 is $Aaj_{38}Amj_{17}Aja_{12}Ama_6Aaa_5Jar_5Tpe_4Anj_3Aal_2Naj_1Alu_1Mfh_1Tte_1$. The end-member composition of the type "(2)" is $Aaj_{22}Amj_{20}Ama_{16}Aaa_{12}Aja_5Jar_5Alu_3Tpe_3Aal_3Anj_2Naj_2Ana_1Naa_1Fhu_1Hua_1Tte_1Cbe_1Chi_1R_{<1}$, where Cbe is a "calciobeudantite" HEM; and T = As+S and $X = 5OH^- + H_2O$ in the As-substituted end-members. A clear enrichment in As-free ammoniojarosite (of 11 mol%) and ammonioalunite (of 14 mol%) end-members is seen when comparing the latter end-member with the former one, thus following decreasing As enrichment when passing from the type "(1)" to the type "(2)" composition. The type "(3)" average composition clearly fits the dominant Aaj HEM. The *T*-site content is shown in Appendix Figure SF24. Multiple projections related to the above species, representing variable levels of As substitution, can be observed. The normality test and Kendall statistical results are shown in Appendix Tables ST28 and ST29, respectively.

Substitution of As into the original P-bearing AAJ leads to formation of minor amounts of a Fe-rich Al,S-bearing phosphate that commonly forms atoll-like aggregates, up to ca. 45 m in diameter, of microcrystals (reaching ~10 microns in diameter). The average composition of this phase is (wt.%): 2.83 SO_3, 33.34 P_2O_5, 45.55 Fe_2O_3, 2.35 Al_2O_3, and 0.24 MgO, with occasional enrichment in Ti (up to 0.22), Ca (up to 0.30), Cl (up to 0.16), and possibly Si. This data may be recalculated, based on 4 cations, to

$$(Fe_{3.53}Al_{0.41}Mg_{0.04}Ca_{0.01})_{4.00}[(PO_4)_{2.90}(SO_4)_{0.24}]_{3.14}[(OH)_{2.73}(H_2O)_{0.26}Cl_{0.01}]_{3.00}$$

($n = 7$), or ideally $(Fe,Al)_4(PO_4,SO_4)_3(OH,H_2O)_3$. As such, it would correspond to a ferric hydroxyphosphate crystallizing in an Fe-deficient, ordered $Fe_2(PO_4)O$-like structure, that is also related to a $Al_4(PO_4)_3(OH)_3$ prototype structure (monoclinic, *C*2/*c*; Iijaali et al., 1989). The latter possibly corresponds to "dehydrated vantasselite". The As experiment is also one of few where in addition to exchanged AAJ an additional phase bearing the particular element of interest was detected. It is the triclinic phase $Fe_7(AsO_4)_6$ (first synthesized by Weil, 2004, by chemical transport reactions at 400°C), with the following refined unit cell dimensions: $a = 6.616(4)$, $b = 8.059(7)$, $c = 9.600(7)$ Å; $= 105.89(7)$, $= 107.22(7)$, $= 101.77(7)°$.

SELENIUM EXPERIMENT

The Se experiment yielded the three following phases:

- a finely-crystalline, BSE-bright SeO-FeSK(P) phase with trace Cl, Si, Ti, Mg and Na, that corresponds to an Se-exchanged AAJ (Fig. 1C.);
- large (~40 μm on average), BSE-brighter SeO_2 crystals, in places in aggregates >100 μm in diameter, and
- an Al-dominant Se,Fe,K-rich sulphate, bearing traces of Si and Cl, found as a minor phase within the SeO_2 crystals.

These phases correspond to variable EDS spectra (Appendix Fig. SF25).

Two general types of Se-enriched AAJ were found (Appendix Table ST30). The average (GM) SeO_2 content is 8.83 wt.%. The Se-rich composition ($n = 4$, GM of 33.18 wt.% SeO_2) is

$$[(NH_4)_{0.47}K_{0.26}Na_{0.12}Ca_{0.11}Mg_{0.03}]_{0.99}(Fe_{1.73}Al_{1.22}Ti_{0.05})_{3.00}[(SeO_3)_{1.58}(SO_4)_{0.35}(PO_4)_{0.08}]_{2.00}[(OH)_{6.00}Cl_{0.08}]_{6.08}$$

(*T*-site normalized, with Si removed due to large excess negative charge). The single Se-richest analysis, with 44.86 wt.% SeO_2, recasts to

$$[(NH_4)_{0.60}K_{0.28}Na_{0.05}Mg_{0.05}Ca_{0.02}]_{1.00}(Fe_{2.26}Al_{0.70}Ti_{0.05})_{3.00}[(SeO_3)_{1.55}(SO_4)_{0.41}(PO_4)_{0.04}]_{2.00}[(OH)_{6.09}Cl_{0.02}]_{6.11}$$

(after *T*-site normalization, Si removed). This formula seems to truly represent the alunite-type structure due to the *X*-site content close to the ideal one and the related stoichiometric character of the compound. The ideal composition of the related HEM would thus be $(NH_4)Fe_3(SeO_3)_2(OH)_6$. The low-Se composition ($n = 6$, GM of 3.65 wt.% SeO_2), with 2.90 wt.% SeO_2 as the lowest content measured, is

$$[(NH_4)_{0.61}K_{0.28}Na_{0.06}Ca_{0.02}Mg_{0.03}]_{1.00}(Al_{1.81}Fe_{1.18}Ti_{0.02})_{3.01}[(SO_4)_{1.70}(SeO_3)_{0.23}(PO_4)_{0.07}]_{2.00}[(OH)_{5.96}Cl_{0.07}]_{6.03}.$$

Both low-Se and Se-enriched exchanged AAJ materials are relatively rich in Cl, though still bearing lower Cl amounts than the unsubstituted AAJ.

An important issue of the Se-for-S substitution is a crystallochemical separation of selenate(IV) (selenite) and sulphate(VI). They occur separately in minerals such as munakataite, $Pb_2Cu_2(SeO_3)(SO_4)(OH)_4$ and pauladamsite, $Cu_4(SeO_3)(SO_4)(OH)_4 \cdot 2H_2O$. This is even true for selenate(VI) as recorded by olsacherite, $Pb_2(SeO_4)(SO_4)$. Indeed, Campostrini and Gramaccioli (2001), who characterized secondary Se minerals from the Baccu Locci site (Sardinia, Italy), reported only tiny amounts of sulphur – listed as wt.% SO_2 and not SO_3 – in chalcomenite, $CuSeO_3 \cdot 2H_2O$ (up to 0.08 wt.%), and mandarinoite, $Fe_2(SeO_3)_3 \cdot 6H_2O$ (up to 0.10 wt.%). They also mention a Se-bearing variety of spangolite, ideally $Cu_6Al(SO_4)(OH)_{12}Cl.3H_2O$, with 2.87 wt.% SeO_3 (and not SeO_2) reported in the relevant table. However, according to

Goldschmidt, a diadochy threshold between ions is 15% (e.g., Misra, 2012). The ionic radii of the SO_4^{2-} and SeO_3^{2-} are 258 and 239 pm, respectively (Constantino et al., 2017). The difference is 7%, thus suggesting diadochy being possible in this system. The SeO_3^{2-} ion entering the *T*-sites is somewhat reminiscent of the CO_3^{2-} substitution in the apatite group – another guest-loving crystal-structure type – at the nominally phosphate- and/or silicate- + sulphate-dominant *T*-sites (Fleet and Liu, 2008). In an earlier paper (Fleet and Liu, 2009) they pinpoint the CO_3^{2-} anion as located "on the sloping faces of the substituted phosphate group". Such a phenomenon could, possibly, involve the SeO_3^{2-} - SO_4^{2-} system of the Se-substituted AAJ. Se-for-S substitution may be indicated via a relatively high r^2 value of 0.68 (negative trend). The SiO_2 *vs.* SO_3+SeO_2+P_2O_5 diagram does not show an obvious trend; if present, a negative trend is related to an r^2 of just 0.53. This seems to be, in part, in accordance with Si removal from the *T*-site in the above formulae. Trials of recasting the obtained analyses of the Se-exchanged AAJ into different stoichiometries (i.e., using different sums of cations in the factor) did not bring any conclusive results. The *T*-site content is shown in Appendix Figures SF26 and SF27. The first figure shows the dataset plotting in a relatively similar fashion as in the As experiment. The latter, oxide-based one, shows a possible additional trend of the compositional shift towards more siliceous/phosphatian end-members. The normality test and Kendall statistical results are shown in Appendix Tables ST31 and ST32, respectively.

LANTHANUM EXPERIMENT

Low and occasional enrichment of La in the AAJ necessitated use of the Sigma system to show La in the EDS spectra (Appendix Fig. SF28). The Ama reflections are, again, much stronger than the Amj ones. The latter, though evident, are diffuse. Still, they are not shoulder-like. Any additional, unascribed reflections, are at 3.33 (possibly from muscovite), 3.324 and 3.250 Å. The average La_2O_3 content is just 0.19 wt.%. The composition of the lanthanum-exchanged AAJ (Appendix Table ST33) is

$$[(NH_4)_{0.95}K_{0.04}Na_{0.02}Mg_{0.01}]_{1.00}(Al_{1.56}Fe_{1.44}Ti_{0.01})_{3.01}[(SO_4)_{1.74}(SiO_4)_{0.02}(PO_4)_{0.02}]_{1.78}[(OH)_{6.38}Cl_{0.05}]_{6.43}$$

(n = 11). It is thus more ammonian than the average AAJ base. After normalization to T = 2 apfu the formula is:

$$[(NH_4)_{0.95}K_{0.04}Na_{0.02}Mg_{0.01}]_{1.00}(Al_{1.56}Fe_{1.44}Ti_{0.01})_{3.01}[(SO_4)_{1.96}(SiO_4)_{0.02}(PO_4)_{0.02}]_{2.00}[(OH)_{5.93}Cl_{0.05}]_{5.98}.$$

Any lanthanum enrichment thus cannot be seen in such a crystallochemical compositional representation. The same is true for the jarosite-dominant normalized composition:

$$[(NH_4)_{0.92}K_{0.04}Na_{0.02}Mg_{0.01}Ca_{0.01}]_{1.00}(Fe_{1.61}Al_{1.39}Ti_{0.01})_{3.01}[(SO_4)_{1.93}(SiO_4)_{0.04}(PO_4)_{0.02}]_{1.99}[(OH)_{5.93}Cl_{0.05}]_{5.98}.$$

The alunite-dominant composition, also normalized, is:

$$[(NH_4)_{0.93}K_{0.05}Na_{0.02}]_{1.00}(Al_{1.70}Fe_{1.30}Ti_{0.01})_{3.01}[(SO_4)_{1.97}(PO_4)_{0.02}(SiO_4)_{0.01}]_{2.00}[(OH)_{5.95}Cl_{0.05}]_{6.00}.$$

Only a single analysis showed traces of La, corresponding to the formula

$$[(NH_4)_{0.92}K_{0.04}Na_{0.02}Ca_{0.01}\mathbf{La_{0.01}}]_{1.00}(Fe_{1.56}Al_{1.44}Ti_{0.01})_{2.01}[(SO_4)_{1.92}(SiO_4)_{0.05}(PO_4)_{0.02}]_{1.99}[(OH_{5.92}Cl_{0.05}]_{5.97}.$$

This then corresponds to the end-member composition $Amj_{48}Ama_{45}Jar_2Alu_2Naj_1Naa_1(Hua+Caj+Mgh+Mfh)_1$, where the content of La-dominant end-members is below 0.1%. Chlorine enrichment is, again, not observed. The *A*-site content is shown in Appendix Figure SF29. The strong ammonian character of the material can be seen. The normality test and Kendall statistical results are shown in Appendix Tables ST34 and ST35, respectively.

CERIUM EXPERIMENT

A typical Ce-exchanged AAJ occurs as very small (up to ca. 10 μm) elongated crystals among BSE-bright aggregates of a Ce-rich oxide. However, the presence of Ce can only barely be seen in the related EDS spectrum (Appendix Fig. SF30). The PXRD pattern of the AAJ only shows Ama reflections. The average Ce_2O_3 content (all Ce is assumed to be trivalent) is just 1.2 wt.%, and the element is only recorded in 4 of the 7 analyses. Unexpectedly, La was also observed (it may be derived from an impure Ce-chloride solution), with average La_2O_3 content of 0.35 wt.%, which is almost twice as large as in the La experiment. The whole-series composition (n = 7, *T*-site-normalized, Appendix Table ST36) is

$$[(NH_4)_{0.84}Na_{0.06}K_{0.06}\mathbf{Ce_{0.02}}La_{0.01}Ca_{0.01}]_{1.00}(Al_{1.87}Fe_{1.12}Ti_{0.01})_{3.01}[(SO_4)_{1.88}(SiO_4)_{0.09}(PO_4)_{0.06}]_{2.02}\{[(OH)_{5.76}Cl_{0.05}]_{5.81}(H_2O)_{0.19}\}.$$

This corresponds to an $Ama_{55}Amj_{31}Alu_4Jar_3Naj_3Naa_3(Mga+Caj+Mgj+Hua+\mathbf{Flc}+Fll+\mathbf{Ffc}+Ffl)_1$ end-member composition, where Flc is florencite-(Ce), Fll is florencite-(La), Ffc is "ferriflorencite-(Ce) HEM, and Ffl is "ferriflorencite-(La)" HEM. The jarosite-dominant composition, n = 2, is more cerian (and lanthanian):

$$[(NH_4)_{0.75}Na_{0.11}K_{0.07}\mathbf{Ce_{0.05}}La_{0.02}]_{1.00}(Fe_{1.94}Al_{1.06}Ti_{0.01})_{3.01}[(SO_4)_{1.92}(PO_4)_{0.09}(SiO_4)_{0.01}]_{2.02}[(OH)_{5.99}Cl_{0.04}]_{6.03},$$

or $Amj_{52}Ama_{28}Naj_8Jar_5Naa_4Alu_3(Caj+Mfh+Hua+Mgh+\mathbf{Ffc}+\mathbf{Flc}+Fll)_{<1}$ (Ti-dominant HEMs omitted). The alunite-dominant composition, n = 5, stoichiometrically normalized, is:

$$[(NH_4)_{0.87}K_{0.06}Na_{0.04}Mg_{0.01}\mathbf{Ce_{0.01}}Ca_{0.01}]_{1.00}(Al_{2.20}Fe_{0.80}Ti_{0.01})_{3.01}[(SO_4)_{1.84}(SiO_4)_{0.13}(PO_4)_{0.05}]_{2.02}\{[(OH)_{5.68}Cl_{0.05}]_{5.73}(H_2O)_{0.27}\},$$

or $Ama_{66}Amj_{24}Alu_4Naa_3Jar_2Naj_1(Hua+Mgh+Caj+Mfh+\mathbf{Ffc}+Flc)_{<1}$. Chlorine levels are identical to those in the La experiment and are twice as low as in the unsubstituted AAJ. The normality test and Kendall statistical results are shown in Appendix Tables ST37 and ST38, respectively.

PRASEODYMIUM EXPERIMENT

As opposed to both Ce and La, Pr was found to be relatively strongly sorbed to the AAJ studied. The EDS spectrum obtained (Appendix Fig. SF31) shows a siliceous, (Al,Fe)-rich Pr-bearing sulphate species that is also clearly enriched rich in Cl and P, with small admixtures of Ti and Ca, but practically devoid of other components (discluding N).

As in the Ce case, the PXRD pattern shows strong Ama reflections, while the Amj ones are barely recognizable. However,

it was possible to obtain the series composition (Appendix Table 39, n = 9, with an average of 3.00 wt.% Pr_2O_3):

$$[(NH_4)_{0.87}\mathbf{Pr_{0.11}}Ca_{0.02}]_{1.00}(Fe_{2.02}Al_{0.92}Ti_{0.07})_{3.01}[(SO_4)_{1.57}(PO_4)_{0.43}]_{2.00}[(OH)_{5.78}Cl_{0.13}]_{5.91}.$$

The formula shown corresponds to $Amj_{64}Ama_{29}\mathbf{Ffp_3}Caj_2\mathbf{Flp_1}Hua_1(Mgh+Mfh+Jar+Alu)_{<1}$, where Ffp is a "ferriflorencite-(Pr)" HEM and Flp is a "florencite-(Pr)" HEM. Silicon substitution at the *T*-sites does not seem to be necessary for surplus positive charge (from Pr^{3+}) balance, as suggested by a lacking trend in the SiO_2-SO_3 Pearson diagram (r^2 < 0.5). The Pr_2O_3-P_2O_5 diagram, by contrast, shows a positive trend, though not very evident (r^2 = 0.46). Substitution of Pr at the *A*-site is indicated by a clear positive trend (r^2 = 0.69) in the Pr_2O_3-$(NH_4)_2O$ diagram. Praseodymium thus follows typical REE behavior, that is, their occurrence at the *A*-site, e.g., in the florencite group. Praseodymium is quite clearly correlated with the $(NH_4)_2O$ (negative trend, r^2 = 0.69), but it also shows a positive correlation with both Al_2O_3 (r^2 = 0.51) and Fe_2O_3 (r^2 = 0.65). Due to lacking trends in any systems involving Ti, the Ti-dominant HEMs are omitted here. The praseodymium experiment is the second one after the indium experiment where chlorine was found in amounts larger than in the non-exchanged AAJ. The *A*-site content is shown in Appendix Figure SF32. The datapoints plot to a narrow area, thus confirming a relatively stable composition of the Pr-exchanged AAJ. The normality test and Kendall statistical results are shown in Appendix Tables ST40 and ST41, respectively.

TANTALUM EXPERIMENT

Among the species detected in thin section, there are:

- a BSE-bright, finely-crystalline TaO-MgAlSiPSFe (CaTiKClNa) phase, with individuals up to ca. 18 μm in diameter;
- a BSE-dark, finer-crystalline matrix of the phase above, comprising chaotic finely crystalline aggregates, with O, Ta, S, Al, and Fe as major elements, and smaller amounts of Mg, K, P, Cl and Na;
- a medium-BSE-bright SiAlTaSFeO-K(CaPClMg) phase intergrown with the first one;
- another phase forming chaotic aggregates, that seems to be a Ta-exchanged AAJ, with S, O, Al and Fe as major; Ta, Cl, P, K as subordinate; and Ti, Na and Ca as trace components; and
- larger, BSE-bright crystals, that seem to be a Mg-Ta-rich aluminosilicate with subordinate P, S, Al and Fe, and trace Na.

Variable EDS spectra of these phases were obtained (Appendix Fig. SF33).

The results of the EPMA data for the tantalum experiment are complex (Appendix Table ST 42) and most of the data does not suggest Ta entering the AAJ structure. The average content of Ta_2O_5 is very high, at 70.6 wt.%. One may consider Ta not fitting into the AAJ structure, with Ta existing as Ta_2O_5 (i.e., due to hydrolysis of the $TaCl_5$ used). As such, the results would rather come from a mixture of compounds. The average formula of the AAJ would then be

$$[(NH_4)_{0.70}Na_{0.18}Ca_{0.06}K_{0.04}Mg_{0.02}]_{1.00}(Fe_{2.42}Al_{0.32}Ti_{0.26})_{3.00}[(SO_4)_{1.55}(PO_4)_{0.32}(SiO_4)_{0.13}]_{2.00}\{[(OH)_{5.75}Cl_{0.01}]ó_{5.76}(H_2O)_{0.24}\}_{6.0}$$

(n = 7). Note the relatively low amount of H_2O molecules.

The first of the analyses listed differs from the others in terms of apfu(Ta) calculated based on B = 3. The related Ta-free formula of the AAJ would be

$$[(NH_4)_{0.49}Ca_{0.19}Na_{0.18}K_{0.10}Mg_{0.04}]_{1.00}(Fe_{1.61}Al_{1.11}Ti_{0.28})_{3.00}[(SO_4)_{0.96}(PO_4)_{0.74}(SiO_4)_{0.30}]_{2.00}[(OH)_{5.14}Cl_{0.03}]_{5.17}.$$

The remainder of the *X*-site may be attributed to water molecules or hydronium cations. However, the analysis may also be recalculated into a supposedly Ta-exchanged AAJ, with the related formula:

$$[(NH_4)_{0.49}Ca_{0.19}Na_{0.18}K_{0.10}Mg_{0.04}]_{1.00}(Fe_{1.38}Al_{0.95}Ta_{0.42}Ti_{0.24})_{2.99}[(SO_4)_{0.96}(PO_4)_{0.74}(SiO_4)_{0.30}]_{2.00}[(OH)_{5.91}Cl_{0.03}]_{5.94}.$$

This formula is very close to an ideal water-free alunitic stoichiometry, and this could be an argument for Ta entering the AAJ structure. This, however, must be confirmed via additional analytical techniques in the future. The normality test and Kendall statistical results are shown in the Appendix Tables ST43 and ST44, respectively.

STATISTICAL ANALYSIS

Result of the statistical analysis are juxtaposed in Table 1.

OTHER EXPERIMENTS

Many other experiments were run, for PXRD data but EPMA data are not yet available. They include baths with solutions of ammonium chloride, sodium (NaCl), calcium chloride, magnesium ($MgCl_2{\cdot}6H_2O$), aluminum ($Al_2(SO_4)_3{\cdot}H_2O$) scandium ($Sc_2(SO_4)_3{\cdot}5H_2O$), vanadium ($(NH_4)VO_3$ and K_3VO_4 for V(V), $(VO)SO_4{\cdot}5H_2O$ for V(IV) and $V_2(SO_4)_3{\cdot}nH_2O$ for V(III)), chromium ($CrCl_3{\cdot}6H_2O$ for Cr(III) and K_2CrO_4 for Cr(VI)), iron ($FeCl_3$), nickel ($NiSO_4{\cdot}7H_2O$), cobalt ($Co(NO3)_2{\cdot}6H_2O$), germanium ($Cs_2[GeCl_6]$), bromine (NH_4Br and CsBr), yttrium ($YCl_3{\cdot}6H_2O$), molybdenum (K_2MoO_4), ruthenium ($RuCl_3{\cdot}3H_2O$), palladium ($PdCl_2$), silver ($AgNO_3$), cadmium (CdI_2), tin(II) ($SnSO_4$), tin(IV) ($(NH_4)_2[SnCl_6]$), antimony (III) ($SbCl_3$), antimony(V) $[K[Sb(OH)_6]$, iodine (NH_4I), barium ($BaCl_2$), cerium(IV) ($Ce(SO_4)_2{\cdot}4H_2O$), neodymium ($NdCl_3{\cdot}6H_2O$), samarium ($Sm_2(SO_4)_3{\cdot}8H_2O$), dysprosium ($DyCl_3{\cdot}6H_2O$), europium ($EuCl_3{\cdot}6H_2O$), terbium ($TbCl_3{\cdot}6H_2O$), holmium ($HoCl_3{\cdot}6H_2O$), thulium ($TmCl_3{\cdot}6H_2O$), lutetium ($LuCl_3{\cdot}6H_2O$), tungsten ($Na_2WO_4{\cdot}2H_2O$), gold ($H[AuCl]_4$), lead ($Pb(NO_3)_2$) and bismuth ($Bi(NO_3)_3{\cdot}5H_2O$). Interaction of AAJ with V(III) and V(IV) solutions produced rich blackish-greenish-yellow sediments. The PXRD data of this treated material shows both AAJ reflections and a single, broad reflection centred around 10.5 Å. The reflection could fit both bokite, $Al_{1.3}(V^{5+},V^{4+})_8O_{20}{\cdot}7.4H_2O$, and kazakhstanite, $Fe_5V^{4+}{}_3V^{5+}{}_{21}O_{39}(OH)_9{\cdot}9H_2O$, but this identification must be treated with caution.–Their synthetic counterparts might have formed by the following exchange and redox reactions:

(1) $0.43(NH_4,K)Al_3(SO_4)_2(OH)_6 + 4V_2(SO4)_3 + 10O_2 \rightarrow Al_{1.3}(V^{5+},V^{4+})_8O_{20}{\cdot}7.4H_2O + 0.43(NH_4,K) + 12.86SO_4^{2-} + 2.58OH^-$

(2) $0.6(NH,K)Fe_3(SO_4)_2(OH)_6 + 24(VO)SO_4{\cdot}5H_2O \rightarrow Fe_5V^{4+}{}_3V^{5+}{}_{21}O_{39}(OH)_9{\cdot}9H_2O + 0.6(NH_4,K) + 25.2SO_4^{2-} + 105.6H_2O + 5.4H^+ + 7.5O_2$

Table 1

Juxtaposition of the results of the statistical analysis for the experimentally exchanged AAJ

Experiment	Strong correlation pairs[1]		Other correlations		Isolinear vectors[2]	Opposite vectors
	positive	negative	positive	negative		
$Li_2SO_4 \cdot H_2O$	KMg	AlFe	ClAl, ClP, KSi, MgSi, CaP; KTi, MgAl, MgTi, MgP, CaSi, CaS, AlP, AlS, SiTi	ClFe, KFe, MgFe, FeP, FeS, TiS	NaTi(Fe), AlKMg(S)	
KI	MgCa, FeS	KAl, SiNa	ClS, NaFe, NaTi, MgAl, CaAl, CaFe, FeTi	KS, ClSi, NaP, SiP, SiS	ClS	K-S, Ca-Na
Rb_2CO_3	NaS, KAl, ClNa	AlFe, ClFe	ClK, ClP, ClS, NaK, NaAl, KP, RbK, RbTi, KS, MgP, CaFe, CaSi, AlP	NaFe, KFe, FeS, MgS, FeP	PAlCl(Fe), KNa(Fe)	Rb-Ca, Rb-Ti
CsCl	ClAl, ClSi, ClS, NaSi, NaP, KFe, KCs, CsFe, CsSi, CsP, CaS, AlS, SiP	ClNa, NaAl, NaS, KTi, MgTi, FeTi, PS	ClTi, NaK, MgCs, KMg, KSi, KRb, KAl, CsCa, MgFe, CaAl, CaSi, FeSi, FeP	ClCs, ClFe, NaTi, CsTi, CsS, FeS	CsNaP, KRb, SiK, AlS	MgTi, ClFe, AlFe
$Sr(NO_3)_2$	ClAl, KAl, KSi, KTi, MgCa, SiTi, ClNa, ClK, ClCa, ClSi, NaAl, NaS, KMg, MgSi, AlSi, AlTi, SiP	ClSr, FeP, MgSr, NaSr, KSr, SrAl, SrSi	MgAl, MgP, CaSi, CaTi, MgP, AlP, TiP	KFe, MgFe, CaSr, SrTi, FeSi, FeTi	CaP(Fe), TiMg, KSi	SrNa
$ZrO(NO_3)_2 \cdot 2H_2O$	MgSi, ClCa, KMg, KSi, FeS, KTi	MgS, KFe, KS, FeSi	ClZr		KMgSi(S), CaCl(Fe), ZrP	
$CuSO_4 \cdot 5H_2O$	CuFe, CuP, FeP, AlS, ClCu, KSi	MgCu, MgS, ClK, CuSi	ClS, MgSi, MgP, CuTi, FeTi, TiP	ClMg, KCu, MgAl, MgTi, CuAl, AlFe, Al, FeS, PS	MgAl(TiFe)	PAl
$Ga(NO_3)_3 \cdot 9H_2O$	GaTi, FeP, FeS, PS, ClAl	ClGa, ClTi, KFe	KSi, FeGa, GaP, GaS, TiP, TiS	ClFe, ClP, ClS, KS, FeSi, SiP, SiS	TiGa, PFe	GaAl, GaCl, SSi, PFe
$InCl_3$	FeIn, AlS, FeTi, TiP, FeP, SiS	AlTi, AlS, TiS, KIn, CaS, AIe, AlIn, FeSi, FeS	KSi, KS, CaTi, AlSi	SiP, PS, ClK, ClCa, KCa, KFe, KTi, KP, CaAl, SiTi	TiFe(Al), InP(S), ClMg	
KH_2AsO_4	KMg, SiMg, AlMg, AsP, MgCl, FeP, café, SCl, KCl, CaAs, FeAs, AlCl, PTi	AsMg, MgTi, SFe, SAs, SP, KCa, KFe, KAs, KP, CaCl, FeAlFeCl, AsAl, AsCa, AlP, AlTi	SK, FeTi	ClP, ClTi, CaMg, MgP, NaMg		
K_2SeO_3		SSe, SeAl, SP, STi, KSe, FeSi, FeP, SeSi, SeMg, SiTi	SK, SeTi, SiMg, SAl, SSi, SMg, SCl, KAl, KCl, CaNa, CaP, CaTi, NaCa, NaCl, NaP, AlSi, AlMg, PTi	MgP, MgTi, SCa, KP, KTi, NaS, AlTi	SeTi(MgAl), NaCaP(KS)	
$LaCl_3 \cdot 7H_2O$		AlFe, NaFe, NaS, KFe, TiS	NaAl, NaLa, KAl, MgP, AlS, FeSi, NaK, KS, MgFe, AlLa	ClK, ClMg, ClCa, ClP, ClS, NaMg, NaTi, NaP, KSi, KP, MgLa, AlSi, AlTi, FeLa, FeS, LaTi		
$PrCl_3 \cdot 6H_2O$	FeP, PrS	ClPr, ClS	ClCa, AlP, AlS, FePr>AlPr, PrTi, PrP, SiTi	ClAl, ClFe, ClTi, CaAl, CaS, FeSi	AlP	PrCl, CaS
$TaCl_5$	CaFe, KFe, KCl, KTi, CaCl, FeCl, ClTi, CaSi	SFe, STi	KCa, KNa, KAl, KMg, CaMg, CaTi, FeSi, AlTi, SiMg, SiCl, SiTi, MgCl	SK, SSi, SCl, TaSi, TaMg		SCa, TaSi, TaCl, TaTi, TaFe, TaAl

[1] – t-values above/below ~0.70/–0.70, and p-values 0.05; [2] – elements represented by collinear but opposite vectors given in parentheses, while these with long(est) vectors are underlined

DISCUSSION

In this paper we have shown variations in the level of accommodation of various elements by the structure of a member of the ammonioalunite-ammoniojarosite solid solution of known initial composition. Although the physico-chemical conditions of our experiments, including their relative stability and high dissolved element concentrations, may not fully reproduce natural ones, the results gained might be useful in relation to some industrial processes.

Observation of not only major but also additional (including "shoulder"-type) reflection in diffractograms of some of the treated AAJ samples reflects the complex and somewhat chaotic interactions of the base AAJ materials with the particular solutions. Although trials of inputting more than four alunite-type structures in the *TOPAS* software were attempted, they always resulted in erroneous peak attributions by the Rietveld-refinement-type approach. As such, the refinements were reduced to a maximum of 4 phases, considering the best PDF database standards.

Microbially-mediated oxidative synthesis of jarosite-type compounds in a Li-rich medium does not produce any precipitate, as opposed to other group-1 elements and NH_4^+ (Ivarson et al., 1981). Lithium was not found also by Fairchild (1933) during trials of synthesis of various *A*-content jarosites from $Fe_2(SO_4)_3$ solutions. Similar observations concerned both Cs, Cu, and Au. According to Dutrizac and Jambor (1987), a Li-dominant jarosite does not exist. A maximum Li concentration of ~0.2 wt.% was measured by them in synthetic jarosite. They observed that its content is independent of the K_{aq} parameter. Kosova et al. (2020) note that although DFT calculations suggest the possible existence of a complete solid solution of $Na_{1-x}Li_xFe_3(SO_4)_2(OH)_6$, this mixed compound, formed during Li cycling in a cell, undergoes amorphization and decomposition. Nevertheless, their paper suggests Li intercalation in the synthetic natrojarosite studied. Interestingly, their formula for the Li-exchanged phase after ten cycles is given as $Na_{0.13}Li_{0.87}Fe_3(SO_4)_2(OH)_6$, which actually points to Li dominance. After the 30th cycle, however, $Li_2SO_4{\cdot}H_2O$ is the Li phase found, with reflections corresponding to the (20-1) and (113) planes becoming either very diffuse or completely diminished. Behaviour of halogens during precipitation of jarosite-type compounds was studied by Dutrizac and Chen (2009), who point to very minor iodide being incorporated due to rapid oxidation of the I^- ions to elemental iodine by the Fe^{3+} ions. All these observations would explain the likely lacking (Li) and lacking to very minor (I) substitution in the AAJ studied here.

To the best knowledge of the authors, a single work related to potential Mn sorption on the ASM seems to be that by Tam and Tran (1991). However, they found "alunite" precipitation from a Mn sulphate solution, corresponding to removal of exclusively the alunite-type elements from it. Very minor Mn enrichment of the AAJ in Mn was eventually confirmed by us, but this case needs further studies.

Gräfe et al. (2008) studied surface sorption of Cu and As on the ASM. Their work was, however, devoted to the precipitation of a few Cu arsenate species. No such species were observed during the current study, neither during the SEM-EDS nor PXRD measurements. Dijkhuis (2009) described precipitation of Cu- and Al-bearing synthetic jarosite, but did not report either the composition of the product or its unit-cell dimensions, only reporting the Cu contents in a neutral-leach calcine and the so-called Budel Leach Product of 0.29 and ~0.4 wt.%, respectively. Dutrizac (1984) pointed to Cu incorporation into jarosite being a function of hydrolysis of Cu^{2+}, $C(Fe^{3+})$, (i.e., the lower the $C(Fe^{3+})$ the higher the Cu^{2+} sorbed), and the occupancy of the *A*-site. In particular, K dominance was found to favor copper, among other impurities, to enter the structure. In turn, NH_4-dominant compositions seemed to disfavor this phenomenon. Dutrizac's (1984) jarosite had 2 wt.% Cu. According to him, Zn behavior is similar but Cu is incorporated preferentially over Zn. This author has also observed that at higher pH (~2) more Zn enters into synthetic natrojarosite (1 wt.%), with just 0.2% at the pH of 0.7. Arabyarmohammadi et al. (2016) studied the efficiency of Zn removal from alunite ore, but only via adsorption. They report a loading capacity of natural alunite of 3.92 mg/g (3920 ppm). The preferential Cu-over-Zn enrichment seems to be confirmed in our experiments. Still, the sorbed Cu levels are low, even though both P and Si – carriers of surplus negative charge needed to neutralize surplus positive Cu charge – are available in the material studied.

A mixed, non-stoichiometric iron-gallium-ammonium-rich ASM compound was synthesized by Kamoun et al. (1989). Their Ga-dominant material's chemistry can be expressed as $(NH_4)_{1.01}(Ga_{0\text{-}2.93}Fe_{2.72\text{-}0})_{2.74}(SO_4)_{1.99}[(OH)_{5.25}(H_2O)_{1.80}]$. A representative intermediate composition, corresponding to 5-mol Ga_{aq}, is $(NH_4)_{1.00}(Fe_{1.38}Ga_{1.35})_{2.73}(SO_4)_2[(OH)_{5.19}(H_2O)_{1.97}]$. Rudolph and Schmidt (2011) also studied synthetic Ga-alunites. They hydrothermally synthesized stoichiometric $AGa_3(SO_4)_2(OH)_6$ compounds, with *A* = Na, K, Rb, H_3O and NH_4. Their PXRD study shows that with increasing ionic radii of the *A*-site occupants the *c* unit-cell parameter is clearly lengthened, with just a minor impact on the *a* parameter. Their ammonian product, $(NH_4)Ga_{2.97}(SO_4)_{2.00}(OH)_{6.20}$, has the following unit-cell parameters: *a* = 7.162 Å, *c* = 17.751 Å. Although the *a* parameter of our Ga-exchanged AAJ is 0.61% larger, the *c* parameter is closest to that of the ammonian member of Rudolph's and Schmidt's (2011) suite (0.58% difference, compared to ~1% difference when compared with their Rb-Ga-alunite, 2.8% with the K-Ga one, 3.7% with the H_3O-Ga one, and 6.1% compared to the Na-Ga one). The *a* parameter of synthetic H_3O-Fe-ASM (hydroniumjarosite) equals 7.355 Å due to the longer Fe-O(3)H bond length. This could explain the 0.61% difference of our *a* parameter, due to the mixed Ga-Al-Fe character of our product. Rudolph and Schmidt (2011) observed a displacement of the (00*l*) but not the (*hk*0) reflections alongside the changing *A*-site content which mostly influences the *c* parameter (7% difference) as compared to ~0.4% difference in the *a* parameter. Kydon et al. (1968) attributed their synthetic hydrated Ga-ASM to two possible phases, $(H_3O)Ga_3(SO_4)_2(OH)_6$ or $Ga_3(SO_4)_2[(OH)_5(H_2O)]{\cdot}H_2O$. They suggest the H_3O^+ ion as charge-balancer due to the supposed invariable content of alkali metals in alunite which is now known not to be true. Their H_3O-Ga-alunite is also *R*-3*m*-structured, with *a* = 7.18 and *c* = 17.17 Å (a/c = 0.419). This ratio is larger than that of our precursor AAJ (0.399 for the Al-dominant, and 0.405 for the Fe-dominant composition), but is closer to that obtained for Al-rich Ga-exchanged AAJ (a/c = 0.408). Dutrizac and Chen (2000) analyzed the behaviour of gallium during precipitation of synthetic jarosite (material heated at 200°C). They reported the Fe-Ga solid solution as being nearly complete. They point to pH as an unimportant factor regarding the amount of Ga absorbed, although elevated pH slightly promotes Ga-over-Fe precipitation. They also point to similar Ga and In behavior. Their precipitate corresponding to the highest Ga_{aq} content includes, however, just 1.4 wt.% Ga. About 75% of the Ga_{aq} enters the precipitate. The element is uniformly distributed though the aggregates obtained. In a further experiment with higher Ga_{aq}, the precipitate has 39 wt.% Ga. Their synthetic $NaGa_3(SO_4)_2(OH)_6$ has the following major reflections: *d* = 3.056(100), *d* = 3.020(92), *d* = 4.996(78), *d* = 1.794(36), and *d* = 5.594(35). Ga substitution for Fe induces cell contraction, with the *a* parameter

getting shorter, and the *c* parameter getting longer. This observation is only partially in accordance to ours: although the parameter *c* of our jarositic Ga-exchanged AAJ gets, indeed, substantially larger, parameter *a* remains very similar to that in the precursor phase.

In a microbially-mediated oxidation of Fe^{3+} in a Rb-bearing medium, Ivarson et al. (1981) found 99% of Rb_{aq} reacted after 17 weeks to form a Rb-exchanged synthetic ASM (room-temperature conditions), with the chemical composition $[Rb_{0.86}(H_3O)_{0.14}]_{1.00}Fe_{2.92}[(SO_4)_{1.86}(PO_4)_{0.04}]_{1.90}(OH)_6$. Precipitation of Rb was said by them to be faster than in the NH_4 and Na case, but slower than in the K case. "Rubidium-jarosite" was also synthesized by Fairchild (1933), in his study of K-Cs separation. The product includes 9.5 wt.% Rb_2O as compared to 2.8 wt.% K_2O. The author stated that 5 g of K_2SO_4 may be removed from a solution bearing 2 mg of Cs_2SO_4 without incorporation of Cs in the precipitate. The latter statement would explain low level of the Cs incorporation in our AAJ. Still, the cause of the similar low-level absorption of Rb remains unknown.

According to Dutrizac and Jambor (1987), Cs-dominant jarosite is non-existent. They did, however, note >2 wt.% Cs in synthetic jarosite prepared at 97°C, with a lesser amount in natrojarosite and still lesser in Rb-dominant jarosite. For the Cs-richest composition, with 3.03 wt.% Cs, they reported the formula of $[K_{0.74}(H_3O)_{0.15}Cs_{0.11}]_{1.00}Fe_{2.58}(SO_4)_{2.00}(OH)_6$ which, however, is largely unbalanced, suggesting just 4.74 OH and the occurrence of as many as 1.26 H_2O molecules pfu. Their Na- and Rb-dominant jarosites bear just up to 0.04 apfu Cs and thus somewhat resemble the level of Cs enrichment in our study. Interestingly, the *a*/*c* ratios in our Rb- and Cs-exchanged AAJ are identical for both the Al- and Fe-dominant phases (0.4 for the Al-rich and 0.398 for the Fe-rich one, respectively).

We were unable to find any data on natural Sr-dominant analogues of huangite and walthierite, although such a compound was synthesized by Okada et al. (1987). May et al. (1963) reported up to 3 wt.% SrO in an ASM representative. Natural, type-locality walthierite bears just 0.02 wt.% SrO (Li et al., 1992). Hikov (2013), who studied element behavior in hydrothermally altered porphyry rocks of the Asarel deposit (Bulgaria), reports strong Sr affinity not only to (Sr-dominant) phosphate species of the svanbergite-woodhouseite solid solution, but also to a svanbergite-woodhouseite-alunite solid solution. The alunitic rocks studied by them contain 1590 ppm Sr (GM), along with 52 ppm Pb, 42 ppm Ce and 21 ppm La. These authors also listed separate values for a supposedly different rock suite, with average 1708 ppm Sr, 61 ppm Pb and 6.3 ppm Ga. Alunite of monoquartzites showed 3870 ppm Sr, 562 ppm Pb, 87 ppm Ce, 50 ppm Ga and 43 ppm La. Our Sr-exchanged AAJ is largely crystallographically different to the Sr-free precursor, with strongly elongated *a* and moderately reduced *c* (Al-dominant phase), and both moderately changed *a* and *c* (Fe-dominant one) parameters. Interestingly, the unit-cell parameters of Okada's phase, *a* = 6.9847 and *c* = 33.86 Å (*a*/*c* = 0.206), are completely incongruent to those calculated for our Sr-exchanged Al-rich AAJ (*a*/*c* = 0.418).

Although Zr is unknown to exist in the *B*-site in the alunite supergroup, the ionic radius of $^{VI}Zr^{4+}$ (0.60) is similar to that of $^{VI}Fe^{3+}$ (0.72). In particular, the crystal and ionic radii differ by 16 and 20%, respectively, being only slightly above the theoretical diadochy limit of 15% (Pauling, 1961). On the other hand, according to Kolitsch (2015), minor Zr may enter the *A*-site. This interferes with the existence of the Th-rich member of the ASM - eylettersite. On the other hand, the difference for the Zr-K system it is 35-36% depending on coordination, and for the Zr-NH_4^+ system it equals 51%. Even though the r^2 coefficients for the Zr-NH_4, Zr-K, and Zr-Na systems are very low (up to 0.15), alternative recasting of the analyses considering an *A*-site occurrence of Zr was conducted. The empirical formula for the Si-rich material would then be

$$[(NH_4)_{0.67}K_{0.14}Zr_{0.09}Na_{0.05}Mg_{0.03}Ca_{0.02}]_{1.00}(Al_{1.51}Fe_{0.23}Ti_{0.02})_{1.76}$$
$$[(SiO_4)_{1.27}(SO_4)_{0.71}(PO_4)_{0.02}]_{2.00}[(H_2O)_{5.94}Cl_{0.05}(OH)_{0.01}]_{6.00};$$

the *B*-site occupancy is far below the published deficiency, at just 59%. Recasting the composition without Si entering the *T*-site induces, in turn, high surplus *B*-site occupancy. However, for the moderately siliceous material, the empirical formula seems to represent the ASM stoichiometry requirements:

$$[(NH_4)_{0.76}Zr_{0.13}K_{0.08}Na_{0.01}Mg_{0.01}C_{a0.01}]_{1.00}(Al_{2.12}Fe_{0.65}Ti_{0.03})_{2.80}$$
$$[(SO_4)_{1.53}(SiO_4)_{0.45}(PO_4)_{0.02}]_{2.00}[(OH)_{4.84}(H_2O)_{1.10}Cl_{0.06}]_{6.00}.$$

In the Zr-rich material case, positioning Zr at the *A*-site and considering *T* = 2 gives a high surplus positive charge that would require 2.17 additional OH groups. The r^2 values for the Zr-Ca system are much higher, being 0.66 for the low- and moderate-Zr compositions, and 0.72 for the whole series (positive trends in both cases). Nevertheless, the amount of Ca in the *B*-site-Zr recasting version is low. Changes in the unit-cell parameters due to Zr incorporation resemble those found for the Sr-exchanged AAJ. Indeed, the *a*/*c* ratios for the Al- and Fe-dominant species are 0.401 and 0428, respectively.

Titanium, due to its position in the periodic table, is expected to follow the behaviour of Zr. Indeed, Ti is a frequent substituent at the *B*-site in various AAJ studied here. However, as opposed to Al and Fe, Ti-Zr correlation is described by a very low r^2 of 0.14. Much higher values were obtained for the Ga-Ti (0.87), In-Ti (0.86) and Ti-Se (0.70) systems (Figs. 3 and 5).

Arsenic enrichment in the ASM is a well-known phenomenon. However, the composition of the As-exchanged AAJ somewhat resembles that of the mineral pharmacosiderite, $KFe_4(AsO_4)_3(OH)_4 \cdot 6\text{-}7H_2O$. This species is much rarer in the environment than the ASM. Neither of the two As- or AsS-dominant HEMs, corresponding to arsenate-dominant "ammoniojarosite", seem to have been synthesized before. The same is true for their Al analogues. The only similar compound that we were able to locate a publication on is $(NH_4)[Fe(AsO_4)F]$ (Bazán et al., 2003). Meanwhile, there are numerous papers devoted to ammonium-free As-bearing ASM. Sunyer and Borrell (2013), for instance, conducted various synthesis experiments resulting in formation of analogues of arsenian natroalunite. Relatively protracted synthesis at 100–200°C gave the latter phase, probably associated with amorphous As species and an equivalent of mansfieldite, $AlAsO_4 \cdot 2H_2O$. Brief experiments, at 160–180°C, were lacking the latter species among the products, while two-hour experiments, at 160°C, had the ASM species, exclusively. Its highest As content was just 3.43 wt.%, with a 1.91 wt.% GM average. A much higher content of 14 wt.% As concerned synthetic H_3O-Ca- natroalunite formed in an experiment with Ca but without Na added. Interestingly, these authors noted a single occurrence of a synthetic analogue of natropharmacoalumite (the NaAl-analogue of pharmacosiderite). They also characterized an "arsenical-natroalunite" generated from industrial waste. A sample with a maximum content (~80%) of this species had 9.85 wt.% As, and maximum apfu(As) of 0.28. Hudson-Edwards (2019) reported typical levels of As incorporation in alunite, natroalunite, jarosite and schlossmacherite, at 3.6, 2.8–1.5, 1.6 and 0.03 wt.%, respectively. She pointed to the limiting factors of the As substitution being charge difference, *B*-site deficiency,

and substitution of H_2O molecules for the OH^- groups. She showed the *c* parameter increases in alunitic structures and both *c* and *a* parameters increase in jarositic structures due to As substitution. The jarosite case was also confirmed by Paktunc and Dutrizac (2003). We confirm similar changes, except the *c* parameter for the jarositic material, for which we observe a minor (0.23%) reduction when compared with the base AAJ. According to Paktunc and Dutrizac (2003) As substitution is mostly affected by Fe occupancy, as the Fe-O(OH) sites are adjacent to the *T*-sites; the limitation is said to be at the ~17 mol% level. Partial protonation of both the AsO_4^{3} and SO_4^{2} anions is suggested as the charge balancer. Pure samples (devoid of "scorodite") of the synthetic material of these authors show 0.68–5.34 wt.% As, corresponding to (after correction of the wrong OH contents reported in their Table 1, and disregarding the supposed though not confirmed anion protonation)

$$[K_{0.89}(H_3O)_{0.11}]_{1.00}Fe_{2.48}[(SO_4)_{1.85}(AsO_4)_{0.16}]_{2.01}[(OH)_{4.26}(H_2O)_{1.74}]_{6.00}.$$

Our samples did not seem to show the substitutional limitation noted, as both their initial and final composition was much more complex than the relatively simple NH_4-Fe-S(As)-O-H system. Also, the formation processes were different, i.e., mostly based on diffusion and/or recrystallization than simple solution crystallization.

Paktunc and Dutrizac (2003) described $NaFe_3(SO_4,SeO_4)_2(OH)_6$ as a complete solid solution. Se(VI)-dominant analogues of jarosite and natrojarosite were synthesized and characterized by Dutrizac et al. (1981). Their SeO_4^{2-} contents were found to be 51.06 and 50.33 wt.% in the Na- and K-dominant phases, respectively. Such compounds are expected during oxidative ore leaching in hydrometallurgy. However, in our case, we do not suspect oxidation of the solution-contained SeO_3^{2-} due to lacking or low Fe^{3+}_{aq}. Also, we observed many SeO^2 aggregates, in which the Se valency is also +4.

Dutrizac and Dou Mingmin (1993) reported a complete solid solution between synthetic natrojarosite and its In analogue. De-la-Cruz-Moreno et al. (2021) reported synthetic natrojarosite as a major component of a post-Zn-refining waste, with 86 ppm In, along with 1.1 wt.% Cu, 1.1 wt.% Mn, 1.4 wt.% Si and 8.8 wt.% Zn. Synthesis of $(NH_4)In_3(SO_4)_2(OH)_6$ was reported by Zhao et al. (2019). The $[In_3(SO_4)_2(OH)_6]$- layers of the compound are shown by them to cyclically exchange cations such as Pb^{2+}. The unit cell parameters of this material *a* = 7.6899 and *c* = 17.711 Å are different from ours (especially in terms of the parameter *a*) which is also reflected in the *a*/*c* ratios difference of 0.434 *versus* our 0.397. This discrepancy is due to both the mixed character of our In-exchanged AAJ's *B*-site content and its P enrichment.

Dutrizac (2004) could not synthesize – in 95–98°C conditions – end-member REE-jarosites and this would explain the low and somewhat individual substitution of Ce and La in our AAJ. The synthetic natrojarosite and jarosite precipitated incorporated <0.3 wt.% REE, with even lesser amounts in Pb-jarosite, and with higher pH and Fe_{aq} contents only slightly influencing this. The purely natrojarositic samples had up to 0.24 wt.% La, up to 1.06 (or 1.54 at higher pH) wt.% Ce, and up to 0.72 wt.% Pr. The maximum content of La in jarosite was 0.15 wt.%, and in Pb-jarosite just 0.05 wt.%. Neither this data nor the descending crystal ionic radii from La to Pr (e.g., Pauling, 1961) explain the preferential Pr substitution in our material. More studies are needed to confirm this behaviour to be, possibly, due to some characteristics of the reagents used. Following the ideal 0.75 apfu occupancy of Th^{4+} in eylettersite, $Th_{0.75}Al_3(PO_4)_2(OH)_6$, the ideal composition of a Ce(III)-dominant Al-rich sulphate HEM would be $Ce_{0.33}Al_3(SO_4)_2(OH)_6$, or $(Ce_{0.33}[]_{0.67})Al_3(SO_4)_2(OH)_6$. However, no data regarding the existence of such a HEM was found. The $Fe^{2+}/Fe(OH)_3$ boundary in a pH-Eh diagram (e.g., Nakada et al., 2013) is below, i.e., at lower Eh, than the Ce^{3+}/Ce^{4+} zone. Thus, it is not expected to have Ce^{3+} oxidized to Ce^{4+} in a Fe^{3+}-rich system, unless plentiful Mn(IV) is present. Inclusion of Ce(III) and not Ce(IV) in the AAJ also follows the known existence of alunite-structured species like florencite-(Ce).

CHLORIDE AND POTASSIUM FIXATION

According to a study of Dutrizac and Chen (2009), in synthetic jarosite precipitated under conditions typical of hydrometallurgical processes from halogen-bearing solutions, as much as 0.7 wt.% Cl or 1.1 wt.% Br is incorporated from >4M solutions. Importantly as regards the current study, these authors pointed to natro- and ammoniojarosite as phases much less readily absorbing these elements. They also reported that neither pH nor temperature greatly influence the process. Meanwhile, the Cl content of the AAJ products of our praseodymium experiment is even larger, in six of the nine analyses presented, and may reach 1.04 wt.%. Concentration of Cl greater than 0.7 wt.% was also found, in some cases, for the products of the Li, KI, Rb and Zr experiments, disregarding the base material. Metal-chloride bond length, that would correspond to the ease of the bond breakage, does not influence the amount of chloride sorbed by the AAJ, as it does not seem to correlate with the chloride available in the experimental solutions. The highest Cl contents concern the praseodymium and indium experiments, while the longest metal-chloride bonds were found for CsCl, $LaCl_3$ and $CeCl_3$ (The Materials Project, 2020).

The (calculated) concentration of ammonium in the treated AAJ is largely invariable, with the exception of Se- (especially the Se-rich variety) and Zr-exchanged (especially the siliceous variety) materials and the Sr-dominant AAJ. A completely different picture concerns potassium. The material of the Se-experiment (both Se-low and Se-rich varieties) is clearly enriched, and this is also true for the siliceous Zr-exchanged one (>0.25 apfu K, GM, for all three types). The As-exchanged materials and one of the Zr-exchanged AAJ follow, at around 0.15 apfu. Other AAJ are clearly depleted, with the lowest levels measured in the moderately In-rich AAJ, the strontian and rubidian ones.

COMPOSITIONAL CORRELATION PROBLEM

Simple diagrams with Pearson correlation factors are commonly used in geochemistry. However, many recent papers, by both statisticians and geologists, strongly suggest such statistics as irrelevant for correct data analysis and conclusions. In particular, derivation of r^2 from Pearson-type relations seems to be unreasonable from the mathematical point of view. Instead, these authors (e.g., Aitchison and Greenackle; , 2002; Egozcue et al., 2005; Filzmoser et al., 2010; Hron et al., 2013; Buccianti et al., 2014; Kynčlova et al., 2017) suggest data transformation (with a logratio procedure often suggested to be insufficient) and inclusion in a multidimensional statistical approach. For such reasons (i.e., total sum constraint) the Pearson-type correlation may just represent partial correlation, thus leading to false conclusions. This, however, does not clearly suggest high-r^2 trends not representing elemental relations close to the real ones, especially since different authors suggest different statistical approaches. Nevertheless, the elemental relations noted in this text should be treated with care.

SILICON PROBLEM

SiO_2-SO_3 diagrams for various AAJ samples usually show more or less evident trends. However, potential Si enrichment varies through the experiments, with the highest contents measured for the Zr-exchanged AAJ, followed by the Cs, Mn, Cu, Zn, Li and KI experiments. Elevated Si contents in the Sr- and In-low but not Sr- and In-high AAJ can, probably, be explained by a causal phenomenon. For the Li experiment, the negative trend has an r^2 of 0.68; Cu experiment – 0.94; KI experiment – 0.92; Zr experiment – 0.90 for the high-Si material but only 0.50 for the whole analytical series (thus likely confirming heterogeneous Zr fixation); Zn experiment – 0.77 (providing a single Si-rich analysis is included); Ce experiment – 0.52; and Rb experiment – 0.44. No trend, however, or non-evident ones were seen for other experiments, e.g., the La one. For the CsCl experiment the related r^2 is as low as 0.25. In the Sr experiment, r^2 < 0.1 was obtained for "typical" AAJ, i.e., with low to moderate Si content. In the Ga experiment, the r^2 was as low as 0.28 for the Ga-exchanged Si-low AAJ, 0.87 for four Si-rich (or very rich) analyses, and grew from 0.28 to 0.50 when the whole series was used. In the In experiment, only the high-Si series of the AAJ gave a negative correlation, with a very high r^2 of 0.92.

The ionic radii of the SO_4^{2-} and SiO_4^{4-} groups, both tetrahedral, are broadly similar. Known as isoelectric ortho-oxyanions, their corrected sum of covalent radii is 1.68 and 1.61 Å, respectively (Ptáček, 2016).This leads to SO_4-SiO_4 heterovalent diadochy being quite common among minerals, e.g., in the apatite supergroup (e.g., in ellestadites, Eakle and Rogers, 1914), the pyrometamorphic mineral flamite, $Ca_{8-x}(Na,K)_x(SiO_4)_{4-x}(PO_4)_x$, pyrometamorphic olivines and clinopyroxenes and other species or groups.

CONCLUSIONS

A long-term (one year) sorption experiment involving a natural ammoniojarosite-ammonioalunite solid solution gave analytical results indicate that:

- germanium (and silicon) are likely not the exclusive tetravalent elements capable of entering the AAJ structure; zirconium is another candidate, while its substitution, as well as the behavior of Ti(IV), Ta(V) and Sn(IV), need further studies;
- strontium, gallium, indium, and praseodymium were found substituted in relatively high amounts
- strontium was locally dominant, consistent with synthesis of the Sr analogue of huangite (Ca-dominant AAJ member) and walthierite (Ba-dominant);
- copper, rubidium, cesium, cerium and lanthanum, were also detected, in low amounts;
- substitution of manganese, iodine and zinc, seems possible, but to a very limited extent; the related phenomena need more studies;
- Ga-dominant compositions were found, as opposed to the case of In; however, both experiments led to formation of mixed Al-Fe-Ga and Al-Fe-In compounds;
- the highest changes in the particular unit-cell parameters of the base AAJ concern the *a* parameter of the alunitic Sr-dominant AAJ (+6.7%), Se-enriched AAJ (+5.9%) and Zr-enriched AAJ (+4.4%); elevated values obtained for La-, Cs-, and Rb-bearing AAJ are somewhat suspicious, or accidental, considering the very low amounts incorporated;
- the largest shifts of the *c* parameter of the jarositic AAJ were found for Zr (–4%), Pr (–3.8%), Sr (–3.6% and Ga (+3.5%);
- the use of a chloride-containing source did not cause elevated Cl substitution in the already Cl-bearing AAJ.

Acknowledgements. This work was financially supported by the statutory funds of the Ministry of Higher Education and Science for the Institute of Geological Sciences, Polish Academy of Sciences (for 2018, 2019, and 2020). We are thankful to L. Jeżak and P. Jokubauskas for help with details of the EPMA.

REFERENCES

Aitchison, J., Greenacre, M., 2002. Biplots of compositional data. Applied Statistics, **51**: c375–392; https://doi.org/10.1111/1467-9876.00275

Akar, T., Celik, S., Ari, A.G., Akar, S.T., 2013. Removal of Pb^{2+} ions from contaminated solutions by microbial composite: combined action of a soilborne fungus *Mucor plumbeus* an alunite matrix. Chemical Engineering Journal, **215–216**: 626–634; https://doi.org/10.1016/j.cej.2012.11.001

Arabyarmohammadi, H., Salarirad, M.M., Mohammadi, A., 2016. Characterization and utilization of alunite ore for adsorptive removal of zinc: batch and column study. Environmental Engineering and Management Journal, **15**: 2761–2770; https://doi.org/10.30638/eemj.2016.003

Asokan, P., Saxena, M., Asolekar, S.R., 2006. Jarosite characteristics and its utilisation potentials. Science of the Total Environment, **359**: 232–243; https://doi.org/10.1016/j.scitotenv.2005.04.024

Asta, M.P., Ayora, C., Román-Ross, G., Cama, J., Acero, P., Gault, A.G., Charnock, J.M., Bardelli, F., 2010. Natural attenuation of arsenic in the Tinto Santa Rosa acid stream (Iberian Pyritic Belt, SW Spain): The role of iron precipitates. Chemical Geology, **271**: 1–12; https://doi.org/10.1016/j.chemgeo.2009.12.005

Basciano, L.C., Peterson, R.C., 2007. The crystal structure of ammoniojarosite, $(NH_4)Fe_3(SO_4)_2(OH)_6$ and the crystal chemistry of the ammoniojarosite–hydroniumjarosite solid-solution series. Mineralogical Magazine, **71**: 427–441; https://doi.org/10.1180/minmag.2007.071.4.427

Bayliss, P., Kolitsch, U., Nickel, E.H., Pring, A., 2010. Alunite supergroup: recommended nomenclature. Mineralogical Magazine, **74**: 919–927; https://doi.org/10.1180/minmag.2010.074.5.919

Bazán, B., Mesa, J.L., Pizarro, J.L., Aguayo, A.T., Arriortua, M.I., Rojo, T., 2003. $Fe(AsO_4)$ a new iron(III) arsenate synthesized from thermal treatment of $(NH_4)[Fe(AsO_4)F]$. Chemical Communications (Cambridge), **7**: 622–623; https://doi.org/10.1039/b210998k

Brown, J.B., 1970. A chemical study of some synthetic potassium-hydronium jarosites. Canadian Mineralogist, **10**: 696–703.

Buccianti, A., Egozcue, J.J., Pawlowsky-Glahn, V., 2014. Variation diagrams to statistically model the behavior of geochemical

variables: Theory an applications. Journal of Hydrology, **519** (A): 988–998; https://doi.org/10.1016/j.hydrol.2014.08.028

Constantino, L.V., Quirino, J.N., Monteiro, A.M., Abrão, T., Parreira, P.S., Urbano, A., Santos, M.J., 2017. Sorption-desorption of selenite and selenite on Mg-Al layered double hydroxide in competition with nitrate, sulfate and phosphate. Chemosphere, **181**: 627–634; https://doi.org/10.1016/j.chemosphere.2017.04.071

De-la-Cruz-Moreno, J.E., Ceniceros-Gómez, A.E., Morton-Bermea, O., Hernandéz-Álvarez, E., 2021. Recovery of indium from jarosite residues of zinc refinery by a hydrometallurgical process. Hydrometallurgy, **203**, 105697; https://doi.org/10.1016/j.hydromet.2021.105697

Dijkhuis, R.J.E., 2009. The minimization of copper losses during iron and aluminium precipitation from zinc leach liquors. M.Sc. thesis, Technical University of Delft, The Netherlands; http://resolver.tudelft.nl/uuid:8b703039-58b3-4ec8-bae9-7714db515ed8

Drouet, C., Navrotsky, A., 2003. Synthesis, characterization, and thermochemistry of K-Na-H_3O jarosites. Geochimica et Cosmochimica Acta, **67**: 2063–2076; https://doi.org/10.1016/S0016-7-7037(02)01299-1

Drouet, C., Baron, D., Navrotsky, A., 2003. On the thermochemistry of the solid solution between jarosite and its chromate analog. American Mineralogist, **88**: 1949–1954; https://doi.org/10.2138/am-2003-11-1238

Drouet, C., Pass, K.L., Baron, D., Draucker, S., Navrotsky, A., 2004. Thermochemistry of jarosite-alunite and natrojarosite-natroalunite solid solutions. Geochimica et Cosmochimica Acta, **68**: 2197–2205; https://doi.org/10.1016/j.gca.2003.12.001

Dutrizac, J.E., 1984. The behaviour of impurities during jarosite precipitation. In: Hydrometallurgical Process Fundamentals (ed. R.G. Bautista, R.G.): 125–169. Springer, New York, USA; https://doi.org/10.1007/978-1-4899-2274-8_6

Dutrizac, J.E., 1991. The precipitation of lead jarosite from chloride media. Hydrometallurgy, **26**: 327–346; https://doi.org/10.1016/0304-386X(91)90008-A

Dutrizac, J.E., 2004. The behaviour of the rare earths during the precipitation of sodium, potassium and lead jarosites. Hydrometallurgy, **73**: 11–30; https://doi.org/10.1016/j.hydromet.2003.07.009

Dutrizac, J.E., Chen, T.T., 1981. The synthesis of mercury jarosite and the mercury concentration in jarosite-family minerals. Canadian Mineralogist, **19**: 559–569.

Dutrizac, J.E., Chen, T.T., 2000. The behaviour of gallium during jarosite precipitation. Canadian Metallurgical Quarterly, **39**: 1–14; https://doi.org/10.1179/cmq.2000.39.1.1

Dutrizac, J.E., Chen, T.T., 2004. Factors affecting the incorporation of cobalt and nickel in jarosite-type compounds. Canadian Metallurgical Quarterly, **43**: 305–319; https://doi.org/10.1016/j.hydromet.2003.07.009

Dutrizac, J.E., Chen, T.T., 2008. Behaviour of the alkaline earth elements (beryllium to radium) during the precipitation of jarosite-type compounds. Canadian Metallurgical Quarterly, **47**: 387–401; https://doi.org/10.1179/cmq.2008.47.4.387

Dutrizac, J.E., Chen T.T., 2009. The behavior of halides during the precipitation of jarosite-type compounds. World of Metallurgy – Erzmetall, **62**: 151–163.

Dutrizac, J.E, Jambor, J.L., 1987. Behaviour of cesium and lithium during the precipitation of jarosite-type compounds. Hydrometallurgy, **17**: 251–265; https://doi.org/10.1016/0304-386X(87)90056-9

Dutrizac, J.E., Jambor, J.L., 2000. Jarosites and Their Application in Hydrometallurgy. Reviews in Mineralogy and Geochemistry, **40**: 405–452; https://doi.org/10.2138/rmg.2000.40.8

Dutrizac, J.E., Kaiman, S., 1976. Synthesis and properties of jarosite-type compounds. Canadian Mineralogist, **14**: 151–158.

Dutrizac, J.E., Mingmin, D., 1993. The behaviour of indium during jarosite precipitation. In: World Zinc '93 (ed. I.G. Matthew): 365–372. Australasian Institute of Mining and Metallurgy, Parkville, Australia.

Dutrizac, J.E., Dinardo, O., Kaiman, S., 1981. Selenate analogues of jarosite-type compounds. Hydrometallurgy, **6**: 327–337; https://doi.org/10.1016/0304-386X(81)90049-9

Dutrizac, J.E., Hardy, D.J., Chen, T.T., 1996. The behaviour of cadmium during jarosite precipitation. Hydrometallurgy, **41**: 269–285; https://doi.org/10.1016/0304-386X(95)00062-L

Dutrizac, J.E., Chen, T.T., Beauchemin, S., 2005. The behaviour of thallium(III) during jarosite precipitation. Hydrometallurgy, **79**: 138–153; https://doi.org/10.1016/j.hydromet.2005.06.003

Eakle, A.S., Rogers, A.F., 1914. Wilkeite, a new mineral of the apatite group, and okenite, its alteration product, from southern California. American Journal of Sciences, 4th series, **37**: 262–267.

Egozcue, J.J., Pawlowsky-Glahn, V., 2005. Groups of parts and their balances in compositional data analysis. Mathematical Geology, **37**: 795–828; https://doi.org/10.1007/s11004-005-7381-9

Fairchild, J.G., 1933. Artificial jarosites – the separation of potassium from cesium. American Mineralogist, **18**: 543–547.

Figueiredo, M.-O., Pereira da Silva, T., 2011. The Positive Environmental Contribution of Jarosite by Retaining Lead in Acid Mine Drainage Areas. International Journal of Environmental Research and Public Health, **8**: 1575–1582; https://doi.org/10.3390/ijerph8051575

Filzmoser, P., Hron, K., Reimann, C., 2010. The bivariate statistical analysis of environmental (compositional) data. Science of the Total Environment, **19**: 4230–4238; https://doi.org/10.1016/j.scitotenv.2010.05.011

Fleet, M.E., Liu, X., 2008. Accommodation of the carbonate ion in fluorapatite synthesized at high pressure. American Mineralogist, **93**: 1460–1469; https://doi.org/10.2138/am.2008.2786

Fleet, M.E., Liu, X., 2009. Coupled substitution of type A and B carbonate in sodium-bearing apatite. Biomaterials, **28**: 916–926; https://doi.org/10.1016/j.1016/j.biomaterials.2006.11.003

Franzblau, R.E., Loick, N., Weisner, C.G., 2014. Investigating the effects of the Se solid phase substitution in jarosite minerals influenced by bacterial reductive dissolution. Minerals, **4**: 17–36; https://doi.org/10.3390/min40100017

Frost, R.L., Bahfenne, S., Čejka, J., Sejkora, J., Plášil, J., Palmer, S.J., Keefe, E.C., Nemec, I., 2011. Dussertite, $BaFe^{3+}{}_3(AsO_4)_2(OH)_5$ - a Raman spectroscopic study of a hydroxy-arsenate mineral. Journal of Raman Spectroscopy, **42**: 56–61; https://doi.org/10.1002/jrs.2612

Gräfe, M., Beattie, D.A., Smith, E., Skinner, W.M., Singh, B., 2008. Copper and arsenate co-sorption at the mineral–water interfaces of goethite and jarosite. Journal of Colloid and Interface Science, **322**: 399–413; https://doi.org/10.1016/j.jcis.2008.02.044

Grey, I.E., Mumme, W.G., Mills, S.J., Birch, W.D., Wilson, N.C., 2009. The crystal chemical role of Zn in alunite-type minerals: Structure refinements for kintoreite and zincian kintoreite. American Mineralogist, **94**: 676–683; https://doi.org/10.2138/am.2009.3083

Hage, J.L.T., Schuiling, R.D., 2000. Comparative column elution of jarosite waste and its autoclaved product – evidence for the immobilization of deleterious elements in jarosite. Minerals Engineering, **13**: 287–296; https://doi.org/10.1016/S0892-6875(00)00008-X

Hammer, O., Harper, D.AT., Ryan, P.D., 2001. PAST: paleontological statistics software package for education and data analysis. Palaeontologia Electronica, **4**: 1–9.

Hikov, A., 2013. Geochemistry of hydrothermally altered rocks from the Asarel porphyry copper deposit, Central Srednogorie. Geologia Balcanica, **42**: 3–28; https://doi.org/10.52321/GeolBalc.42.1-3.3

Hron, K., Filzmoser, P., Donevska, S., Fišerová, E., 2013. Covariance-based variable selection for compositional data. Mathematical Geosciences, **45**: 487–498; https://doi.org/10.1007/s11004-013-9450-9

Hudson-Edwards, K.A., 2019. Uptake and release of arsenic and antimony in alunite-jarosite and beudantite group minerals. American Mineralogist, **104**: 633–640; https://doi.org/10.2138/am-2019-6591

Hudson-Edwards, K.A., Wright, K., 2011. Computer simulations of the interactions of the (0 1 2) and (0 0 1) surfaces of jarosite with Al, Cd, Cu^{2+} and Zn. Geochimica et Cosmochimica Atca, **75**: 52–62; https://doi.org/10.1016/j.gca.2010.10.004

Iijaali, M., Malaman, M., Gleitzer, C., 1989. $Fe_4(PO_4)_3(OH)$. A ferric hydroxyphosphate with an ordered iron-deficient -$Fe_2(PO_4)O$ structure. European Journal of Solid State Inorganic Chemistry, **26**: 73–89.

Ivarson, K.C., Ross, G.J., Miles, N.M., 1981. Formation of rubidium jarosite during the microbiological oxidation of ferrous iron at room temperature. Canadian Mineralogist, **19**: 429–434.

Jambor, J.L., 1999. Nomenclature of the alunite supergroup. The Canadian Mineralogist, **37**: 1232–1341; https://doi.org/10.2113/gscanmin.38.5.1298

Jones, F., 2017. Crystallization of Jarosite with Variable Al^{3+} Content: The Transition to Alunite. Minerals, **7**; https://doi.org/10.3390/min7060090

Kamoun, F., Lorenz, M., Kempe, G., 1989. Contributions to the formation of oxidic iron(III) compounds in the presence of foreign cations. Journal of Materials Science, **24**: 726–730; https://doi.org/10.1007/BF01107466

Kaufman, E.A., Zeller, M., Norquist, A.J., 2010. A slow leak synthetic route to organically templated gallium sulfates. Crystal Growth and Design, **10**: 4656–4661; https://doi.org/10.1012/cg1009412

Kavak, D., 2008. Removal of boron from aqueous solutions by batch adsorption on calcined alunite using experimental design. Journal of Hazardous Materials, **163**: 308–314; https://doi.org/10.1016/j.hazmat.2008.06.093

Kim, H.-S., Park, J.-W., An, Y.-J., Bae, J.-S., Han, C., 2011. Activation of ground granulated blast furnace slag cement by calcined alunite. Materials Transactions, **52**: 210–218; https://doi.org/10.2320/matertrans.M2010350

Kolitsch, U., 2015. Crystal structures of the hydrothermally synthesized chromates $KSc_3(CrO_4)_2(OH)_6$, $KIn_3(CrO_4)_2(OH)_6$, $RbIn_3(CrO_4)_2(OH)_6$, and $AgIn_3(CrO_4)_2(OH)_6$: a contribution to the crystal chemistry of the alunite supergroup. The Canadian Mineralogist, **53**: 833–844; https://doi.org/10.3749/canmin.1400103

Kolitsch, U., Pring, A., 2001. Crystal chemistry of the crandallite, beudantite and alunite groups: a review and evaluation of the suitability as storage materials for toxic metals. Journal of Mineralogical and Petrological Sciences, **96**: 67–78; https://doi.org/10.2465/jmps.96.67

Kosova, N.V., Shindrov, A., Kabanov, A.A., 2020. Theoretical and experimental study of reversible intercalation of Li ions in the Jarosite $NaFe_3(SO_4)_2(OH)_6$ structure. Electrochimica Acta, **359**: 136950; https://doi.org/10.1016/j.electacta.2020.136950

Kydon, D.W., Pintar, M., Petch, H.E., 1968. NMR evidence of H_3O^+ ions in gallium sulfate. Journal of Chemical Physics, **48:** 5348–5351.

Kynčlová, P., Hron, K., Filzmoser, P., 2017. Correlation between compositional parts based on symmetrical balances. Mathematical Geosciences, **49**: 777–796; https://doi.org/10.1007/s11004-016-9669-3

Lehmann, E.L., 1975. Nonparametrics: Statistical Methods Based on Ranks. Holden-Day, San Francisco; ISBN978-0-387-35212-1.

Lengauer, C.L., Giester, G., Irran, E., 2013. $KCr_3(SO_4)_2(OH)_6$: Synthesis, characterization, powder diffraction data, and structure refinement by the Rietveld technique and a compilation of alunite-type compounds. Powder Diffraction, **9**: 265–271; https://doi.org/10.1017/S0885715600018984

Li, G., Peacor, D.R., Essene, E.J., Brosnahan, D.R., Beane, R.E., 1992. Walthierite, $Ba_{0.5}Al_3(SO_4)_2(OH)_6$, and huangite, $Ca_{0.5}Al_3(SO_4)_2(OH)_6$, two new minerals of the alunite group from the Coquimbo region, Chile. American Mineralogist, **77**: 1275–1284.

Liu, C., Ling, Z., Cao, F., Chen, J., 2017. Comparative Raman and visible near-infrared spectroscopic studies of jarosite endmember mixtures and solid solutions relevant to Mars. Journal of Raman Spectroscopy, **48**: 1676–1684; https://doi.org/10.1002/jrs.5286

Luddington, S., Bookstrom, A.A., Kamilli, R.J., Walker, B.M., Klein, D.P., 1995. Climax Mo deposits (Model 16). Summary of relevant geologic, geoenvironmental, and geophysical information. Chapter 10. In: Preliminary Compilation of Descriptive Geoenvironmental Mineral Deposit Modelsdu (ed. E.A. Bray): 70–74. Open-File Report 95-831, U.S. Department of the Interior, U.S. Geological Survey, USA; https://doi.org/10.1002/jrs.5286

May, I., Schnepfe, M.M., Naeser, C.R., 1963. Strontium Sorption Studies on Crandallite. Contributions to Geochemistry, Geological Survey Bulletin, **1114-C**: C1–C17; https://doi.org/10.3133/tei819

Mindat, 2022. www.mindat.org, data retrieved on 20.08.2022.

Misra, K.C., 2012. Ionic substitution in crystals. Chapter 3.3. In: Introduction to Geochemistry, Principles and Applications (ed. K.C. Misra). Wiley-Blackwell, Hoboken, New Jersey, USA; ISBN978-1-4443-5095-1

Murray, J., Kirschbaum, A., Dold, B., Guimaraes, E.M., Panunzio Miner, E.V., 2014. Jarosite *versus* soluble iron-sulfate formation and their role in acid mine drainage formation at the Pan de Azúcar MineTailings (Zn-Pb-Ag), NW Argentina. Minerals, **4**: 477–502; https://doi.org/10.3390/min4020477

Nakada, R., Takanashi, Y., Tanimizu, M., 2013. Isotopic and speciation study on cerium during its solid-water distribution with implication for Ce stable isotope as a paleo-redox proxy. Geochimica et Cosmochimica Acta, **103**: 49–62; https://doi.org/10.1016/j.gca.2012.10.045

Nheta, W., Makhata, M.E., 2013. Leaching of Nickel from a Jarosite Precipitate with Hydrochloric Acid. International Conference on Chemical and Environmental Engineering, April 15–16, Johannesburg, South Africa, (abstract book): 18–21.

Okada, K., Soga, H., Ossaka, J., Otsuka, N., 1987. Syntheses of minamiite type compounds, $M_{0.5}Al_3(SO_4)_2(OH)_6$ with M = Sr^{2+}, Pb^{2+} and Ba^{2+}. Neues Jahrbuch für Mineralogie – Monatshefte: 64–70; https://doi.org/10.1002/jrs.5286

Paktunc, D., Dutrizac, J.E., 2003. Characterization of arsenate-for-sulfate substitution in synthetic jarosite using X-Ray Diffraction and X-Ray Absorption Spectroscopy. The Canadian Mineralogist, **41**: 905–919; https://doi.org/10.2113/gscanmin.41.4.905

Parafiniuk, J., Kruszewski, Ł., 2010. Minerals of the ammonioalunite-ammoniojarosite series formed on a burning coal dump at Czerwionka, Upper Silesian Coal Basin, Poland. Mineralogical Magazine, **74**: 731–745; https://doi.org/10.1180/minmag.2010.074.4.731

Pauling, L., 1961. The nature of the chemical bond. Cornell University Press, Ithaca, New York, USA; http://abulafia.mt.ic.ac.uk/shannon (visited 22.12.2022).

Ptáček, P., 2016. Substituents and Dopants in the Structure of Apatite. Chapter 6. In: Apatites and their Synthetic Analogues - Synthesis, Structure, Properties and Applications Intechopen (ed. P. Ptáček): 289–334, Amazon.com; https://doi.org/10.5772/62213

Reyes, I.A., Mireles, I., Patińo, F., Pandiyan, T., Flores, M.U., Palacios, E.G., Gutiérrez, E.J., Reyes, M., 2016. A study on the dissolution rates of K-Cr(VI)-jarosites: kinetic analysis and implications. Geochemical Transactions, **17**; https://doi.org/10.1186/s12932-016-0035-7

Rudolph, W.W., Schmidt, P., 2011. Studies on synthetic galloalunites $AGa_3(SO_4)_2(OH)_6$: Synthesis, thermal analysis, and X-ray characterization. Thermochimica Acta, **521**: 112–120; https://doi.org/10.1016/j.tca.2011.04.013

Rytuba, J.J., John, D.A., Foster, A., Ludington, S.D., Kotlyar, B., 2003. Hydrothermal Enrichment of Gallium in Zones of Advanced Argillitic Alteration – Examples from the Paradise Peak and McDermitt Ore Deposits, Nevada. Chapter C. In: Contributions to Industrial-Minerals Research, Bulletin 2209-C (eds J.D. Bliss, P.R. Moyle and K.R. Long). U.S. Department of the Interior, U.S. Geological Survey.

Strawn, D., Doner, H., Zavarin, M., McHugo, S., 2002. Microscale investigation into the geochemistry of arsenic, selenium, and iron in soil developed in pyritic shale materials. Geoderma, **108**: 237–257; https://doi.org/10.1016/S0016-7061(02)00133-7

Sunyer i Borrell, A., 2013. Arsenic intertization through alunite-type phases: Application to copper pyrometallurgy. Ph.D. thesis, Universitat de Barcelona.

Tam, T.H., Tran, T., 1991. Kinetic study on the precipitation of alunite from manganese sulphate solutions. Hydrometallurgy, **27**: 85–97; https://doi.org/10.1016/0304-386X(91)90080-6

Teixeira, L.A., Tavares, L.Y., 1986. Precipitation of jarosite from manganese sulphate solutions. International Symposium on Iron Control in Hydrometallurgy, October 19–22, Toronto, Ontario, Canada, IV, chapter 21, p. 431, 24 pp.

The Materials Project, 2020. Materials Data on CsCl by Materials Project; (…) CeCl3; (…) LaCl3; USA;

https://doi.org/10.17188/1199031; 10.17188/1199061; 10.17188/1199330; 10.17188/1309795; https://www.osti.gov/dataexplorer/biblio/dataset/, retrieved on 22.08.2022.

Wang, L., Xue, N., Zhang, Y., Hu, P., 2021. Controlled hydrothermal precipitation of alunite and natroalunite in high-aluminium vanadium-bearing aqueous system. Minerals, .**11**: 892; https://doi.org/10.3390/min11080892

Weil, M., 2004. $Fe^{II}_3Fe^{III}_4(AsO_4)_6$, the first arsenate adopting the $Fe_7(PO_4)_6$ structure type. Acta Crystallographica Section E - Structure Reports, **60**: i139–i141; https://doi.org/10.1107/S1600536804026182

White, D.T., Gillaspie, J.D., 2013. Acid leaching of nickel laterites with jarosite precipitation. In: Ni-Co 2013 (eds. Battle, T., Moats, M., Cocalia, V., Oosterhof, H., Alam, S., Allanore, A., Jones, R., Stubina, N., Anderson, C., Wang, S.): 75–95. The Minerals, Metals and Materials Society, Springer, Cham, Switzerland; https://doi.org/10.1007/978-3-319-48147-0_4

Žáček, V., Škoda, R., Laufek, F., 2008. Mo-bearing jarosite from supergene zone of medieval Au-Ag deposit at Hůrky near Rakovník, Czech Republic (in Czech with English summary). Bulletin mineralogicko-petrologického Odděleni Národního Muzea v Praze, **16**: 190–193; ISSN 1211-0329

Zema, M., Callegari, A.M., Tarantino, S.C., Gasparini, E., Ghigna, P., 2012. Thermal expansion of alunite up to dehydroxylation and collapse of the crystal structure. Mineralogical Magazine, **76**: 613–623; https://doi.org/10.1180/minmag.2012.076.3.12

Zhang, H. (ed.), 2011. Building Materials in Civil Engineering. Woodhead Publishing Limited, Sawston, Cambridge, UK; ISBN 9781845699567.

Zhao, Y.-Y.S., McLennan, S.M., Schoonen, M.A.A., 2014. Behavior of bromide, chloride, and phosphate during low-temperature aqueous Fe(II) oxidation processes on Mars. Journal of Geophysical Research: Planets, **119**: 998–1002; https://doi.org/10.1002/2013JE004417

Zhao, R., Li, Y., Chan, C.K., 2016. Synthesis of jarosite and vanadium jarosite analogues using microwave hydrothermal reaction and evaluation of composition-dependent electrochemical properties. The Journal of Physical Chemist C, **120**: 9702–9712; https://doi.org/10.1021/acs.jpcc.6b03195

Zhao, Y., Hu, K., Wang, D., Zhang, S., Wang, P., Dong, W., Chen, H., Zhao, W., Huang, F., 2019. Synthesis, crystal structure and excellent selective Pb^{2+} ion adsorption of new layered compound $(NH_4)In_3(SO_4)_2(OH)_6$. European Journal of Inorganic Chemistry, **47**: 5000–5007; https://doi.org/10.1002/ejic.201901015

APPENDIX

Table ST1. PXRD reflection positions and unit cell parameters of the base and experimentally exchanged AAJ

	Ama[1]	Amj	Alu	Jar	Δ, Ama [%]	Δ, Amj [%]
	base (R_{wp}=12.59, GOF=1.67)[2]					
main reflections[3] [Å]	3.0168[4]	3.1006[4]				
a [Å]	7.0319(5)	7.078(1)		7.224(6)		
c [Å]	17.629(2)	17.517(6)		17.35(4)		
	Rb_2CO_3 (R_{wp}=5.10, GOF=1.58)[3]					
main reflections [Å]	3.0185	unclear				
a [Å]	7.244(9)	7.069(3)			3	-0.24
c [Å]	18.13(328)	17.76(1)			2.8	1.4
	CsCl (R_{wp}=6.02, GOF=1.71)					
main reflections [Å]	3.0168 (3.0174)	3.096?		3.1097?		
a [Å]	7.249(1)	7.068(3)			3.1	-0.27
c [Å]	18.13(28)	17.751(9)			2.8	(1.3)
	$Sr(NO_3)_2$ (R_{wp}=16.66, GOF=5.64)					
main reflections [Å]	2.967?		2.994, 3.017			
a [Å]	7.50(1)	7.191(5)		8.363(2)	6.7	1.5
c [Å]	17.93(20)	16.89(2)		16.8716(6)	1.7	-3.6
	$ZrCl_4$ (R_{wp}=4.09, GOF=1.33)					
main reflections [Å]	3.0178 (3.0184)	3.073?				
a [Å]	7.34(2)	7.194(4)	7.023(4)		4.4	1.5
c [Å]	18.03(47)	16.82(1)	17.44(2)		2.3	-4
	$MnSO_4 \cdot H_2O$ (R_{wp}=8.05, GOF=2.78)					
main reflections [Å]	3.0193 (3.0193)	3.065?	3.0249			
a [Å]	7.25(1)	7.070(2)			3.1	-0.16
c [Å]	18.00(7)	17.745(6)			2.1	1.5
	$CuSO_4 \cdot 5H_2O$ (R_{wp}=5.32, GOF=1.43)					
main reflections [Å]	3.0191		3.0065			
a [Å]	7.26(9)	7.076(3)			3.2	-0.16
c [Å]	18.13(24)	18.13(3)			2.8	1.5
	$Ga(NO_3)_3 \cdot 9H_2O$ (R_{wp}=7.29, GOF=3.01)					
main reflections [Å]	3.024 (3.0214)	3.0664 (3.0556)				
a [Å]	7.206(2)	7.084(2)			2.5	-0.04
c [Å]	17.648(4)	18.13(1)			0.11	3.5
	$InCl_3$ (R_{wp}=5.77, GOF=2.01)					
main reflections [Å]	3.0175 (3.0192)	3.0678	3.0218			
a [Å]	7.195(6)	7.051(3)		7.28(6)	2.3	-0.51
c [Å]	18.13(3)	17.686(9)		16.89(4)	2.8	0.97
	KH_2AsO_4 (R_{wp}=3.68, GOF=1.44)					
main reflections [Å]	3.0178	3.0609				
a [Å]	6.99(2)	7.272(3)			-0.6	2.6
c [Å]	18.121(1)	17.482(9)			2.7	-0.23
	K_2SeO_3 (R_{wp}=7.77, GOF=2.86)					
main reflections [Å]	3.0135	3.063		3.10		
a [Å]	7.45(1)	7.275(3)		7.280(6)	5.9	2.7
c [Å]	17.43(1)	17.566(8)		16.84(1)	-1.1	0.26
	$LaCl_3 \cdot 7H_2O$ (R_{wp}=6.31, GOF=1.95)					
main reflections [Å]	3.0195 (3.0195)	3.084?				
a [Å]	7.011(5)	7.063(3)			5.9	-0.34
c [Å]	17.45(18)	17.72(1)			-1	1.1
	$CeCl_3 \cdot 7H_2O$ (R_{wp}=4.74, GOF=1.46)					

main reflections [Å]	3.0219 (3.018)	3.0699?		
a [Å]	7.224(7)	7.060(3)	2.7	-0.38
c [Å]	18.00(24)	17.70(1)	2.1	1

Table ST1 - continuation

	$PrCl_3 \cdot 6H_2O$ (R_{wp}=5.76, GOF=1.50)			
main reflections [Å]	3.023 (3.0177)			
a [Å]	7.21(1)	7.087(4)	2.5	0
c [Å]	17.93(26)	16.86(2)	1.7	-3.8

[1] – Ama – ammonioalunite, Amj – ammoniojarosite, Alu – alunite (or a species with similar PXRD pattern, or a second alunitic phase), Jar – jarosite or hydroniumjarosite (or a second jarositic phase); [2] – refinement quality statistics: R_{wp} – residual weighted-pattern, GOF – goodness of fit (χ^2); [3] – reflection's barycentric position, reflections at *d*=4.974 and 5.216 Å are more intense in the base sample for ammonioalunite and ammoniojarosite, respectively

Table ST2. Results of chemical analyses of AAJ contacting with a solution of $Li_2SO_4 \cdot H_2O$

	1	2	3	4	5	6	7
				[wt.%]			
P_2O_5[1]	0.77	0.71	0.81	0.81	0.99	0.80	0.93
SO_3	34.29	35.02	36.02	39.75	34.45	35.81	34.52
SiO_2	9.25	4.96	6.75	2.52	9.76	10.73	5.44
TiO_2	0.49	0.19	0.18	0.16	0.86	0.19	0.17
Al_2O_3	38.71	26.67	44.57	51.36	48.99	42.05	31.11
Fe_2O_3	12.27	16.24	11.30	9.57	8.82	10.49	16.41
MgO	0.26	0.11	0.17	0.15	0.30	0.27	0.14
CaO	0.21	0.12	0.18	0.22	0.25	0.35	0.47
K_2O	1.18	0.91	1.13	0.94	1.29	1.31	0.89
Na_2O	0.54	0.42	0.46	0.45	0.55	0.43	0.40
Cl	0.49	0.49	0.66	0.83	0.84	0.56	0.57
Σ	98.47	85.82	102.23	106.76	107.11	102.99	91.03
H_2O[1]	14.17	10.82	18.19	23.23	18.70	14.12	13.30
$(NH_4)_2O$[2]	2.27	1.85	2.64	3.01	2.71	2.38	2.06
				apfu (mpfu), *B* = 3 basis (assuming all Si entering the *T*-site)			
P	0.04	0.04	0.03	0.03	0.04	0.04	0.05
S	1.41	1.81	1.33	1.32	1.20	1.40	1.59
Si	0.51	0.34	0.33	0.11	0.45	0.56	0.33
Ti	0.02	0.01	0.01	0.01	0.03	0.01	0.01
Al	2.50	2.16	2.58	2.68	2.69	2.59	2.24
Fe	0.50	0.84	0.42	0.32	0.31	0.41	0.76
Mg	0.02	0.01	0.01	0.01	0.02	0.02	0.01
Ca	0.01	0.01	0.01	0.01	0.01	0.02	0.03
K	0.08	0.08	0.07	0.05	0.08	0.09	0.07
Na	0.06	0.06	0.04	0.04	0.05	0.04	0.05
Cl	0.05	0.06	0.06	0.06	0.07	0.05	0.06
NH_4[3]	0.83	0.85	0.86	0.89	0.84	0.83	0.84
OH	5.17	4.96	5.96	6.86	5.86	4.92	5.43
				end members, [%]			
Ama[4]	69	61	74	79	75	71	63
Amj	14	24	12	9	9	11	21
Alu	7	6	6	5	7	8	5
Jar	1	2	1	1	1	1	2
Naa	5	4	4	3	4	4	4
Naj	1	2	1	<1	1	1	1
Hua	1	1	1	1	1	2	2
Caj	<1	<1	<1	<1	<1	<1	1
Mgh	2	1	1	1	2	2	1
Mfh	<1	<1	<1	<1	<1	<1	<1

[1] – Mn was measured but not detected (under the detection limit); [2] – below detection limit; [3] – exclusively OH-derived, backward-calculated from OH *mpfu* content assuming lacking H_3O^+ and H_2O molecules in the structure; [4] –backward-calculated from NH_4^+ *mpfu* content; 3 calculated by stoichiometry (filling the *A*-site to the occupancy of 1); [5] – by charge balance; [6] – Ama – ammoniojarosite (and hydroniumjarosite), Amj – ammonioalunite (and schlossmacherite), Alu – alunite, Jar – jarosite, Naa – natroalunite, Naj – natrojarosite, Hua – huangite, Caj – "calciojarosite" HEM, Mgh – "magnesiohuangite" HEM, Mgj – "magnesioferrihuangite" HEM

Table ST3. Results of chemical analyses of AAJ contacting with a solution of KI

	1	2	3	4	5	6	7	8	9
	[wt.%]								
P_2O_5[1]	0.36	0.53	0.42	0.50	0.51	0.62	0.33	0.48	0.44
SO_3	38.10	38.61	39.70	40.46	37.53	38.24	36.91	36.53	38.35
SiO_2	6.46	1.21	3.55	2.45	2.71	5.09	9.73	7.37	4.25
TiO_2	0.18	0.17	0.15	0.08	0.17	0.16	0.18	0.12	0.23
Al_2O_3	43.22	47.09	43.26	48.09	39.76	41.66	44.74	45.81	42.74
Fe_2O_3	14.51	14.26	14.30	14.63	13.93	13.64	13.72	12.84	15.39
MgO	0.13	0.11	0.07	0.12	0.09	0.11	0.10	0.19	0.13
CaO	0.11	0.11	0.08	0.12	0.07	0.09	0.04	0.18	0.17
K_2O	1.10	0.87	0.94	0.83	1.12	1.05	0.83	0.96	0.96
Na_2O	0.29	0.26	0.35	0.24	0.27	0.22	0.28	0.26	0.34
Cl	0.74	0.82	0.79	0.66	0.70	0.63	0.53	0.61	0.66
Σ	105.19	104.03	103.60	108.18	96.86	101.49	107.37	105.35	103.66
H_2O[2]	18.46	23.60	19.73	23.15	18.50	17.88	17.35	19.12	19.78
$(NH_4)_2O$[3]	2.75	3.03	2.78	3.11	2.54	2.67	2.89	2.86	2.76
apfu (mpfu), *B* = 3 basis (assuming all Si entering the *T*-site)									
P	0.01	0.02	0.02	0.02	0.02	0.03	0.01	0.02	0.02
S	1.39	1.31	1.45	1.35	1.47	1.45	1.32	1.29	1.39
Si	0.31	0.05	0.17	0.11	0.14	0.26	0.46	0.35	0.21
Ti	0.01	0.01	0.01		0.01	0.01	0.01		0.01
Al	2.47	2.51	2.48	2.51	2.45	2.48	2.51	2.54	2.44
Fe	0.53	0.49	0.52	0.49	0.55	0.52	0.49	0.46	0.56
Mg	0.01	0.01		0.01	0.01	0.01	0.01	0.01	0.01
Ca	0.01	0.01		0.01				0.01	0.01
K	0.07	0.05	0.06	0.05	0.07	0.07	0.05	0.06	0.06
Na	0.03	0.02	0.03	0.02	0.03	0.02	0.03	0.02	0.03
Cl	0.06	0.06	0.06	0.05	0.06	0.05	0.04	0.05	0.05
NH_4[4]	0.89	0.91	0.90	0.92	0.89	0.90	0.92	0.90	0.89
OH[5]	5.97	7.13	6.39	6.84	6.46	6.03	5.51	6.01	6.39
	end members [%]								
Ama[5]	73	77	74	77	72	74	77	76	72
Amj	16	15	16	15	16	16	15	14	17
Alu	6	4	5	4	6	6	4	5	5
Jar	1	1	1	1	1	1	1	1	1
Naa	2	2	3	2	2	2	2	2	3
Naj	1	<1	1	<1	1	<1	<1	<1	<1
Hua	1	<1	<1	1	<1	<1	<1	1	1
Caj	<1	<1	<1	<1	<1	<1	<1	<1	<1
Mgh	1	1	<1	1	1	1	1	1	1
Mfh	<1	<1	<1	<1	<1	<1	<1	<1	<1

[1] – Mn was measured but not detected (under the detection limit); [2] – exclusively OH-derived, backward-calculated from OH *mpfu* content assuming lacking H_3O^+ and H_2O molecules in the structure; [2] – backward-calculated from NH_4^+ *mpfu* content; [3] – calculated by stoichiometry (filling the *A* site to the occupancy of 1); [4] – by charge balance; [5] – Ama – ammoniojarosite (and hydroniumjarosite), Amj – ammonioalunite (and schlossmacherite), Alu – alunite, Jar – jarosite, Naa – natroalunite, Naj – natrojarosite, Hua – huangite, Caj – "calciojarosite" HEM, Mga – "magnesiohuangite" HEM, Mfh – "magnesioferrihuangite" HEM

Table ST4. Results of chemical analyses of AAJ contacting with a solution of Rb_2CO_3

	1	2	3	4	5	6	7	8	9	10	11	12
						[wt.%]						
P_2O_5[1]	0.54	0.58	0.63	0.59	0.46	0.53	0.48	0.58	0.59	0.57	0.44	0.63
SO_3	35.61	37.10	33.80	36.55	36.23	35.66	32.76	35.89	35.32	36.64	35.51	36.21
SiO_2	0.31	bdl	0.22	bdl	0.73	bdl	2.00	0.61	0.11	bdl	0.07	0.60
TiO_2	0.14	0.14	0.15	0.16	0.10	0.15	0.14	0.12	0.10	0.14	0.13	0.11
Al_2O_3	25.12	32.63	23.91	36.08	21.40	20.38	19.71	39.48	27.76	36.87	21.07	34.99
Fe_2O_3	25.44	20.63	29.31	20.53	27.13	28.36	29.30	19.49	26.17	20.52	27.95	20.04
MgO	0.32	0.41	0.62	0.34	0.28	0.50	0.53	0.52	0.58	0.45	0.28	0.42
CaO	0.14	0.23	0.25	0.22	0.21	0.21	0.24	0.19	0.18	0.13	0.16	0.16
Rb_2O	0.43	0.48	0.58	0.53	0.50	0.45	0.39	0.33	0.44	0.62	0.43	0.37
K_2O	0.36	0.42	0.46	0.62	0.41	0.36	0.33	0.65	0.40	0.78	0.29	0.47
Na_2O	0.23	0.26	0.19	0.36	0.25	0.22	0.20	0.25	0.22	0.32	0.18	0.25
Cl	0.54	0.73	0.53	0.78	0.51	0.49	0.45	0.71	0.55	0.68	0.47	0.70
Σ	89.25	93.62	90.68	96.74	88.22	87.34	86.59	98.82	89.43	97.72	86.98	94.99
H_2O[3]	15.99	18.42	17.24	20.51	14.06	14.54	13.98	21.95	18.02	20.99	14.76	19.39
$(NH_4)_2O$[4]	2.17	2.38	2.14	2.52	1.99	1.95	1.96	2.69	2.29	2.53	2.06	2.50
						apfu (mpfu), *B* = 3 basis (assuming all Si entering the *T*-site)						
P	0.03	0.03	0.03	0.03	0.03	0.03	0.03	0.02	0.03	0.02	0.02	0.03
S	1.64	1.54	1.51	1.42	1.78	1.77	1.62	1.32	1.51	1.40	1.74	1.45
Si	0.02		0.01		0.05		0.13	0.03	0.01			0.03
Ti	0.01	0.01	0.01	0.01	0.01	0.01	0.01	0.01	0.01	0.01	0.01	
Al	1.82	2.13	1.68	2.20	1.66	1.58	1.54	2.28	1.87	2.21	1.62	2.19
Fe	1.18	0.86	1.31	0.80	1.34	1.41	1.46	0.72	1.13	0.79	1.37	0.80
Mg	0.03	0.03	0.05	0.03	0.03	0.05	0.05	0.04	0.05	0.03	0.03	0.03
Ca	0.01	0.01	0.02	0.01	0.01	0.02	0.02	0.01	0.01	0.01	0.01	0.01
Rb	0.02	0.02	0.02	0.02	0.02	0.02	0.02	0.01	0.02	0.02	0.02	0.01
K	0.03	0.03	0.03	0.04	0.03	0.03	0.03	0.04	0.03	0.05	0.02	0.03
Na	0.03	0.03	0.02	0.04	0.03	0.03	0.03	0.02	0.02	0.03	0.02	0.03
Cl	0.06	0.07	0.05	0.07	0.06	0.05	0.05	0.06	0.05	0.06	0.05	0.06
NH_4[5]	0.89	0.88	0.85	0.87	0.87	0.86	0.86	0.88	0.87	0.86	0.90	0.89
OH[5]	6.55	6.81	6.85	7.07	6.15	6.40	6.17	7.17	6.87	7.12	6.42	6.88
						end members [%]						
Ama[6]	56	65	51	66	50	48	47	69	57	66	50	67
Amj	36	26	40	24	41	43	44	22	34	23	43	25
Alu	2	2	2	3	2	2	2	3	2	4	1	2
Jar	1	1	2	1	2	1	1	1	1	1	1	1
Naa	2	2	1	3	2	2	1	2	2	2	1	2
Naj	1	1	1	1	1	1	1	1	1	1	1	1
Rba	1	1	1	1	1	1	1	1	1	1	1	1
Rbj	1	1	1	1	1	1	1	<1	1	1	1	<1
Hua	<1	1	1	1	<1	<1	<1	<1	<1	<1	<1	<1
Caj	<1	<1	<1	<1	<1	<1	<1	<1	<1	<1	<1	<1
Mgh	1	1	2	1	1	1	1	2	2	1	1	1
Mfh	1	1	1	<1	1	1	1	1	1	1	1	1

[1] – Mn was measured but not detected (under the detection limit); [2] – below detection limit; [3] – exclusively OH-derived, backward-calculated from OH *mpfu* content assuming lacking H_3O^+ and H_2O molecules in the structure; [4] – backward-calculated from NH_4^+ *mpfu* content; 3 calculated by stoichiometry (filling the *A* site to the occupancy of 1); [5] – by charge balance; [6] – Ama – ammoniojarosite (and hydroniumjarosite), Amj – ammonioalunite (and schlossmacherite), Alu – alunite, Jar – jarosite, Naa – natroalunite, Naj – natrojarosite, Hua – huangite, Rba – "rubidioalunite" HEM, Rbj – "rubidiojarosite" HEM, Caj – "calciojarosite" HEM, Mgh – "magnesiohuangite" HEM, Mfh – "magnesioferrihuangite" HEM

Table ST5. Shapiro-Wilk (S-W) normality test results, rubidium experiment

	S-W	p-v
Cl	**0.90**	0.18
Na_2O	**0.95**	0.65
K_2O	**0.94**	0.56
Rb_2O	**0.99**	0.99
MgO	**0.93**	0.40
CaO	**0.94**	0.55
Al_2O_3	**0.90**	0.14
Fe_2O_3	0.84	**0.02**
SiO_2	**0.97**	0.91
TiO_2	**0.88**	0.10
P_2O_5	**0.90**	0.14
SO_3	0.76	**0.004**

p-v – the *p*-values; meaningful values are given in bold

Table ST6. Element correlation based on Kendall's τ coefficients and uncorrected ρ-values (given in the parentheses), rubidium experiment

	Cl	Na_2O	K_2O	Rb_2O	MgO	CaO	Al_2O_3	Fe_2O_3	SiO_2	TiO_2	P_2O_5	SO_3
Cl		**0.66 (0.003)**	**0.58 (0.008)**	0.15 (0.49)	-0.08 (0.73)	-0.06 (0.78)	**0.78 (0.0004)**	**-0.68 (0.002)**	-0.04 (0.90)	0.08 (0.73)	**0.57 (0.01)**	**0.54 (0.02)**
Na_2O	**0.66 (0.003)**		**0.62 (0.005)**	0.18 (0.40)	-0.23 (0.30)	-0.15 (0.48)	**0.56 (0.01)**	**-0.58 (0.008)**	**0.40** (0.17)	0.20 (0.36)	0.29 (0.20)	**0.72 (0001)**
K_2O	**0.58 (0.008)**	**0.62 (0.005)**		**0.31** (0.16)	0.17 (0.45)	-0.06 (0.78)	**0.75 (0.0007)**	**-0.52 (0.02)**	0.21 (0.46)	0.17 (0.44)	**0.49 (0.03)**	**0.39** (0.07)
Rb_2O	0.15 (0.49)	0.18 (0.40)	**0.31** (0.16)		-0.02 (0.94)	0.18 (0.40)	0.11 (0.63)	0.14 (0.52)	-0.25 (0.38)	**0.36** (0.11)	0.13 (0.57)	0.29 (0.19)
MgO	-0.08 (0.73)	-0.23 (0.30)	0.17 (0.45)	-0.02 (0.94)		0.29 (0.19)	0.09 (0.68)	0.06 (0.78)	0.07 (0.80)	0.06 (0.78)	**0.36** (0.10)	**-0.43** (0.05)
CaO	-0.06 (0.78)	-0.15 (0.48)	-0.06 (0.78)	0.18 (0.40)	0.29 (0.19)		-0.26 (0.24)	**0.36** (0.10)	**0.40** (0.17)	0.14 (0.53)	0.16 (0.47)	-0.21 (0.33)
Al_2O_3	**0.78 (0.0004)**	**0.56 (0.01)**	**0.75 (0.0007)**	0.11 (0.63)	0.09 (0.68)	-0.26 (0.24)		**-0.78 (0.0004)**	0 (1)	0 (1)	**0.43** (0.05)	**0.46 (0.04)**
Fe_2O_3	**-0.68 (0.002)**	**-0.58 (0.008)**	**-0.52 (0.02)**	0.14 (0.52)	0.07 (0.78)	**0.36** (0.10)	**-0.78 (0.0004)**		-0.11 (0.71)	0.10 (0.67)	**-0.37** (0.09)	**-0.53 (0.02)**
SiO_2	-0.04 (0.90)	0.40 (0.17)	0.21 (0.46)	-0.25 (0.38)	0.07 (0.80)	**0.40** (0.17)	0 (1)	-0.11 (0.71)		-0.11 (0.71)	-0.07 (0.80)	-0.09 (0.76)
TiO_2	0.08 (0.73)	0.20 (0.36)	0.17 (0.44)	**0.36** (0.11)	0.06 (0.78)	0.14 (0.53)	0 (1)	0.10 (0.67)	-0.11 (0.71)		0.18 (0.43)	0.29 (0.19)
P_2O_5	**0.57 (0.01)**	0.29 (0.20)	**0.49 (0.03)**	0.13 (0.57)	**0.36** (0.10)	0.16 (0.47)	**0.43** (0.05)	**-0.37** (0.09)	-0.07 (0.80)	0.18 (0.43)		0.07 (0.74)
SO_3	**0.53 (0.02)**	**0.72 (0.001)**	**0.39** (0.07)	0.29 (0.20)	**-0.43** (0.05)	-0.21 (0.33)	**0.46 (0.04)**	**-0.53 (0.02)**	-0.09 (0.76)	0.29 (0.19)	0.07 (0.74)	

Strong correlations are given in bold

Table ST7. Results of chemical analyses of AAJ contacting with a solution of CsCl

	1	2	3	4	5	6	7	8
				wt.%				
P_2O_5[1]	0.54	0.52	0.62	0.83	0.78	0.91	0.83	0.94
SO_3	38.69	37.33	36.53	31.30	29.27	25.91	26.41	28.61
SiO_2	4.74	6.11	4.38	11.72	9.87	11.62	11.23	16.47
TiO_2	0.16	0.25	0.15	0.12	0.09	0.23	0.12	0.09
Al_2O_3	47.24	45.25	44.66	16.65	14.33	11.66	13.46	17.44
Fe_2O_3	11.73	10.74	9.26	27.22	28.54	25.82	26.85	27.90
MgO	0.10	0.12	0.16	0.13	0.17	0.12	0.14	0.17
CaO	0.15	bdl[2]	bdl	0.20	0.10	0.13	0.09	0.30
Cs_2O	0.24	0.28	0.27	0.97	0.90	0.88	0.83	1.07
Rb_2O	bdl	bdl	bdl	0.28	0.32	0.28	0.30	0.31
K_2O	0.61	0.90	0.70	1.04	1.23	0.83	0.98	1.16
Na_2O	0.15	0.24	0.25	0.31	0.31	0.35	0.35	0.39
Cl	0.45	0.47	0.45	0.37	0.36	0.34	0.36	0.35
Σ	104.80	102.20	97.43	91.12	86.26	79.08	81.96	95.22
H_2O[3]	20.49	18.46	18.70	5.68	6.38	3.51	5.04	4.14
$(NH_4)_2O$[4]	3.01	2.80	2.73	1.57	1.46	1.28	1.39	1.56
apfu (mpfu), B=3 basis (assuming all Si entering the T site)								
P	0.02	0.02	0.03	0.05	0.05	0.07	0.06	0.06
S	1.35	1.36	1.38	1.75	1.71	1.75	1.64	1.55
Si	0.22	0.30	0.22	0.87	0.77	1.05	0.93	1.19
Ti	0.01	0.01	0.01	0.01	0.01	0.02	0.01	
Al	2.58	2.60	2.64	1.46	1.32	1.24	1.32	1.48
Fe	0.41	0.39	0.35	1.53	1.68	1.75	1.68	1.51
Mg	0.01	0.01	0.01	0.01	0.02	0.02	0.02	0.02
Ca	0.01			0.02	0.01	0.01	0.01	0.02
Cs		0.01	0.01	0.03	0.03	0.03	0.03	0.03
Rb				0.01	0.02	0.02	0.02	0.01
K	0.04	0.06	0.04	0.10	0.12	0.10	0.10	0.11
Na	0.01	0.02	0.02	0.04	0.05	0.06	0.06	0.05
Cl	0.04	0.04	0.04	0.05	0.05	0.05	0.05	0.04
NH_4[5]	0.93	0.91	0.91	0.78	0.76	0.77	0.77	0.75
OH[5]	6.34	6.00	6.26	2.83	3.32	2.10	2.79	1.99
				end members, %				
Ama[6]	80	79	81	39	34	33	35	38
Amj	13	12	11	41	44	46	44	39
Alu	3	5	4	5	6	4	5	5
Jar	1	1	1	5	7	6	6	6
Naa	1	2	2	2	2	3	3	3
Naj	<1	<1	<1	2	3	4	3	3
Csa	0.4	0.5	0.5	2	1	1	1	2
Csj	0.1	0.1	0.1	2	2	2	2	2
Rba				1	1	1	1	1
Rbj				1	1	1	1	1
Hua	1			<1	<1	<1	<1	1
Caj	<1							
Mgh	1	1	1	<1	1	<1	<1	1
Mfh	<1	<1	<1	<1	1	1	1	1

[1] – Mn was measured but not detected (under the detection limit); Rb was detected as an impurity; [2] – below detection limit; [3] – exclusively OH-derived, backward-calculated from OH *mpfu* content assuming lacking H_3O^+ and H_2O molecules in the structure; [4] – backward-calculated from NH_4^+ *mpfu* content; 3 calculated by stoichiometry (filling the *A* site to the occupancy of 1); [5] – by charge balance; [6] – Ama – ammoniojarosite (and hydroniumjarosite), Amj – ammonioalunite (and schlossmacherite), Alu – alunite, Jar – jarosite, Naa – natroalunite, Naj – natrojarosite, Hua – huangite, Csa – “caesioalunite” HEM, Csj – “caesiojarosite” HEM, Rba – “rubidiolunite” HEM, Rbj – “rubidiojarosite” HEM, Caj – “calciojarosite” HEM, Mgh – “magnesiohuangite” HEM, Mfh – “magnesioferrihuangite” HEM

Table ST8. Shapiro-Wilk (S-W) normality test results, caesium experiment

	S-W	p-v
Cl	**0.83**	**0.05**
Na_2O	**0.89**	0.21
K_2O	**0.97**	0.86
Rb_2O	**0.90**	0.42
Cs_2O	0.76	**0.01**
MgO	**0.95**	0.72
CaO	**0.94**	0.66
Al_2O_3	0.80	**0.03**
Fe_2O_3	0.74	**0.006**
SiO_2	**0.89**	0.24
TiO_2	**0.92**	0.44
P_2O_5	**0.88**	0.19
SO_3	**0.88**	0.21

p-v – the *p*-values; meaningful values are given in bold

Table ST9. Element correlation based on Kendall's τ coefficients and uncorrected ρ-values (given in the parentheses), caesium experiment

	Cl	Na_2O	K_2O	Rb_2O	Cs_2O	MgO	CaO	Al_2O_3	Fe_2O_3	SiO_2	TiO_2	P_2O_5	SO_3
Cl		**-0.77 (0.008)**	**-0.30** (0.30)	0 (1)	**-0.44** (0.12)	**-0.30** (0.30)	0 (1)	**0.64 (0.03)**	**-0.44** (0.12)	**-0.57 (005)**	**0.42** (0.15)	**-0.79 (0.006)**	**0.82 (0.005)**
Na_2O	**-0.77 (0.008)**		**0.44** (0.12)	0.12 (0.77)	**0.59 (0.04)**	**0.44** (0.12)	0.07 (0.84)	**-0.64 (0.03)**	**0.37** (0.20)	**0.72 (0.01)**	**-0.42** (0.15)	**0.87 (0.002)**	**-0.82 (0.005)**
K_2O	**-0.30** (0.30)	**0.44** (0.12)		**0.74** (0.07)	**0.71 (0.01)**	**0.57 (0.05)**	0.07 (0.85)	**-0.33** (0.26)	**0.79 (0.006)**	**0.47** (0.10)	**-0.62 (0.03)**	**0.33** (0.26)	-0.29 (0.32)
Rb_2O	0 (1)	0.12 (0.77)	**0.74** (0.07)		**0.32** (0.44)	**0.95 (0.02)**	0.11 (0.80)	**0.53** (0.20)	**0.74** (0.07)	-0.22 (0.59)	**-0.89 (0.03)**	-0.22 (0.59)	**0.32** (0.44)
Cs_2O	**-0.44** (0.12)	**0.59 (0.04)**	**0.71 (0.01)**	**0.32** (0.44)		**0.43** (0.14)	**0.47** (0.19)	**-0.33** (0.26)	**0.64 (0.03)**	**0.76 (0.008)**	**-0.47** (0.10)	**0.62 (0.03)**	**-0.43** (0.14)
MgO	**-0.30** (0.30)	**0.44** (0.12)	**0.57 (0.05)**	**0.95 (0.02)**	**0.43** (0.14)		-0.07 (0.85)	-0.25 (0.38)	0.50 (0.08	0.18 (0.53)	**-0.69 (0.02)**	0.25 (0.38)	-0.29 (0.32)
CaO	0 (1)	0.07 (0.84)	0.07 (0.85)	0.11 (0.80)	**0.47** (0.19)	-0.07 (0.85)		**0.47** (0.19)	0.07 (0.85)	**0.41** (0.24)	-0.14 (0.70)	0.28 (0.44)	0.20 (0.57)
Al_2O_3	**0.64 (0.03)**	**-0.64 (0.03)**	**-0.33** (0.26)	**0.53** (0.20)	**-0.33** (0.26)	-0.25 (0.38)	**0.47** (0.19)		-0.25 (0.38)	**-0.44** (0.12)	0.22 (0.44)	**-0.52** (0.07)	**0.84 (0.004)**
Fe_2O_3	**-0.44** (0.12)	**0.37** (0.20)	**0.79 (0.006)**	**0.74** (0.07)	**0.64 (0.03)**	**0.50** (0.08)	0.07 (0.85)	-0.25 (038)		**0.55** (0.06)	**-0.69 (0.02)**	**0.40** (0.17)	-0.21 (0.46)
SiO_2	**-0.57 (0.05)**	**0.71 (0.01)**	**0.47** (0.10)	-0.22 (0.59)	**0.76 (0.008)**	0.18 (0.53)	**0.41** (0.24)	**-0.44** (0.12)	**0.55** (0.06)		-0.22 (0.44)	**0.74 (0.01)**	**-0.55** (0.06)
TiO_2	**0.42** (0.15)	**-0.42** (0.15)	**-0.62 (0.03)**	**-0.89 (0.03)**	**-0.47** (0.10)	**-0.69 (0.02)**	-0.14 (0.70)	0.22 (0.44)	**-0.69 (0.02)**	-0.22 (0.44)		**-0.41** (0.16)	0.25 (0.38)
P_2O_5	**-0.79 (0.006)**	**0.87 (0.003)**	**0.33** (0.26)	-0.22 (0.59)	**0.62 (0.03)**	0.25 (0.38)	0.28 (0.44)	**-0.52** (0.07)	**0.40** (0.17)	**0.74 (0.01)**	**-0.41** (0.16)		**-0.69 (0.02)**
SO_3	**0.82 (0.005)**	**-0.82 (0.005)**	-0.29 (0.32)	**0.32** (0.44)	**-0.43** (0.14)	-0.29 (0.32)	0.20 (0.57)	**0.84 (0.004)**	-0.21 (0.46)	**-0.55** (0.06)	0.25 (0.38)	**-0.69 (0.02)**	

Strong correlations are given in bold

Table ST10. Results of chemical analyses of AAJ contacting with a solution of $Sr(NO_3)_2$

	1	2	3	4	5	6	7[1]	8	9	10	11
	Sr-dominant	medium Sr-rich						Sr-low			
	[wt.%]										
P_2O_5[1]	0.38	0.37	0.28	0.33	0.44	0.48	0.47	0.37	0.39	0.84	0.71
SO_3	36.40	34.11	36.78	34.91	37.41	27.55	35.02	36.50	35.16	36.19	34.07
SiO_2	1.57	0.78	1.57	2.37	2.09	3.98	0.32	2.60	5.27	7.66	5.62
TiO_2	0.12	0.11	0.13	0.11	0.11	0.11	0.07	0.10	0.17	0.35	0.19
Al_2O_3	20.30	18.59	22.53	19.16	26.79	20.01	11.80	26.04	28.31	44.59	33.45
Fe_2O_3	20.24	28.20	25.09	24.70	24.19	19.87	16.35	25.13	23.24	11.24	11.49
MgO	0.09	bdl	0.07	0.04	0.06	0.15	0.03	bdl	0.12	0.34	0.09
CaO	0.13	bdl	0.07	0.06	0.10	0.17	0.04	bdl	0.07	0.14	bdl
SrO	10.25	2.50	2.62	4.93	1.59	1.59	18.70[1]	0.31	0.68	0.50	0.73
K_2O	0.35	0.26	0.48	0.41	0.43	0.55	0.20	0.39	1.10	1.02	0.80
Na_2O	0.15	0.20	0.22	0.16	0.24	0.09	0.15	0.24	0.21	0.40	0.21
Cl	0.42	0.40	0.45	0.37	0.52	0.48	0.26	0.61	0.56	0.69	0.48
Σ	90.41	85.51	90.28	87.54	93.99	75.03	83.40	92.27	95.27	103.94	87.84
H_2O[3]	10.25	14.50	13.59	11.57	15.13	10.62	7.89	14.79	14.23	17.57	12.77
$(NH_4)_2O$[4]	0.00	1.84	1.87	1.49	2.17	1.60	0.00	2.32	2.18	2.61	2.11
	apfu (mpfu), *B* = 3 basis (assuming all Si entering the *T*-sites)										
P	0.02	0.01	0.02	0.02	0.02	0.03	0.05	0.02	0.02	0.03	0.04
S	2.09	1.78	1.82	1.91	1.69	1.61	3.00[1]	1.65	1.55	1.33	1.59
Si	0.12	0.05	0.10	0.17	0.13	0.31	0.04	0.16	0.31	0.37	0.35
Ti	0.01	0.01	0.01	0.01	0.01	0.01	0.01		0.01	0.01	0.01
Al	1.83	1.52	1.75	1.64	1.90	1.83	1.59	1.85	1.96	2.57	2.45
Fe	1.16	1.47	1.24	1.35	1.10	1.16	1.41	1.14	1.03	0.41	0.54
Mg	0.01		0.01		0.01	0.02			0.01	0.02	0.01
Ca	0.01				0.01	0.01	0.01			0.01	
Sr	0.45	0.10	0.10	0.21	0.06	0.07	1.24[1]	0.01	0.02	0.01	0.03
K	0.03	0.02	0.04	0.04	0.03	0.05	0.03	0.03	0.08	0.06	0.06
Na	0.02	0.03	0.03	0.02	0.03	0.01	0.03	0.03	0.02	0.04	0.03
Cl	0.05	0.05	0.05	0.05	0.05	0.06	0.05	0.06	0.06	0.06	0.05
NH_4[5]	0.00	0.85	0.82	0.72	0.87	0.83	0.00	0.93	0.86	0.85	0.88
OH[5]	5.23	6.22	5.97	5.62	5.20	5.50	6.01	5.96	5.59	5.74	5.30
	end members [%]										
Ama[6]		43	51	44	57	53		58	57	75	73
Amj		42	36	37	33	34		36	30	12	16

Alu	4	2	2	2	2	3	11	2	6	6	5
Jar	2	1	2	2	1	2	10	1	3	1	1
Naa	3	2	2	1	2	1	12	2	2	3	2
Naj	2	1	1	1	1	1	11	1	1	1	
Srh	52	1	3	6	2	2	27	5	1	1	1
Sfh	33	0.4	2	5	1	2	24	5	0.4	0.1	0.2
Hua	1		<1	<1	<1	1	1		<1	<1	
Caj	1		<1	<1	<1	<1	1		<1	<1	
Mgh	1		<1	<1	<1	1	1		<1	1	<1
Mfh	1		<1	<1	<1	<1	1		<1	<1	<1
Goy[7]	1		<1	<1	<1		1	0.1			0.1
Ben	<1			<1		<1	1	0.1			

[1] – excess SrO recasted as 1.09 $SrSO_4$; [2] – Mn was measured but not detected (under the detection limit); [3] – exclusively OH-derived, backward-calculated from OH *mpfu* content assuming lacking H_3O^+ and H_2O molecules in the structure; [4] – backward-calculated from NH_4^+ *mpfu* content; 3 calculated by stoichiometry (filling the *A* site to the occupancy of 1); [5] – by charge balance; [6] – Ama – ammoniojarosite (and hydroniumjarosite), Amj – ammonioalunite (and schlossmacherite), Alu – alunite, Jar – jarosite, Naa – natroalunite, Naj – natrojarosite, Hua – huangite, Srh – “strontiohuangite” HEM, Sfh – “strontioferrihuangite” HEM, Caj – “calciojarosite” HEM, Mgh – “magnesiohuangite” HEM, Mfh – “magnesioferrihuangite” HEM, goy – goyazite, Ben – benauite; [7] – crandallite and related end members omitted due to very low content

Table ST11. Shapiro-Wilk (S-W) normality test results, strontium experiment

	S-W	p-v
Cl	**0.97**	0.83
Na_2O	**0.94**	0.50
K_2O	**0.96**	0.74
MgO	**0.98**	0.97
CaO	**0.95**	0.68
SrO	**0.97**	0.84
Al_2O_3	**0.97**	0.87
Fe_2O_3	0.83	**0.02**
SiO_2	**0.95**	0.60
TiO_2	**0.88**	0.10
P_2O_5	**0.91**	0.22
SO_3	0.71	**0.0007**

p-v – the p-values; meaningful values are given in bold

Table ST12. Element correlation based on Kendall's τ coefficients and uncorrected ρ-values (given in the parentheses), strontium experiment

	Cl	Na_2O	K_2O	MgO	CaO	SrO	Al_2O_3	Fe_2O_3	SiO_2	TiO_2	P_2O_5	SO_3
Cl		**0.57 (0.01)**	**0.55 (0.02)**	**0.65 (0.02)**	**0.43** (0.14)	**-0.80 (0.0007)**	**0.70 (0.003)**	-0.13 (0.58)	**0.59 (0.01)**	**0.45** (0.05)	0.26 (0.27)	0.23 (0.32)
Na_2O	**0.57 (0.01)**		0.29 (0.21)	0.14 (0.60)	0.18 (0.53)	**-0.54 (0.02)**	**0.51 (0.03)**	0.09 (0.69)	0.26 (0.27)	0.22 (0.34)	0.04 (0.88)	**0.51 (0.03)**
K_2O	**0.55 (0.02)**	0.29 (0.21)		**0.67 (0.01)**	0.29 (0.32)	**-0.55 (0.02)**	**0.64 (0.006)**	**-0.33** (0.16)	**0.67 (0.004)**	**0.72 (0.002)**	0.27 (0.24)	0.06 (0.81)
MgO	**0.65 (0.02)**	0.14 (0.60)	**0.67 (0.01)**		**0.64 (0.03)**	**-0.65 (0.02)**	**0.50** (0.06)	**-0.39** (0.14)	**0.56 (0.04)**	**0.70 (0.008)**	**0.39** (0.14)	-0.15 (0.59)
CaO	**0.43** (0.14)	0.18 (0.53)	0.29 (0.32)	**0.64 (0.03)**		**-0.40** (0.17)	0.29 (0.32)	-0.29 (0.32)	**0.36** (0.22)	**0.40** (0.17)	0.29 (0.32)	0.11 (0.69)
SrO	**-0.80 (0.0007)**	**-0.54 (0.02)**	**-0.55 (0.02)**	**-0.65 (0.02)**	**-0.40** (0.17)		**-0.59 (0.01)**	0.06 (0.81)	**-0.59 (0.01)**	**-0.37** (0.11)	-0.26 (0.27)	-0.08 (0.74)
Al_2O_3	0.**70 (0.003)**	**0.51 (0.03)**	**0.64 (0.006)**	**0.50** (0.06)	0.29 (0.32)	**-0.59 (0.01)**		-0.29 (0.21)	**0.67 (0.004)**	**0.69 (0.003)**	**0.35** (0.14)	0.25 (0.28)
Fe_2O_3	-0.13 (0.58)	0.09 (0.69)	**-0.33** (0.16)	**-0.39** (0.14)	-0.29 (0.32)	0.06 (0.81)	-0.29 (0.21)		**-0.40** (0.08)	**-0.41** (0.08)	**-0.73 (0.002)**	0.16 (0.51)
SiO_2	**0.59 (0.01)**	0.26 (0.27)	**0.67 (0.004)**	**0.56 (0.04)**	**0.36** (0.22)	**-0.59 (0.01)**	**0.67 (0.004)**	**-0.40** (0.08)		**0.54 (0.02)**	**0.45 (0.05)**	-0.10 (0.68)
TiO_2	**0.45** (0.05)	0.22 (0.34)	**0.72 (0.002)**	**0.70 (0.008)**	**0.40** (0.17)	**-0.37** (0.11)	**0.69 (0.004)**	**-0.41** (0.08)	**0.54 (0.02)**		**0.31** (0.18)	0.06 (0.80)
P_2O_5	0.26 (0.27)	0.04 (0.88)	0.27 (0.24)	**0.39** (0.14)	0.29 (0.32)	-0.26 (0.27)	**0.35** (0.14)	**-0.73 (0.002)**	**0.45 (0.05)**	**0.31** (0.18)		-0.21 (0.36)
SO_3	0.23 (0.32)	**0.51 (0.03)**	0.06 (0.80)	-0.15 (0.59)	0.11 (0.69)	-0.08 (0.74)	0.25 (0.28)	0.16 (0.51)	-0.10 (0.68)	0.06 (0.80)	-0.21 (0.36)	

Strong correlations are given in bold

Table ST13. Results of chemical analyses of AAJ contacting with a solution of $ZrCl_4$

	1	2	3	4	5	6	7	8	9	10	11	12
	[wt.%]											
	Si-rich Zr-exchanged AAJ				moderately siliceous Zr-exchanged AAJ						Zr phase	
P_2O_5	0.02	0.69	0.52	0.65	1.06	0.24	0.22	0.18	0.23	0.32	0.18	0.18
SO_3	27.73	18.93	13.39	18.72	30.22	27.50	28.20	32.42	32.73	31.91	20.56	21.87
SiO_2	14.12	25.91	39.32	35.03	6.69	8.21	9.43	4.78	2.87	9.45	0.75	1.04
ZrO_2	4.38	5.25	2.65	3.33	4.25	7.94	3.86	2.44	4.44	1.54	17.56	16.14
TiO_2	0.32	0.37	1.02	0.50	3.01	0.09	0.19	0.17	0.17	0.30	bdl[1]	0.11
Al_2O_3	32.11	25.71	24.55	25.82	29.50	24.69	25.49	26.74	24.88	30.61	10.60	15.36
Fe_2O_3	9.11	6.43	3.71	6.24	7.23	12.49	14.01	14.83	15.44	13.49	10.75	12.59
MgO	0.29	0.38	0.57	0.57	0.14	0.15	0.24	0.10	bdl	0.23	bdl	bdl
CaO	0.43	0.45	0.34	0.46	0.52	0.36	0.15	bdl	bdl	0.15	0.49	0.53
K_2O	2.04	2.00	2.87	2.42	1.41	1.04	1.26	0.66	0.61	0.99	0.27	0.47
Na_2O	0.63	0.49	0.46	0.73	0.61	bdl	bdl	bdl	bdl	bdl	bdl	bdl
Cl	0.88	0.69	0.55	0.56	1.05	0.48	0.48	0.47	0.47	0.46	0.83	0.46
Σ	92.05	87.30	89.93	95.01	85.69	83.20	83.52	82.79	81.85	88.42	61.98	68.74
H_2O[2]	11.21	8.54	6.80	8.36	11.88	11.01	10.89	11.81	11.94	12.04	11.27	11.49
$(NH_4)_2O$[3]	1.65	1.22	0.82	0.98	1.67	1.83	1.81	2.05	2.05	2.10		
apfu (mpfu), *B* = 3 basis (assuming all Si entering the *T*-site); analyses 11 and 12: *B* = 2 basis												
P		0.05	0.04	0.04	0.06	0.01	0.01	0.01	0.01	0.02	0.01	0.01
S	1.33	1.12	0.89	1.14	1.53	1.46	1.49	1.66	1.71	1.52	1.06	0.93
^{T}Si	0.67	0.83	1.07	0.82	0.41	0.53	0.50	0.33	0.28	0.46	0.05	0.06
Zr	0.14	0.20	0.11	0.13	0.14	0.27	0.13	0.08	0.15	0.05	0.58	0.44
Ti	0.02	0.02	0.07	0.03	0.15		0.01	0.01	0.01	0.01		
Al	2.41	2.39	2.57	2.46	2.34	2.06	2.12	2.15	2.04	2.29	0.86	1.02
Fe	0.44	0.38	0.25	0.38	0.37	0.66	0.74	0.76	0.81	0.65	0.56	0.53
Mg	0.03	0.04	0.08	0.07	0.01	0.02	0.03	0.01		0.02		
Ca	0.03	0.04	0.03	0.04	0.04	0.03	0.01			0.01	0.04	0.03
K	0.17	0.20	0.32	0.25	0.12	0.09	0.11	0.06	0.05	0.08	0.02	0.03
Na	0.08	0.08	0.08	0.11	0.08							
Cl	0.09	0.09	0.08	0.08	0.12	0.06	0.06	0.05	0.05	0.05	0.10	0.04
NH_4[4]	0.70	0.64	0.49	0.53	0.75	0.86	0.85	0.93	0.95	0.89	0.94	0.94
OH[4]	4.77	4.50	4.03	4.51	5.34	5.20	5.11	5.37	5.53	5.11	5.17	5.27
	end members [%]											
Ama[5]	56	49	40	42	60	58	59	66	63	68		
Amj	10	8	4	6	9	19	21	23	25	19		
Alu	13	15	27	20	10	6	8	4	4	6		
Jar	2	2	2	3	2	2	3	1	1	2		
Naa	6	6	7	9	6							
Naj	1	1	1	1	1							
Hua	1	1	1	1	1	<1	<1			<1		
Caj	<1	<1		<1	<1	<1	<1			<1		
Mgh	2	3	6	6	1	1	2	1		2		
Mfh	<1	1	1	1	<1	<1	1	<1		1		
Azs[6]	2	3	2	2	1	3	1	1	1	0.4		
Pzs	0.4	1	1	1	0.2	0.3	0.2					
Szs	0.2	0.4	0.3	0.3	0.1							
Mzs	0.1	0.2	0.3	0.2		0.1						
Czs	<0.1	<0.1	<0.1	<0.1	<0.1	<0.1						
Azu	3	4	2	2	4	8	4	3	5	1		
Pzu	1	1	1	1	1	1	1	0.2	0.3	0.1		
Szu	0.4	1	0.3	1	0.4							
Mzu	0.1	0.3	0.3	0.3	0.1	0.1	0.1					
Czu	<0.1	0.1	<0.1	<0.1	<0.1	0.1	<0.1					
R	<1	4	4	4	4	1	1	1	1	1		

[1] – below detection limit; [2] – exclusively OH-derived, backward-calculated from OH *mpfu* content assuming lacking H_3O^+ and H_2O molecules in the structure; [3] – backward-calculated from NH_4^+ *mpfu* content; 3 calculated by stoichiometry (filling the *A* site to the occupancy of 1); [4] – by charge balance; [5] – Ama – ammoniojarosite (and hydroniumjarosite), Amj – ammonioalunite (and schlossmacherite), Alu – alunite, Jar – jarosite, Naa – natroalunite, Naj – natrojarosite, Hua – huangite, Caj – "calciojarosite" HEM, Mgh – "magnesiohuangite" HEM, Mfh – "magnesioferrihuangite" HEM; *R* – remaining P-, Ti- and Cl-dominant HEMs; [6] – Zr-dominant analogues: see the main text for explanations

Table ST14. Shapiro-Wilk (S-W) normality test results, zirconium experiment

	S-W	p-v
Cl	0.81	**0.02**
Na_2O	**0.93**	0.58
K_2O	**0.95**	0.67
MgO	**0.95**	0.67
CaO	0.78	**0.02**
Al_2O_3	**0.84**	**0.04**
Fe_2O_3	**0.89**	0.18
SiO_2	**0.95**	0.65
TiO_2	**0.93**	0.48
ZrO_2	**0.97**	0.92
P_2O_5	**0.86**	0.08
SO_3	0.81	**0.02**

p-v – the p-values are given in parentheses; meaningful values are given in bold

Table ST15. Element correlation based on Kendall's τ coefficients and uncorrected ρ-values (given in the parentheses), zirconium experiment

	Cl	Na_2O	K_2O	MgO	CaO	Al_2O_3	Fe_2O_3	SiO_2	TiO_2	ZrO_2	P_2O_5	SO_3
Cl		0.20 (0.62)	**0.48** (0.05)	0.14 (0.60)	**0.69 (0.02)**	0.21 (0.39)	**-0.43** (0.08)	0.25 (0.31)	**0.43** (0.08)	**0.30** (0.23)	**0.39** (0.12)	**-0.33** (0.19)
Na_2O	0.20 (0.62)		0 (1)	-0.20 (0.62)	**0.40** (0.33)	**0.53** (0.20)	**0.40** (0.33)	-0.20 (0.62)	-0.20 (0.62)	0 (1)	0 (1)	0.20 (0.62)
K_2O	**0.48** (0.050	0 (1)		**0.72 (0.007)**	0.29 (0.32)	0.07 (0.78)	**-0.82 (0.001)**	**0.78 (0.002)**	**0.56 (0.03)**	-0.07 (0.79)	0.20 (0.42)	**-0.80 (0.001)**
MgO	0.14 (0.60)	-0.20 (0.62)	**0.72 (0.007)**		0.07 (0.80)	-0.17 (0.52)	**-0.61 (0.02)**	**1 (0.0002)**	**0.50** (0.06)	0 (1)	0.11 (0.68)	**-0.82 (0.002)**
CaO	**0.69 (0.02)**	**0.40** (0.33)	0.29 (0.32)	0.07 (0.80)		0.15 (0.61)	**-0.43** (0.14)	0.07 (0.80)	**0.50** (0.08)	0.29 (0.32)	**0.43** (0.14)	-0.25 (0.38)
Al_2O_3	0.21 (0.39)	**0.53** (0.20)	0.07 (0.78)	-0.17 (0.52)	0.15 (0.61)		0.02 (0.93)	0.02 (0.93)	0.21 (0.40)	-0.26 (0.30)	-0.07 (0.78)	0.17 (0.50)
Fe_2O_3	**-0.43** (0.08)	**0.40** (0.33)	**-0.82 (0.001)**	**-0.61 (0.02)**	**-0.43** (0.14)	0.02 (0.93)		**-0.69 (0.006)**	**-0.64**	0.07 (0.79)	**-0.38** (0.13)	**0.80 (0.001)**
SiO_2	0.25 (0.31)	-0.20 (0.62)	**0.78 (0.002)**	**1 (0.0002)**	0.07 (0.80)	0.02 (0.93)	**-0.69 (0.006)**		**0.51 (0.01)**	-0.11 (0.65)	0.16 (0.53)	**-0.84 (0.0007)**
TiO_2	**0.43** (0.08)	-0.20 (0.62)	**0.56 (0.03)**	**0.50** (0.06)	**0.50** (0.08)	0.21 (0.40)	**-0.64** (0.79)	**0.51 (0.04)**		-0.16 (0.53)	**0.47** (0.06)	**-0.48** (0.05)
ZrO_2	**0.30** (0.23)	0 (1)	-0.07 (0.79)	0 (1)	0.29 (0.32)	-0.26 (0.30)	0.07 (0.13)	-0.11 (0.65)	-0.16 (0.53)		0.11 (0.65)	-0.07 (0.78)
P_2O_5	**0.39** (0.12)	0 (1)	0.20 (0.42)	0.11 (0.68)	**0.43** (0.14)	-0.07 (0.78)	**-0.38** (0.13)	0.16 (0.53)	**0.47** (0.06)	0.11 (0.65)		-0.25 (0.31)
SO_3	**-0.33** (0.19)	0.20 (0.62)	**-0.80 (0.001)**	**-0.82 (0.002)**	-0.25 (0.38)	0.17 (0.50)	**0.80 (0.001)**	**-0.84 (0.0007)**	**-0.48** (0.05)	-0.07 (0.78)	-0.25 (0.31)	

Strong correlations are given in bold

Table ST16. Results of chemical analyses of AAJ contacting with a solution of $MnSO_4 \cdot H_2O$

	1	2	3	4	5	6	7
				[wt.%]			
P_2O_5[1]	0.46	0.60	0.66	0.62	0.67	0.68	0.61
SO_3	35.51	38.76	37.86	38.37	37.96	37.05	36.61
SiO_2	9.83	7.01	2.30	3.04	3.96	6.06	3.73
TiO_2	0.24	0.22	0.19	0.22	0.17	0.14	0.14
Al_2O_3	36.38	38.70	38.00	42.42	47.75	36.74	35.99
Fe_2O_3	13.53	15.07	15.60	14.95	12.15	14.52	16.60
MgO	0.09	0.10	0.09	0.10	0.11	0.11	0.09
CaO	0.04	0.04	0.06	007	0.05	002	0.02
K_2O	1.04	1.56	0.60	1.20	0.70	0.57	0.50
Na_2O	0.15	0.17	0.16	0.23	0.19	0.38	0.26
Cl	0.97	0.82	1.05	0.94	0.53	0.44	0.47
Σ	98.24	103.05	96.57	102.25	104.25	96.72	95.01
H_2O[3]	12.59	15.44	18.22	20.05	21.63	14.97	16.82
$(NH_4)_2O$[4]	2.38	2.47	2.64	2.74	3.05	2.46	2.56
apfu (mpfu), *B* = 3 basis (assuming all Si entering the *T*-site)							
P	0.02	0.03	0.03	0.03	0.03	0.03	0.03
S	1.51	1.53	1.51	1.41	1.31	1.54	1.50
Si	0.56	0.37	0.12	0.15	0.18	0.34	0.20
Ti	0.01	0.01	0.01	0.01	0.01	0.01	0.01
Al	2.42	2.40	2.38	2.45	2.58	2.40	2.32
Fe	0.58	0.60	0.62	0.55	0.42	0.60	0.68
Mg	0.01	0.01	0.01	0.01	0.01	0.01	0.01
K	0.08	0.10	0.04	0.07	0.04	0.04	0.03
Na	0.02	0.02	0.02	0.02	002	0.04	0.03
Cl	0.09	0.07	0.09	0.08	0.04	0.04	0.04
NH_4[5]	0.90	0.87	0.93	0.89	0.93	0.91	0.93
OH[5]	4.75	5.42	6.45	6.55	6.62	5.52	6.13
				end members [%]			
Ama[6]	73	69	74	73	80	72	72
Amj	17	17	19	16	13	18	21
Alu	6	8	3	6	4	3	3
Jar	1	2	1	1	1	1	1
Naa	1	1	1	2	1	3	2
Naj	<1	<1	<1	<1	<1	1	1
Hua	<1	<1	<1	<1	<1	<1	<1
Caj			<1	<1			
Mga	1	1	1	1	1	1	1
Mgj	<1	<1	<1	<1	<1	<1	<1

[1] – Mn was measured but not detected (under the detection limit); [2] – below detection limit; [3] – exclusively OH-derived, backward-calculated from OH *mpfu* content assuming lacking H_3O^+ and H_2O molecules in the structure; [4] – backward-calculated from NH_4^+ *mpfu* content; 3 calculated by stoichiometry (filling the *A* site to the occupancy of 1); [5] – by charge balance; [6] – Ama – ammoniojarosite (and hydroniumjarosite), Amj – ammonioalunite (and schlossmacherite), Alu – alunite, Jar – jarosite, Naa – natroalunite, Naj – natrojarosite, Hua – huangite, Caj – "calcio-jarosite" (hypothetical end member), Flc – florencite-(Ce), Ffc – "ferriflorencite-(Ce)" (hypothetical end member), Mga – "magnesioalunite" (hypothetical end member), Mgj – magnesiojarosite (hypothetical end member)

Table ST17. Results of chemical analyses of AAJ contacting with a solution of $CuSO_4 \cdot 5H_2O$.

	1	2	3	4	5	6	7
				[wt.%]			
P_2O_5[1]	0.64	0.54	0.44	0.53	0.45	0.94	0.75
SO_3	32.83	35.96	38.01	34.74	32.54	30.65	34.49
SiO_2	10.53	5.32	3.26	8.58	9.56	2.95	5.25
TiO_2	0.15	0.19	0.13	0.19	0.18	0.19	0.24
Al_2O_3	40.11	48.65	48.23	46.26	44.46	35.50	43.31
Fe_2O_3	10.03	10.06	9.13	9.31	9.28	13.10	10.28
CuO	0.65	bdl[1]	bdl	bdl	0.58	1.05	0.75
MgO	0.13	bdl	bdl	0.11	0.17	bdl	0.13
CaO	0.12	bdl	bdl	bdl	bdl	bdl	bdl
K_2O	1.56	1.05	1.00	1.22	1.17	0.74	1.04
Na_2O	bdl	bdl	0.38	bdl	0.42	bdl	Bdl
Cl	0.52	0.57	0.58	0.55	0.52	0.58	0.56
Σ	97.25	102.34	101.16	101.48	99.31	85.70	96.79
H_2O[2]	13.56	20.89	21.09	17.54	16.56	17.04	18.36
$(NH_4)_2O$[3]	2.43	3.05	2.89	2.83	2.62	2.49	2.75
apfu (mpfu), *B* = 3 basis (assuming all Si entering the *T*-site)							
P	0.03	0.02	0.02	0.02	0.02	0.05	0.03
S	1.33	1.24	1.34	1.27	1.22	1.31	1.30
Si	0.57	0.25	0.15	0.42	0.48	0.17	0.26
Ti	0.01	0.01	0.01	0.01	0.01	0.01	0.01
Al	2.56	2.64	2.67	2.65	2.62	2.38	2.57
Fe	0.41	0.35	0.32	0.34	0.35	0.56	0.39
Cu	0.03				0.02	0.05	0.03
Mg	0.01			0.01	0.01		0.01
K	0.11	0.06	0.06	0.08	0.07	0.05	0.07
Na			0.03	0.04			
Cl	0.05	0.04	0.05	0.05	0.04	0.06	0.05
NH_4[4]	0.88	0.94	0.91	0.92	0.87	0.95	0.92
OH[4]	4.90	6.43	6.61	5.69	5.53	6.48	6.17
				end members {%}			
Ama[5]	73	81	80	80	75	73	78
Amj	12	11	10	10	10	17	12
Alu	9	5	5	7	6	4	6
Jar	1	1	1	1	1	1	1
Naa			3		4		
Naj			<1		1		
Hua	1						
Caj	<1						
Mgh	1			1	1		1
Mfh	<1			<1	<1		<1
Cbc	<0.5						
Mbc	<0.5				<0.5		<0.5
R	2	2	1	2	2	3	2

[1] – below detection limit; [2] – exclusively OH-derived, backward-calculated from OH *mpfu* content assuming lacking H_3O^+ and H_2O molecules in the structure; [3] – backward-calculated from NH_4^+ *mpfu* content; 3 calculated by stoichiometry (filling the *A* site to the occupancy of 1); [4] – by charge balance; [5] – Ama – ammoniojarosite (and hydroniumjarosite), Amj – ammonioalunite (and schlossmacherite), Alu – alunite, Jar – jarosite, Naa – natroalunite, Naj – natrojarosite, Hua – huangite, Caj – "calcio-jarosite" HEM, Mgh – "magnesiohuangite" HEM, Mfh – "magnesioferrihuangite" HEM, Cbc – "calciobeaverite-(Cu)" HEM, Mbc – "magnesiobeaverite-(Cu)" HEM, *R* – remaining P-, Ti- and Cl-dominant HEMs

Table ST18. Shapiro-Wilk (S-W) normality test results, copper experiment

	S-W	p-v
Cl	0.80	**0.02**
Na_2O	**1**	1
K_2O	**0.93**	0.56
MgO	**0.90**	0.40
CuO	**0.92**	0.53
Al_2O_3	**0.90**	0.27
Fe_2O_3	**0.82**	**0.05**
SiO_2	**0.92**	0.39
TiO_2	**0.92**	0.41
P_2O_5	**0.95**	0.75
SO_3	**0.98**	0.96

p-v – the p-values; meaningful values are given in bold

Table ST19. Element correlation based on Kendall's τ coefficients and uncorrected ρ-values (given in the parentheses), copper experiment

	Cl	K_2O	MgO	CuO	Al_2O_3	Fe_2O_3	SiO_2	TiO_2	P_2O_5	SO_3
Cl		**-0.69 (0.03)**	**-0.55** (0.26)	**0.82** (0.10)	**0.33** (0.30)	0.06 (0.86)	**-0.79 (0.01)**	0.11 (0.73)	0.05 (0.87)	**-0.49** (0.12)
K_2O	**-0.69 (0.03)**		0 (1)	**-0.67** (0.17)	0 (1)	-0.25 (0.43)	**0.90 (0.004)**	-0.20 (0.54)	-0.14 (0.65)	-0.10 (0.76)
MgO	**-0.55** (0.26)	0 (1)		**-1** (0.12)	**-0.33** (0.50)	-0.18 (0.71)	**0.33** (0.50)	**-0.33** (0.50)	**-0.33** (0.50)	**-0.91** (0.06)
CuO	**0.82** (0.10)	**-0.67** (0.17)	**-1** (0.12)		**-0.67** (0.17)	**1 (0.04)**	**-0.67** (0.17)	**0.33** (0.50)	**1 (0.04)**	-0.18 (0.71)
Al_2O_3	**0.33** (0.30)	0 (1)	**-0.33** (0.50)	**-0.67** (0.17)		**-0.62** (0.05)	-0.10 (0.76)	-0.25 (0.43)	**-0.59** (0.06)	**0.85 (0.007)**
Fe_2O_3	0.06 (0.86)	-0.25 (0.43)	-0.18 (0.71)	**1 (0.04)**	**-0.62** (0.05)		-0.25 (0.43)	**0.51** (0.11)	**0.95 (0.003)**	**-0.51** (0.11)
SiO_2	**-0.79 (0.01)**	**0.90 (0.004)**	**0.33** (0.47)	**-0.67** (0.17)	-0.10 (0.76)	-0.25 (0.42)		-0.29 (0.36)	-0.24 (0.45)	-0.20 (0.54)
TiO_2	0.11 (0.73)	-0.20 (0.54)	**-0.33** (0.47)	**0.33** (0.50)	-0.25 (0.43)	**0.51** (0.11)	-0.29 (0.36)		**0.49** (0.12)	-0.25 (0.43)
P_2O_5	0.05 (0.86)	-0.14 (0.65)	**0.33** (0.47)	**1 (0.04)**	**-0.59** (0.06)	**0.95 (0.003)**	-0.24 (0.45)	**0.49** (0.12)		**-0.49** (0.12)
SO_3	**0.49** (0.12)	-0.10 (0.76)	**-0.91** (0.06)	-0.18 (0.71)	**0.85 (0.007)**	**-0.51** (0.11)	-0.20 (0.54)	-0.25 (0.43)	**-0.49** (0.12)	

Strong correlations are given in bold.

Table ST20. Results of chemical analyses of AAJ contacting with a solution of $ZnCl_2$

	1	2	3	4	5	6	7
	[wt.%]						
P_2O_5[1]	0.51	0.40	0.43	0.68	0.46	0.93	0.88
SO_3	34.19	36.62	35.17	31.49	36.00	30.88	36.31
SiO_2	8.69	2.52	9.92	1.29	4.90	13.10[3]	2.53
TiO_2	0.14	0.11	0.16	0.22	1.41	0.22	0.17
Al_2O_3	39.37	48.40	43.59	28.60	45.77	30.91	30.75
Fe_2O_3	14.65	16.98	16.23	19.66	17.36	13.97	16.09
MgO	0.11	bdl[2]	0.14	0.11	0.15	0.11	bdl
CaO	bdl	bdl	bdl	0.20	bdl	0.37	0.18
K_2O	1.00	0.71	1.00	1.48	1.00	2.66	1.45
Na_2O	bdl	bdl	bdl	bdl	bdl	0.61	bdl
Cl	0.66	0.80	0.63	0.70	0.70	0.61	0.44
Σ	99.31	106.53	107.25	84.41	107.74	94.37	88.82
H_2O[4]	15.52	24.85	17.70	16.10	22.81	8.33	14.13
$(NH_4)_2O$[5]	2.66	3.36	2.96	2.10	3.18	1.59	2.12
apfu (mpfu) *B* = 3 basis, assuming all Si entering the *T*-sites							
P	0.02	0.01	0.02	0.04	0.02	0.05	0.05
S	1.34	1.18	1.24	1.46	1.19	1.48	1.69
Si	0.45	0.11	0.47	0.08	0.22	0.83[3]	0.16
Ti	0.01		0.01	0.01	0.05	0.01	0.01
Al	2.42	2.45	2.42	2.08	2.38	2.32	2.24
Fe	0.57	0.55	0.58	0.91	0.58	0.67	0.75
Mg	0.01		0.01	0.01	0.01	0.01	
Ca				0.01		0.02	0.01
K	0.07	0.04	0.06	0.12	0.06	0.22	0.11
Na						0.08	
Cl	0.06	0.06	0.05	0.07	0.05	0.07	0.05
NH_4[6]	0.92	0.96	0.93	0.86	0.93	0.67	0.87
OH[6]	5.40	7.11	5.56	6.62	6.71	3.54	5.83
Ama[7]	73	78	74	58	74	50	64
Amj	17	17	18	26	18	15	21
Alu	5	3	5	8	4	16	8
Jar	1	1	1	3	1	5	3
Naa						6	
Naj						2	
Hua				1		2	1
Caj				<1		1	<1
Mgh	1		1	1	1	1	
Mfh	<1		<1	<1	<1	<1	

[1] – Mn and Zn were measured but not detected (under the detection limit); [2] – below detection limit; [3] – excess possible; [4] – exclusively OH-derived, backward-calculated from OH *mpfu* content assuming lacking H_3O^+ and H_2O molecules in the structure; [5] – backward-calculated from NH_4^+ *mpfu* content; [6] – calculated by stoichiometry (filling the *A* site to the occupancy of 1); [5] by charge balance; [7] – Ama – ammoniojarosite (and hydroniumjarosite), Amj – ammonioalunite (and schlossmacherite), Alu – alunite, Jar – jarosite, Naa – natroalunite, Naj – natrojarosite, Hua – huangite, HEM, Caj – "calciojarosite" HEM, Mgh – "magnesiohuangite" HEM, Mfh – "magnesioferrihuangite" HEM

Table ST21. Results of chemical analyses of AAJ contacting with a solution of $Ga(NO_3)_3 \cdot xH_2O$

	1	2	3	4	5	6	7
	aluminous composition				ferric composition		
	[wt.%]						
P_2O_5[1]	0.40	0.57	0.62	0.46	0.58	0.59	0.58
SO_3	23.53	25.69	28.44	24.82	25.78	27.72	24.12
SiO_2	4.22	1.19	0.36	1.66	2.21	0.32	0.74
TiO_2	0.12	0.14	0.15	bdl	0.17	0.14	bdl
Al_2O_3	8.25	8.48	8.42	13.22	5.76	7.24	4.12
Fe_2O_3	7.94	11.12	12.10	7.34	11.08	15.26	9.46
Ga_2O_3	17.02	20.77	21.03	16.54	21.44	18.62	19.86
MgO	0.11	bdl	bdl	bdl	bdl	bdl	bdl
K_2O	0.31	0.29	0.23	0.46	0.32	0.15	0.32
Cl	0.35	0.31	0.28	0.41	0.23	0.28	0.27
Σ	62.25	68.76	71.80	65.46	67.82	70.58	59.81
H_2O[3]	6.59	8.29	8.03	8.48	7.04	7.93	5.46
$(NH_4)_2O$[4]	3.61	4.43	4.58	4.33	4.01	4.55	3.29
apfu (mpfu), *B* = 3 basis (assuming all Si entering the *T*-site), unnormalized							
P	0.04	0.05	0.05	0.04	0.05	0.05	0.06
S	1.98	1.82	1.96	1.76	2.00	1.95	2.20
Si	0.47	0.11	0.03	0.16	0.23	0.03	0.09
Ti	0.01	0.01	0.01		0.01	0.01	
Al	1.09	0.94	0.91	1.47	0.70	0.80	0.59
Fe	0.67	0.79	0.84	0.52	0.86	1.07	0.86
Ga	1.23	1.26	1.24	1.00	1.42	1.12	1.55
Mg	0.02						
K	0.04	0.03	0.03	0.06	0.04	0.02	0.05
Cl	0.07	0.05	0.04	0.07	0.04	0.04	0.05
NH_4[5]	0.94	0.97	0.97	0.94	0.96	0.98	0.95
OH[5]	4.94	5.22	4.92	5.35	4.86	4.95	4.42
	end members [%]						
Ama[6]	34	30	29	45	22	26	18
Amj	21	25	27	16	27	34	27
Alu	2	1	1	3	1	0.5	1
Jar	1	1	1	1	1	1	1
Mgh	0.6						
Mfh	0.4						
Ags	38	40	39	31	44	36	48
Pgs	2	1	1	2	2	1	2
Mgs	0.7						
R	2	2	2	2	2	2	3

[1] – Na and Ca were measured but not detected (under the detection limit); [2] – below detection limit; [3] – exclusively OH-derived, backward-calculated from OH *mpfu* content assuming lacking H_3O^+ and H_2O molecules in the structure; [4] – backward-calculated from NH_4^+ *mpfu* content; 3 calculated by stoichiometry (filling the *A* site to the occupancy of 1); [5] – by charge balance; [6] – Ama – ammoniojarosite (and hydroniumjarosite), Amj – ammonioalunite (and schlossmacherite), Alu – alunite, Jar – jarosite, Mgh – "magnesiohuangite" HEM, Mfh – "magnesioferrihuangite" HEM, Ags – "ammonium gallium sulfate" HEM, Pgs – "potassium gallium sulfate" HEM, Mgs – "magnesium gallium sulfate" HEM, *R* – remaining end-members

Table ST22. Shapiro-Wilk (S-W) normality test results, gallium experiment

	S-W	p-v
Cl	**0.96**	0.84
K_2O	**0.92**	0.45
Al_2O_3	**0.95**	0.72
Fe_2O_3	**0.96**	0.83
Ga_2O_3	**0.92**	0.50
SiO_2	**0.96**	0.79
TiO_2	**0.98**	0.95
P_2O_5	**0.82**	0.07
SO_3	**0.93**	0.59

p-v – the p-values; meaningful values are given in bold

Table ST23. Element correlation based on Kendall's τ coefficients and uncorrected ρ-values (given in the parentheses), gallium experiment

	Cl	K_2O	Al_2O_3	Fe_2O_3	Ga_2O_3	SiO_2	TiO_2	P_2O_5	SO_3
Cl		0.15 (0.64)	**0.65 (0.04)**	**-0.45** (0.16)	**-0.68 (0.03)**	0.20 (0.54)	**-0.74** (0.07)	**-0.45** (0.16)	-0.29 (0.36)
K_2O	0.15 (0.64)		-0.05 (0.87)	**-0.75 (0.02)**	-0.20 (0.54)	**0.49** (0.12)	0.20 (0.62)	**-0.45** (0.16)	**-0.39** (0.22)
Al_2O_3	**0.65 (0.04)**	-0.05 (0.87)		-0.15 (0.64)	-0.29 (0.36)	0.10 (0.76)	-0.11 (0.80)	-0.05 (0.87)	0.10 (0.76)
Fe_2O_3	**-0.45** (0.16)	**-0.75 (0.02)**	-0.15 (0.64)		**0.49** (0.12)	**-0.59** (0.06)	0.11 (0.80)	**0.75 (0.02)**	**0.68 (0.03)**
Ga_2O_3	**-0.68 (0.03)**	-0.20 (0.54)	-0.29 (0.36)	**0.49** (0.12)		-0.05 (0.88)	**1 (0.01)**	**0.49** (0.12)	**0.43** (0.18)
SiO_2	0.20 (0.54)	**0.49** (0.12)	0.10 (0.76)	**-0.59** (0.06)	-0.05 (0.88)		0 (1)	**-0.59** (0.06)	**-0.43** (0.18)
TiO_2	**-0.74 (**0.07)	0.20 (0.62)	-0.11 (0.80)	0.11 (0.80)	**1 (0.01)**	0 (1)		**0.40** (0.33)	**0.40** (0.33)
P_2O_5	**-0.45** (0.16)	**-0.45** (0.16)	-0.05 (0.87)	**0.75 (0.02)**	**0.49** (0.12)	**-0.59** (0.06)	**0.40** (0.33)		**0.88 (0.006)**
SO_3	**-0.30** (0.36)	**-0.39** (0.22)	0.10 (0.76)	**0.68 (0.03)**	**0.43** (0.18)	**-0.43** (0.18)	**0.40** (0.33)	**0.88 (0.006)**	

Strong correlations are given in bold

Table ST24. Results of chemical analyses of AAJ contacting with a solution of $InCl_3$

	1	2	3	4	5	6	7	8	9	10	11	12	13	14	15
	In-rich						medium-In			In-low					
	[wt.%]														
P_2O_5[1]	3.19	2.89	3.04	1.94	2.28	2.45	2.54	2.18	2.38	0.74	0.78	0.85	0.77	0.62	063
SO_3	12.93	7.56	6.47	14.60	11.66	8.09	8.07	8.34	12.60	35.37	34.21	36.03	36.32	34.98	34.54
SiO_2	0.90	0.40	0.53	0.20	0.55	0.53	0.24	0.24	0.16	6.17	7.80	3.71	2.12	5.29	11.12
TiO_2	0.88	0.87	0.86	0.63	0.70	0.78	0.59	0.58	0.64	0.15	0.26	0.15	0.13	0.28	0.29
Al_2O_3	4.34	2.09	2.11	8.82	6.93	3.77	6.47	4.24	8.74	45.01	42.64	43.44	43.92	43.67	42.69
Fe_2O_3	47.87	44.84	44.68	29.27	34.27	30.88	21.92	26.85	28.48	11.97	12.53	11.28	13.41	12.76	11.77
In_2O_3	17.04	14.84	14.54	10.59	11.53	11.08	7.48	9.02	8.54	0.85	0.81	0.96	1.04	0.89	0.73
CaO	0.20	0.35	0.30	0.19	0.31	0.45	0.25	0.22	026	bdl[2]	bdl	bdl	bdl	bdl	bdl
MgO	0.02	bdl	bdl	bdl	bdl	0.12	bdl	bdl	bdl	0.14	0.18	0.11	0.19	0.14	0.13
K_2O	0.28	bdl	bdl	0.20	bdl	bdl	bdl	bdl	0.17	0.98	1.14	1.04	1.07	1.04	1.19
Cl	0.70	0.32	0.37	0.50	0.47	0.52	0.62	0.61	0.54	0.51	0.47	0.52	0.61	0.49	0.45
Σ	88.35	74.14	72.90	66.92	68.71	58.68	48.19	52.29	62.52	101.88	100.81	98.08	99.57	100.15	103.55
H_2O[3]	5.24	3.40	3.06	5.42	4.61	3.53	3.36	3.35	4.86	12.99	12.90	12.86	12.71	12.72	14.47
$(NH_4)_2O$[4]	0.91	0.58	0.55	0.89	0.79	0.55	0.59	0.59	0.80	2.28	2.30	2.14	2.00	2.17	2.66
	apfu (mpfu), *B* = 3 basis (assuming all Si entering the *T*-site), unnormalized														
P	0.41	0.57	0.65	0.26	0.34	0.48	0.51	0.44	0.35	0.04	0.04	0.05	0.04	0.03	0.03
S	1.46	1.33	1.22	1.71	1.56	1.40	1.43	1.50	1.63	1.59	1.50	1.72	1.82	1.64	1.33
Si	0.14	0.09	0.13	0.03	0.10	0.12	0.06	0.06	0.03	0.37	0.46	0.24	0.14	0.33	0.57
Ti	0.10	0.15	0.16	0.07	0.09	0.14	0.11	0.10	0.08	0.01	0.01	0.01	0.01	0.01	0.01
Al	0.77	0.58	0.62	1.62	1.45	1.03	1.80	1.20	1.77	3.18	2.94	3.25	3.45	3.21	2.59
Fe	5.42	7.93	8.45	3.44	4.59	5.36	3.91	4.84	3.69	0.54	0.55	0.54	0.67	0.60	0.46
In	1.11	1.51	1.58	0.72	0.89	1.11	0.77	0.94	0.64	0.02	0.02	0.03	0.03	0.02	0.02
Ca	0.03	0.09	0.08	0.03	0.06	0.11	0.06	0.06	0.05	bdl	bdl	bdl	bdl	bdl	bdl
Mg	bdl	bdl	bdl	bdl	bdl	0.04	bdl	bdl	bdl	0.01	0.02	0.01	0.02	0.01	0.01
K	0.05	bdl	bdl	0.04	bdl	bdl	bdl	bdl	0.04	0.08	0.09	0.08	0.09	0.08	0.08
Cl	0.18	0.13	0.16	0.13	0.14	0.20	0.25	0.25	0.16	0.05	0.05	0.06	0.07	0.05	0.04
NH_4[5]	0.91	0.91	0.92	0.93	0.94	0.85	0.94	0.94	0.91	0.91	0.90	0.91	0.89	0.90	0.91
OH[5]	5.26	5.33	5.13	5.65	5.48	5.43	5.30	5.35	5.58	5.20	5.04	5.45	5.65	5.29	4.96
	end members [%]														
Ama[6]	7	4	4	23	16	9	19	12	22	76	73	75	72	74	76
Amj	52	50	47	47	50	44	41	50	45	13	14	12	14	14	13
Alu	0.4			1					1	6	7	7	7	7	6
Jar	3			2					2	1	1	1	1	1	1
Hua	0.3	0.4	0.3	1	1	1	1	1	1						
Caj	2	5	4	2	3	6	3	3	2						
Mgh	0.04					0.4				1	1	1	2	1	1
Mfh	0.3					2				0.2	0.2	0.1	0.3	0.2	0.1
Ais	11	10	9	10	10	9	8	10	8	1	1	1	1	1	0.5
Pis	0.6			0.4					0.3	0.04	0.1	0.1	0.1	0.1	0.04
Mis	0.1					0.4				0.01	0.01	0.01	0.01	0.01	0.01
Tte	1	2	2	1	1	2	2	1	1	0.2	0.3	0.2	0.2	0.3	0.4
Tpe	21	29	34	13	18	25	25	25	22	17	2	3	2	2	2

[1] – Na was measured but not detected (under the detection limit); [2] – below detection limit; [3] – exclusively OH-derived, backward-calculated from OH *mpfu* content assuming lacking H_3O^+ and H_2O molecules in the structure; [4] – backward-calculated from NH_4^+ *mpfu* content; 3 calculated by stoichiometry (filling the *A* site to the occupancy of 1); [5] – by charge balance; [6] – Ama – ammoniojarosite (and hydroniumjarosite), Amj – ammonioalunite (and schlossmacherite), Alu – alunite, Jar – jarosite, Mgh – "magnesiohuangite" HEM, Mfh – "magnesioferrihuangite" HEM, Ags – "ammonium gallium sulfate" HEM, Pgs – "potassium gallium sulfate" HEM, Mgs – "magnesium gallium sulfate" HEM, Tte – total Ti-dominant end-members, Tpe – total P-dominant end-members

Table ST25. Shapiro-Wilk (S-W) normality test results, indium experiment

	S-W	p-v
Cl	**0.95**	0.48
K_2O	0.72	**0.003**
MgO	0.70	**0.003**
CaO	**0.97**	0.90
Al_2O_3	0.84	**0.01**
Fe_2O_3	0.87	**0.03**
In_2O_3	0.77	**0.002**
SiO_2	**0.90**	0.10
TiO_2	0.85	**0.02**
P_2O_5	0.82	**0.006**
SO_3	0.82	**0.006**

p-v – the p-value; meaningful values are given in bold

Table ST26. Element correlation based on Kendall's τ coefficients and uncorrected ρ-values (given in the parentheses), indium experiment

	Cl	K_2O	CaO	Al_2O_3	Fe_2O_3	In_2O_3	SiO_2	TiO_2	P_2O_5	SO_3
Cl		**-0.42** (0.12)	**-0.48** (0.08)	0.07 (0.72)	-0.02 (0.92)	0.10 (0.62)	-0.22 (0.25)	-0.12 (0.55)	0.17 (0.37)	0.13 (051)
K_2O	**-0.42** (0.12)		**-0.33** (0.60)	0.23 (0.38)	**-0.42** (0.12)	**-0.54 (0.04)**	**0.70 (0.008)**	**-0.31** (0.24)	**-0.51** (0.05)	**0.41** (0.12)
CaO	**-0.48** (0.07)	**-0.33** (0.60)		**-0.39** (0.14)	0.14 (0.60)	0.08 (0.75)	0.22 (0.40)	**0.31** (0.24)	0.17 (0.53)	**-0.54 (0.04)**
Al_2O_3	0.07 (0.72)	0.23 (0.38)	**-0.39** (0.14)		**-0.60 (0002)**	**-0.58 (0.003)**	**0.36** (0.06)	**-0.73 (0.0001)**	**-0.68 (00004)**	**0.84 (0.00001)**
Fe_2O_3	-0.02 (0.92)	**-0.42** (0.11)	0.14 (0.60)	**-0.60 (0.002)**		**0.88 (0.000004)**	**-0.38 (0.05)**	**0.77 (0.00006)**	**0.66 (0.0006)**	**-0.53 (0006)**
In_2O_3	0.10 (0.62)	**-0.54 (0.04)**	0.08 (0.75)	**-0.58 (0.003)**	**0.88 (0.000001)**		**-0.46 (0.02)**	**0.69 (0.0003)**	**0.70 (0.0003)**	**-0.45 (0.02)**
SiO_2	-0.22 (0.25)	**0.70 (0.008)**	0.22 (0.40)	**0.36** (0.06)	**-0.39 (0.05)**	**-0.46 (0.02)**		**-0.31** (0.11)	**-0.42 (0.03)**	**0.38 (0.05)**
TiO_2	0.12 (0.55)	**-0.31** (0.24)	**0.31** (0.24)	**-0.73 (0.0001)**	**0.77 (0.00006)**	**0.69 (0.0003)**	**-0.31** (0.11)		**0.68 (0.0004)**	**-0.68 (0.0004)**
P_2O_5	0.17 (0.37)	**-0.51** (0.05)	0.17 (0.53)	**-0.68 (0.0004)**	**0.66 (00006)**	**0.70 (0.0003)**	**-0.42 (0.03)**	**0.68 (0.0004)**		**-0.62 (0.001)**
SO_3	0.13 (0.51)	**0.41** (0.12)	**-0.54 (0.04)**	**0.84 (0.00001)**	**-0.53 (0.006)**	**-0.45 (0.02)**	**0.38 (0.05)**	**-0.68 (0.0004)**	**-0.62 (0.001)**	

Strong correlations are given in bold

Table ST27. Results of chemical analyses of AAJ contacting with a solution of KH_2AsO_4

	1	2	3	4	5	6	7	8	9	10	11	12	13	14	15
	high-As					medium-As			low-As[1]						
	[wt.%]														
As_2O_5	45.93	43.30	44.79	44.94	37.38	27.54	28.57	20.33	3.48	7.24	5.60	8.55	7.20	5.27	3.07
P_2O_5[2]	1.05	0.96	1.21	1.18	1.36	0.88	0.98	0.78	0.54	0.77	0.69	0.82	0.75	0.75	0.90
SO_3	**5.77**	**5.76**	**6.50**	**5.87**	11.48	**15.82**	**17.30**	**17.42**	**32.64**	**32.70**	**34.05**	**28.10**	**30.80**	31.60	**24.90**
SiO_2	0.15	bdl[3]	bdl	bdl	0.09	0.95	2.14	1.32	0.68	0.86	0.66	8.27	10.75	6.29	21.28
TiO_2	0.29	0.27	0.38	0.35	0.25	0.20	0.24	0.25	0.18	0.17	0.20	0.22	0.19	0.25	0.29
Al_2O_3	3.02	2.42	1.91	1.87	2.69	8.74	11.51	10.20	40.33	27.32	35.69	32.09	29.84	35.73	16.72
Fe_2O_3	29.81	27.58	31.32	30.77	32.14	27.06	30.21	25.05	13.55	15.41	15.58	13.02	14.21	12.80	16.05
MgO	0.09	0.09	bdl	bdl	0.14	bdl	0.12	bdl	bdl	bdl	bdl	0.13	0.16	0.18	bdl
CaO	0.39	0.22	0.32	bdl	0.15	0.27	0.35	0.38	0.17	0.11	0.19	0.17	0.12	0.12	0.14
K_2O	0.87	0.68	0.74	0.62	1.51	1.28	1.53	1.49	2.12	1.89	1.75	1.96	2.32	2.41	2.26
Na_2O	0.48	bdl	bdl	0.20	0.27	0.33	0.56	0.45	0.40	0.28	0.27	0.25	0.37	0.37	0.47
Cl	0.20	0.22	0.11	0.18	0.24	0.27	0.28	0.34	0.43	0.53	0.48	0.46	0.54	0.43	0.50
Σ	88.06	81.50	87.28	85.98	87.69	83.35	93.78	78.01	94.52	87.29	95.14	94.04	97.23	96.19	86.57
H_2O[4]	0.26	0.00	0.00	0.00	1.54	4.33	6.70	6.01	18.81	11.36	15.96	14.05	13.20	16.22	8.96
$(NH_4)_2O$[5]	2.58	2.83	3.21	3.19	2.64	3.34	3.62	3.11	6.77	5.02	6.51	5.33	4.77	5.54	2.92
	apfu (mpfu), *B* = 3 basis (assuming all Si entering the *T*-site), unnormalized														
As	2.75	2.85	2.69	2.75	2.13	1.40	1.23	1.03	0.09	0.26	0.16	0.28	0.25	0.16	0.15
P	0.10	0.10	0.12	0.12	0.13	0.07	0.07	0.06	0.02	0.04	0.03	0.04	0.04	0.04	0.07
S	0.50	0.54	0.56	0.52	0.94	1.16	1.07	1.26	1.27	1.68	1.42	1.32	1.51	1.37	1.75
Si	0.02				0.01	0.09	0.18	0.13	0.04	0.06	0.04	0.52	0.70	0.36	1.99
Ti	0.02	0.03	0.03	0.03	0.02	0.01	0.02	0.02	0.01	0.01	0.01	0.01	0.01	0.01	0.02
Al	0.41	0.36	0.26	0.26	0.34	1.00	1.12	1.16	2.46	2.20	2.34	2.37	2.29	2.43	1.85
Fe	2.57	2.62	2.71	2.71	2.63	1.98	1.87	1.82	0.53	0.79	0.65	0.62	0.70	0.56	1.13
Mg	0.04	0.04			0.05		0.03					0.03	0.03	0.03	
Ca	0.05	0.03	0.04		0.02	0.03	0.03	0.04	0.01	0.01	0.01	0.01	0.01	0.01	0.01
K	0.13	0.11	0.11	0.09	0.21	0.16	0.16	0.18	0.14	0.16	0.12	0.16	0.19	0.18	0.27
Na	0.11			0.04	0.06	0.06	0.09	0.08	0.04	0.04	0.03	0.03	0.05	0.04	0.09
Cl	0.04	0.05	0.02	0.04	0.04	0.04	0.04	0.06	0.04	0.06	0.05	0.05	0.06	0.04	0.08
NH_4[6]	0.68	0.82	0.85	0.86	0.66	0.75	0.69	0.69	0.81	0.79	0.84	0.77	0.72	0.74	0.63
OH[6]	0.20				1.12	2.81	3.68	3.87	6.50	5.17	5.92	5.88	5.74	6.25	5.60
	end members [%]														
Ama[7]	2	2	2	2	6	14	14	19	63	53	60	49	48	53	43
Amj	9	11	13	12	17	21	19	21	12	16	15	12	13	11	18
Alu	0.3	0.2	0.2	0.1	1	2	3	4	10	9	8	10	12	12	13
Jar	2	2	2	1	5	4	4	6	2	3	2	3	4	3	8
Naa	0.2			0.1	0.2	1	1	2	3	2	2	2	3	3	4
Naj	1			0.6	1	2	2	3	1	1	1	0.5	1	1	2
Hua	0.1	0.1	0.1		0.1	0.4	1	1	1	0.5	1	1	0.5	1	1
Caj	0.6	0.4	0.6		0.4	1	1	1	0.1	0.2	0.2	0.2	0.2	0.1	0.4
Mgh	0.1	0.1			0.2		0.5					2	2	2	
Mfh	0.5	0.5			1		0.9					0.5	1	1	
Aaa	8	8	6	6	5	13	13	11	4	7	6	10	7	6	3
Aaj	49	59	62	63	38	26	22	17	1	3	2	3	2	1	2
Aal	1	1	1	1	2	3	3	3	1	1	1	2	2	1	1
Aja	9	8	8	7	12	5	5	5	0.2	1	0.3	1	1	0.3	1
Ana	1			0.3	0.4	1	2	1	0.2	0.3	0.2	0.4	0.5	0.3	0.3
Anj	7			3	3	2	3	2	0.04	0.1	0.1	0.1	0.1	0.1	0.2

Cbe	0.6	0.4	0.6		0.4	1	1	1	0.1	0.2	0.2	0.2	0.2	0.1	0.4
Chi	0.6	0.3	0.3		0.1	0.5	0.6	0.6	0.1	0.1	0.1	0.1	0.1	0.1	0.1
Mbe	3	3			3		1					0.1	0.1	0.1	
Mhi	0.1	0.1			0.2		0.5					2	2	2	
Tpe	3	3	4	3	4	3	3	3	2	2	2	3	2	2	3
Tte	1	1	1	1	1	0.5	0.5	0.6	0.2	0.3	0.3	0.3	0.3	0.3	0.6

[1] – analyses 9-11: Si-low composition; analyses 12-14: Si-enriched composition, type 1; analysis 15: Si-enriched composition, type 2; [2] – Mn was measured but not detected (under the detection limit); [3] – below detection limit; [4] – exclusively OH-derived, backward-calculated from OH *mpfu* content assuming lacking H_3O^+ and H_2O molecules in the structure; [5] – backward-calculated from NH_4^+ *mpfu* content; 3 calculated by stoichiometry (filling the *A* site to the occupancy of 1); [6] – by charge balance; [7] – Ama – ammoniojarosite (and hydroniumjarosite), Amj – ammonioalunite (and schlossmacherite), Alu – alunite, Jar – jarosite, Naa – natroalunite, Naj – natrojarosite, Hua – huangite, Mgh – “magnesiohuangite” HEM, Mfh – “magnesioferrihuangite” HEM, Aaa – “arsenate ammoniojarosite” HEM, Aaj – “arsenate jarosite” HEM, Aal – “arsenate alunite” HEM, Aja – “arsenate jarosite” HEM, Ana – “arsenate natrojarosite”, Anj – “arsenate natrojarosite” HEM, Cbe – “calciobeudantite” HEM, Chi – “calciohidalgoite” HEM, Mbe – “magnesiobeudantite” HEM, Mhi – “magnesiohidalgoite” HEM

Table ST28. Shapiro-Wilk (S-W) normality test results, arsenic experiment

	S-W	p-v
SO_3	0.83	**0.01**
K_2O	**0.86**	**0.02**
CaO	**0.90**	0.12
Fe_2O_3	0.84	**0.01**
Na_2O	**0.97**	0.93
As_2O_5	**0.86**	**0.02**
Al_2O_3	**0.85**	**0.02**
SiO_2	**0.96**	0.79
MgO	**0.90**	0.40
Cl	**0.93**	0.24
P_2O_5	**0.97**	0.87
TiO_2	**0.95**	0.54

p-v – the p-values; meaningful values are given in bold

Table ST29. Element correlation based on Kendall's τ coefficients and uncorrected ρ-values (given in the parentheses), arsenic experiment

	SO_3	K_2O	CaO	Fe_2O_3	Na_2O	As_2O_5	Al_2O_3	SiO_2	MgO	Cl	P_2O_5	TiO_2
SO_3		**0.61 (0.002)**	**-0.46 (0.04)**	**-0.51 (0.01)**	-0.09 (0.68)	**-0.57 (0.004)**	**0.77 (0.0001)**	-0.07 (0.75)	**0.95 (0.02)**	**0.65 (0.001)**	**-0.55 (0.006)**	**-0.60 (0.003)**
K_2O	**0.61 (0.002)**		**-0.53 (0.02)**	**-0.63 (0.002)**	0.06 (0.78)	**-0.60 (0.003)**	**0.71 (0.0004)**	**0.37** (0.12)	**1 (0.01)**	**0.77 (0.0001)**	**-0.51 (0.01)**	**-0.47 (0.02)**
CaO	**-0.46 (0.04)**	**-0.53 (0.02)**		**0.50 (0.02)**	**0.38** (0.13)	**0.53** (0.10)	**-0.36** (0.10)	**-0.33** (0.18)	**-0.60** (0.14)	**-0.66 (0.003)**	**0.38** (0.08)	**0.45 (0.04)**
Fe_2O_3	**-0.51 (0.01)**	**-0.63 (0.002)**	**0.50 (0.02)**		0.28 (0.210	**0.60 (0.003)**	**-0.66 (0.001)**	-0.11 (0.64)	-0.20 (0.62)	**-0.63 (0.002)**	**0.74 (0.0002)**	**0.55 (0.006)**
Na_2O	-0.09 (0.68)	0.06 (0.78)	**0.38** (0.13)	0.28 (0.21)		0.15 (0.48)	0.02 (0.94)	-0.05 (0.82)	**-0.33** (0.50)	-0.06 (0.78)	0.23 (0.29)	0 (1)
As_2O_5	**-0.57 (0.004)**	**-0.60 (0.003)**	**0.53 (0.02)**	**0.60 (0.003)**	0.15 (0.48)		**-0.52 (0.009)**	-0.29 (0.21)	**-0.80 (0.05)**	**-0.64 (0.002)**	**0.71 (0.0004)**	**0.42 (0.03)**
Al_2O_3	**0.77 (0.0001)**	**0.71 (0.0004)**	**-0.36** (0.10)	**-0.66 (0.001)**	0.02 (0.94)	**-0.52 (0.009)**		-0.05 (0.82)	**0.80 (0.05)**	**0.60 (0.003)**	**-0.61 (0.002)**	**-0.63 (0.002)**
SiO_2	-0.07 (0.75)	**0.37 (**0.12)	**-0.33** (0.18)	-0.11 (0.64)	-0.05 (0.81)	-0.29 (0.21)	-0.05 (0.82)		**1 (0.04)**	0.29 (0.21)	0.02 (0.94)	-0.26 (0.26)
MgO	**0.95 (0.02)**	**1 (0.01)**	**-0.60** (0.14)	-0.20 (0.62)	**-0.33** (0.50)	**-0.80 (0.05)**	**0.80 (0.05)**	**1 (0.04)**		**0.80 (0.05)**	**-0.60** (0.14)	**-0.80 (0.05)**
Cl	**0.65 (0.001)**	**0.77 (0.0001)**	**-0.66 (0.003)**	**-0.63 (0.002)**	-0.06 (0.78)	**-0.64 (0.002)**	**0.60 (0.003)**	0.29 (0.21)	**0.80 (0.05)**		**-0.56 (0.005)**	**-0.57 (0.004)**
P_2O_5	**-0.55 (0.006)**	**-0.51 (0.01)**	**0.38** (0.08)	**0.74 (0.0002)**	0.23 (0.29)	**0.71 (0.0004)**	**-0.61 (0.002)**	0.02 (0.94)	**-0.60** (0.14)	**-0.56 (0.005)**		**0.61 (0.002)**
TiO_2	**-0.60 (0.003)**	**-0.47 (0.02)**	**0.45 (0.04)**	**0.55 (0.006)**	0 (1)	**0.42 (0.03)**	**-0.63 (0.002)**	0.26 (0.26)	**-0.80 (0.05)**	**-0.57 (0.004)**	**0.61 (0.002)**	

Strong correlations are given in bold

Table ST30. Results of chemical analyses of AAJ contacting with a solution of K_2SeO_3

	1	2	3	4	5	6	7	8	9	10
	high-Se				low-Se					
	[wt.%]									
P_2O_5	0.87	1.15	0.97	0.70	0.93	0.85	0.76	0.58	0.44	0.91
SO_3	6.54	2.36	2.32	8.58	20.05	22.71	25.63	31.98	25.04	12.37
SeO_2	20.47	36.60	36.05	44.86	3.07	4.16	2.90	3.27	3.85	5.11
SiO_2	5.05	0.47	0.37	0.03	40.19	1.69	27.81	10.79	23.79	46.80
TiO_2	0.43	0.63	0.58	0.53	0.28	0.40	0.13	0.23	0.14	0.18
Al_2O_3	4.92	11.87	10.34	4.81	15.48	15.01	18.80	28.63	15.32	6.42
Fe_2O_3	12.52	17.33	15.08	24.41	12.84	14.73	16.31	17.21	19.79	12.24
MgO	bdl[1]	0.12	0.11	0.12	0.14	0.11	bdl	0.19	0.23	bdl
CaO	0.26	1.61	1.34	0.14	0.45	0.24	0.22	0.17	bdl	0.17
K_2O	2.17	0.79	0.80	1.76	2.31	3.22	2.35	3.56	1.30	1.06
Na_2O	0.50	0.75	0.42	0.20	0.22	0.50	0.37	0.24	bdl	0.29
Cl	0.61	0.23	0.28	0.09	0.26	0.57	0.32	0.55	0.54	0.28
Σ	54.32	73.89	68.64	86.22	96.21	64.18	95.62	97.38	90.43	85.84
H_2O[2]	2.57	7.16	5.50	2.85	8.79	8.42	10.70	15.49	10.09	1.54
$(NH_4)_2O$[3]	0.51	1.99	1.90	2.16	2.19	1.74	3.27	4.25	3.73	1.54
apfu (mpfu), *B* = 3 basis (assuming Si absent at the *T*-site), unnormalized										
P	0.14	0.11	0.10	0.07	0.08	0.07	0.06	0.03	0.03	0.14
S	0.95	0.19	0.22	0.79	1.61	1.76	1.67	1.54	1.71	1.65
Se	2.14	2.16	2.44	2.98	0.18	0.23	0.14	0.11	0.19	0.49
Ti	0.06	0.05	0.06	0.05	0.02	0.03	0.01	0.01	0.01	0.02
Al	1.12	1.53	1.52	0.70	1.95	1.83	1.92	2.16	1.64	1.34
Fe	1.82	1.42	1.42	2.26	1.03	1.14	1.07	0.83	1.35	1.63
Mg		0.04	0.04	0.05	0.05	0.04		0.04	0.07	
Ca	0.05	0.19	0.18	0.02	0.05	0.03	0.02	0.01		0.03
K	0.53	0.11	0.13	0.28	0.31	0.42	0.26	0.29	0.15	0.24
Na	0.19	0.16	0.10	0.05	0.04	0.10	0.06	0.03		0.10
Cl	0.20	0.04	0.06	0.02	0.05	0.10	0.05	0.06	0.08	0.08
NH_4[4]	0.23	0.50	0.55	0.61	0.54	0.41	0.66	0.63	0.78	0.63
OH[5]	3.31	5.21	4.59	2.34	6.26	5.79	6.20	6.61	6.11	5.29
	end members [%]									
Ama[6]	2	2	2	3	30	21	38	41	38	20
Amj	4	2	2	9	16	13	21	16	31	25
Alu	6	0.4	1	1	18	22	15	19	7	8
Jar	9	0.4	0.5	4	9	14	8	7	6	9
Naa	2	1	0.4	0.2	2	5	4	2		3
Naj	3	1	0.4	1	1	3	2	1		4
Hua	1	1	1	0.1	3	1	1	1		1
Caj	1	1	1	0.3	2	1	1	0.3		1
Mgh		0,2	0,2	0,2	3	2		3	3	
Mfh		0.2	0.2	1	1	1		1	3	
Saa	6	22	25	11	3	3	3	3	4	6
Saj	9	21	23	36	2	2	2	1	3	7
Sea	13	5	6	5	2	3	1	1	1	2
Sej	21	5	5	16	1	2	1	1	1	3
Sna	5	7	5	1	0.3	1	0.3	0.1		1
Snj	7	7	4	3	0.1	0.4	0.2	0.1		1
Shu	1	8	8	0.3	0.3	0.2	0.1	0.1		0.3
Smh		2	2	1	03	0.3		0.2	0.4	
Fsh	2	8	8	1	0.2	0.1	0.1	0.02		0.4
Mis		2	2	3	0.2	0.2		0.1	0.3	

Tpe	4	4	4	2	5	4	3	2	2	6
Tte	2	2	2	2	1	1	0.3	0.4	0.3	1

[1] – below detection limit; [2] – exclusively OH-derived, backward-calculated from OH *mpfu* content assuming lacking H_3O^+ and H_2O molecules in the structure; [3] – backward-calculated from NH_4^+ *mpfu* content; [4] – calculated by stoichiometry (filling the *A* site to the occupancy of 1); [5] – by charge balance; [6] – Ama – ammoniojarosite (and hydroniumjarosite), Amj – ammonioalunite (and schlossmacherite), Alu – alunite, Jar – jarosite, Naa – natroalunite, Naj – natrojarosite, Hua – huangite, Mgh – "magnesiohuangite" HEM, Mfh – "magnesioferrihuangite" HEM, Saa – "selenoammonioalunite" HEM, Saj – "selenoammoniojarosite" HEM, Sea – "selenoalunite" HEM, "Sej" – selenojarosite HEM, Sna – "selenonatroalunite" HEM, Snj – "selenonatrojarosite" HEM, Shu – "selenohuangite" HEM, Smh – "selenomagnesiohuangite" HEM, Fsh – "ferriselenohuangite" HEM, Mis – "magnesium iron selenite" HEM, Tpe – total P-dominant HEM, Tte – total Ti-dominant HEM

Table ST31. Shapiro-Wilk (S-W) normality test results, selenium experiment

	S-W	p-v
SO_3	**0.86**	0.09
K_2O	**0.92**	0.39
CaO	0.82	**0.03**
Fe_2O_3	**0.94**	0.55
Na_2O	**0.95**	074
SeO_2	0.79	**0.01**
Al_2O_3	**0.93**	0.42
SiO_2	**0.90**	0.22
MgO	**0.86**	0.14
Cl	**0.86**	0.08
P_2O_5	**0.93**	0.46
TiO_2	**0.91**	0.29

p-v – the p-values; meaningful values are given in bold

Table ST32. Element correlation based on Kendall's τ coefficients and uncorrected ρ-values (given in the parentheses), selenium experiment

	SO_3	K_2O	CaO	Fe_2O_3	Na_2O	SeO_2	Al_2O_3	SiO_2	MgO	Cl	P_2O_5	TiO_2
SO_3		**0.64 (0.01)**	**-0.42** (0.11)	0.16 (0.52)	-0.29 (0.28)	**-0.68 (0.006)**	**0.61 (0.01)**	**0.31** (0.21)	**0.55** (0.08)	**0.30** (0.24)	**-0.58(0.02)**	**-0.67 (0.007)**
K_2O	**0.64 (0.01)**		**-0.31** (0.24)	0.07 (0.78)	-0.17 (0.52)	**-0.50 (0.04)**	**0.39** (0.12)	0.14 (0.59)	0.25 (0.43)	**0.39** (0.12)	**-0.40** (0.10)	**-0.40** (0.10)
CaO	**-0.42** (0.11)	**-0.31** (0.24)		-0.08 (0.75)	**0.54 (0.04)**	0.08 (0.75)	0.06 (0.83)	-0.17 (0.53)	-0.28 (0.43)	0.03 (0.92)	**0.72 (0.007)**	**0.44** (0.10)
Fe_2O_3	0.16 (0.52)	0.07 (0.78)	-0.08 (0.75)		-0.17 (0.52)	0.16 (0.52)	0.16 (0.52)	**-0.40** (0.10)	0.25 (0.43)	-0.25 (0.31)	**-0.36** (0.15)	0.09 (0.72)
Na_2O	-0.29 (0.28)	-0.17 (052)	**0.54 (0.04)**	0.17 (0.52)		0.17 (0.52)	-0.03 (0.92)	-0.20 (0.46)	-0.14 (0.70)	**0.34** (0.20)	**0.37** (0.17)	0.20 (0.46)
SeO_2	**-0.68 (0.006)**	**-0.50 (0.04)**	0.08 (0.75)	0.16 (0.52)	0.17 (0.52)		**-0.70 (0.004)**	**-0.63 (0.01)**	**-0.35** (0.27)	-0.25 (0.31)	0.27 (0.28)	**0.63 (0.01)**
Al_2O_3	**0.61 (0.01)**	**0.39** (0.12)	0.06 (0.83)	0.16 (0.52)	-0.03 (0.92)	**-0.70 (0.005)**		**0.36** (0.15)	**0.55** (0.08)	0.20 (0.41)	-0.18 (0.47)	**-0.45** (0.07)
SiO_2	**0.31** (0.21)	0.13 (0.59)	-0.17 (0.53)	**-0.40** (0.10)	-0.20 (0.46)	**-0.63 (0.01)**	**0.36** (0.15)		**0.49** (0.12)	0.04 (0.86)	-0.07 (0.79)	**-0.60 (0.02)**
MgO	**0.55** (0.08)	0.25 (0.43)	-0.28 (0.44)	0.25 (0.43)	-0.14 (0.70)	**-0.35** (0.27)	**0.55** (0.08)	**0.49** (0.12)		0.10 (0.76)	**-0.59** (0.06)	**-0.68 (0.03)**
Cl	**0.30** (0.23)	**0.39** (0.12)	0.03 (0.92)	-0.25 (0.31)	**0.34** (0.20)	-0.25 (0.31)	0.20 (0.41)	0.04 (0.86)	0.10 (0.76)		-0.27 (0.28)	-0.18 (0.47)
P_2O_5	**-0.58 (0.02)**	**-0.40** (0.10)	**0.72 (0.007)**	**-0.36** (0.15)	**0.37** (0.17)	0.27 (0.28)	-0.18 (0.47)	-0.07 (0.79)	**-0.59** (0.06)	-0.27 (0.28)		**0.47** (0.06)
TiO_2	**-0.67 (0.007)**	**-0.40** (0.10)	**0.44** (0.10)	0.09 (0.72)	0.20 (0.46)	**0.63 (0.01)**	**-0.45** (0.07)	**-0.60 (0.02)**	**-0.68 (0.03)**	-0.18 (0.47)	**0.47** (0.06)	

Strong correlations are given in bold

Table ST33. Results of chemical analyses of AAJ contacting with a solution of $LaCl_3 \cdot 7H_2O$

	1	2	3	4	5	6	7	8	9	10	11
						[wt.%]					
P_2O_5[1]	0.45	0.42	0.39	0.46	0.37	0.36	0.33	0.35	0.39	0.32	0.41
SO_3	37.96	36.79	36.85	35.73	36.17	37.30	36.89	35.57	36.73	38.53	35.51
SiO_2	0.13	0.81	0.18	0.19	0.33	0.21	0.10	0.31	1.42	0.37	0.17
TiO_2	0.19	0.21	0.24	0.22	0.20	0.20	0.24	0.27	0.21	0.19	0.20
Al_2O_3	25.94	18.94	20.98	16.48	18.34	21.30	24.93	18.42	17.93	27.50	22.56
Fe_2O_3	26.71	32.00	30.79	33.95	32.21	29.44	25.85	31.73	32.77	28.59	28.12
La_2O_3	0.20	0.22	0.17	0.18	0.17	0.20	bdl[2]	0.18	bdl	0.22	0.21
MgO	0.07	0.05	0.06	0.07	0.07	0.05	0.04	0.06	0.06	0.04	0.06
CaO	0.06	0.11	0.04	0.09	0.10	0.12	0.07	0.05	0.05	0.06	0.06
K_2O	0.60	0.44	0.63	0.45	0.53	0.68	0.73	0.42	0.50	0.61	0.54
Na_2O	0.22	0.17	0.12	0.14	0.17	0.19	0.25	0.16	0.18	0.23	0.17
Cl	0.50	0.48	0.45	0.49	0.45	0.36	0.41	0.51	0.50	0.48	0.53
Σ	93.03	90.64	90.80	88.44	89.10	90.41	89.82	88.02	90.73	97.14	88.55
H_2O[3]	16.67	14.42	15.49	14.30	14.58	15.11	16.05	14.62	13.75	18.06	15.75
$(NH_4)_2O$[4]	2.32	2.15	2.21	2.08	2.10	2.14	2.21	2.12	2.12	2.48	2.20
apfu (mpfu), *B* = 3 basis (assuming all Si entering the *T*-site)											
P	0.02	0.02	0.02	0.02	0.02	0.02	0.02	0.02	0.02	0.02	0.02
S	1.69	1.78	1.74	1.79	1.78	1.78	1.70	1.76	1.81	1.61	1.67
Si	0.01	0.05	0.01	0.01	0.02	0.01	0.01	0.02	0.09	0.02	0.01
Ti	0.01	0.01	0.01	0.01	0.01	0.01	0.01	0.01	0.01	0.01	0.01
Al	1.81	1.44	1.55	1.30	1.41	1.59	1.81	1.43	1.38	1.80	1.67
Fe	1.19	1.56	1.45	1.70	1.59	1.41	1.19	1.57	1.62	1.20	1.33
La	0.004	0.01	0.004	0.004	0.004	0.01		0.004		0.004	0.01
Mg	0.01		0.01	0.01	0.01	0.01		0.01	0.01		0.01
Ca		0.01		0.01	0.01	0.01					
K	0.05	0.04	0.05	0.04	0.04	0.06	0.06	0.04	0.04	0.04	0.04
Na	0.03	0.02	0.01	0.02	0.02	0.02	0.03	0.02	0.02	0.02	0.02
Cl	0.05	0.05	0.05	0.06	0.05	0.04	0.04	0.06	0.06	0.05	0.06
NH_4[5]	0.91	0.92	0.92	0.93	0.92	0.90	0.91	0.93	0.93	0.92	0.92
OH[5]	6.58	6.21	6.48	6.36	6.36	6.40	6.57	6.42	6.01	6.70	6.60
end members [%]											
Ama[6]	54	44	47	39	43	47	54	44	42	55	51
Amj	36	47	44	52	48	42	36	48	49	36	40
Alu	3	2	3	2	2	3	3	2	2	3	2
Jar	2	2	2	2	2	2	2	2	2	2	2
Naa	2	1	1	1	1	1	2	1	1	1	1
Naj	1	1	1	1	1	1	1	1	1	1	1
Hua	<1	<1	<1	<1	<1	<1	<1	<1	<1	<1	<1
Caj	<1	<1	<1	<1	<1	<1	<1	<1	<1	<1	<1
Mgh	<1	<1	<1	<1	<1	<1	<1	<1	<1	<1	<1
Mfh	<1	<1	<1	<1	<1	<1	<1	<1	<1	<1	<1

[1] – Mn was measured but not detected (under the detection limit); [2] – below detection limit; [3] – exclusively OH-derived, backward-calculated from OH *mpfu* content assuming lacking H_3O^+ and H_2O molecules in the structure; [4] – backward-calculated from NH_4^+ *mpfu* content; 3 calculated by stoichiometry (filling the *A* site to the occupancy of 1); [5] – by charge balance; [6] Ama – ammoniojarosite (and hydroniumjarosite), Amj – ammonioalunite (and schlossmacherite), Alu – alunite, Jar – jarosite, Naa – natroalunite, Naj – natrojarosite, Hua – huangite, Caj – "calciojarosite" HEM, Mgh – "magnesiohuangite" HEM, Mfh – "magnesioferrihuangite" HEM

Table ST34. Shapiro-Wilk (S-W) normality test results, lanthanum experiment

	S-W	p-v
Cl	**0.95**	0.75
Na_2O	**0.85**	0.12
K_2O	**0.95**	0.69
MgO	0.70	**0.01**
CaO	0.73	**0.007**
Al_2O_3	**0.85**	0.13
Fe_2O_3	**0.90**	0.30
La_2O_3	**0.98**	0.94
Ce_2O_3	0.74	**0.03**
SiO_2	0.73	**0.007**
TiO_2	**0.81**	**0.05**
P_2O_5	**0.87**	0.19
SO_3	**0.90**	0.33

p-v – the p-values; meaningful values are given in bold

Table ST35. Element correlation based on Kendall's τ coefficients and uncorrected ρ-values (given in the parentheses), lanthanum experiment

	Cl	Na_2O	K_2O	MgO	CaO	Al_2O_3	Fe_2O_3	La_2O_3	SiO_2	TiO_2	P_2O_5	SO_3
Cl		-0.10 (0.68)	**-0.44** (0.06)	**0.31** (0.18)	**-0.34** (0.14)	-0.14 (0.56)	0.10 (0.67)	0.18 (0.49)	0.08 (0.74)	-0.04 (0.87)	**0.35** (0.13)	**-0.33** (0.16)
Na_2O	-0.10 (0.68)		**0.43** (0.07)	**-0.41** (0.08)	0.22 (0.35)	**0.54 (0.02)**	**-0.54 (0.02)**	**0.53 (0.05)**	-0.04 (0.88)	**-0.36** (0.12)	**-0.34** (0.15)	**0.55 (0.02)**
K_2O	**-0.44** (0.06)	**0.43** (0.07)		-0.15 (0.52)	0 (1)	**0.50 (0.03)**	**-0.51 (0.03)**	0 (1)	**-0.40** (0.08)	-0.15 (0.51)	**-0.30** (0.20)	**0.40** (0.08)
MgO	**0.31** (0.18)	**-0.41** (0.08)	-0.15 (0.52)		-0.10 (0.69)	-0.26 (0.26)	**0.30** (0.19)	**-0.51** (0.06)	-0.17 (0.48)	-0.13 (0.56)	**0.58 (0.01)**	-0.15 (0.52)
CaO	**-0.34** (0.14)	0.22 (0.35)	0 (1)	-0.10 (0.69)		-0.04 (0.88)	0.04 (0.87)	0.26 (0.33)	0.09 (0.70)	-0.25 (0.29)	0.02 (0.94)	0.11 (0.65)
Al_2O_3	-0.13 (0.56)	**0.54 (0.02)**	**0.50 (0.03)**	-0.26 (0.26)	-0.04 (0.88)		**-0.85 (0.0003)**	**0.41** (0.12)	**-0.37 (0.12)**	**-0.38** (0.10)	-0.26 (0.26)	**0.55 (0.02)**
Fe_2O_3	0.10 (0.67)	**-0.54 (0.02)**	**-0.51 (0.03)**	**0.30** (0.19)	0.04 (0.87)	**-0.85 (0.0003)**		**-0.33** (0.22)	**0.52 (0.02)**	0.19 (0.41)	0.27 (0.25)	**-0.41** (0.08)
La_2O_3	0.18 (0.49)	**0.53 (0.05)**	0 (1)	**-0.51** (0.06)	0.26 (0.33)	**0.41** (0.12)	**-0.32** (0.22)		0.20 (0.45)	-0.36 (0.17)	-0.12 (0.66)	0.19 (0.47)
SiO_2	0.08 (0.74)	-0.04 (0.88)	**-0.40** (0.08)	-0.17 (0.48)	0.09 (0.70)	**-0.37** (0.12)	**0.52 (0.02)**	0.20 (0.45)		-0.13 (0.57)	-0.09 (0.69)	0.06 (0.79)
TiO_2	-0.04 (0.87)	**-0.36** (0.12)	-0.15 (0.51)	-0.13 (0.56)	-0.25 (0.29)	**-0.38** (0.10)	0.19 (0.41)	**-0.36** (0.17)	-0.13 (0.57)		-0.06 (0.80)	**-0.57 (0.01)**
P_2O_5	**0.35** (0.13)	**-0.34** (0.15)	**-0.30** (0.20)	**0.58 (0.01)**	0.02 (0.94)	-0.26 (0.26)	0.27 (0.25)	-0.12 (0.66)	-0.09 (0.69)	-0.06 (0.80)		-0.24 (0.31)
SO_3	**-0.33** (0.16)	**0.55 (0.02)**	**0.40** (0.08)	-0.15 (0.52)	0.11 (0.65)	**0.55 (0.02)**	**-0.41** (0.08)	0.19 (0.47)	0.06 (0.79)	**-0.57 (0.01)**	-0.24 (0.31)	

Strong correlations are given in bold

Table ST36. Results of chemical analyses of AAJ contacting with a solution of $CeCl_3 \cdot 7H_2O$

	1	2	3	4	5	6	7
				[wt.%]			
P_2O_5[1]	0.46	1.54	1.25	0.66	0.62	0.48	0.85
SO_3	37.93	33.77	33.39	37.43	32.29	36.60	26.93
SiO_2	0.11	0.17	0.04	0.81	1.25	5.56	1.70
TiO_2	0.18	0.14	0.14	0.14	0.16	0.29	0.22
Al_2O_3	28.50	11.69	11.84	46.98	20.55	46.11	19.46
Fe_2O_3	24.73	35.13	32.83	11.10	15.96	11.49	18.17
La_2O_3	0.27	0.69	0.55	0.11	bdl[2]	bdl	0.45
Ce_2O_3	bdl	1.74	1.53	bdl	0.38	bdl	1.73
MgO	0.05	bdl	0.05	0.05	0.06	0.09	bdl
CaO	0.06	0.04	0.07	0.02	0.05	0.04	0.19
K_2O	0.80	0.67	0.81	0.99	0.58	0.68	1.32
Na_2O	0.18	0.79	0.76	0.41	0.21	0.28	0.35
Cl	0.48	0.29	0.33	0.53	0.39	0.55	0.42
Σ	93.74	86.65	83.56	99.22	72.50	102.18	71.28
H_2O[3]	17.44	12.15	11.62	22.79	9.99	19.89	11.27
$(NH_4)_2O$[4]	2.37	1.52	1.42	2.86	1.60	2.91	1.43
apfu (mpfu), *B* =3 basis (assuming all Si entering the *T*-site)							
P	0.02	0.10	0.08	0.03	0.04	0.02	0.03
S	1.64	1.89	1.94	1.32	2.01	1.31	1.65
Si	0.01	0.01		0.04	0.10	0.26	0.14
Ti	0.01	0.01	0.01	0.01	0.01	0.01	0.01
Al	1.93	1.03	1.08	2.61	2.01	2.59	1.87
Fe	1.07	1.97	1.92	0.39	0.99	0.41	1.12
La	0.01	0.02	0.02				0.01
Ce		0.05	0.04		0.01		0.05
Mg			0.01		0.01	0.01	
Ca			0.01				0.02
K	0.06	006	0.08	0.06	0.06	0.04	0.08
Na	0.02	0.11	0.11	0.04	0.03	0.03	0.06
Cl	0.05	0.04	0.04	0.04	0.06	0.04	0.06
NH_4[5]	0.91	0.75	0.73	0.90	0.88	0.92	0.78
OH[5]	6.68	6.04	6.01	7.15	5.52	6.32	6.13
				end members [%]			
Ama[6]	59	28	28	78	60	80	47
Amj	33	53	50	12	30	13	28
Alu	4	2	3	5	4	4	5
Jar	2	4	5	1	2	1	3
Naa	1	4	4	3	2	2	4
Naj	1	8	8	1	1	<1	2
Hua	<1	<1	<1	<1	<1	<1	1
Caj	<1	<1	<1	<1	<1	<1	1
Flc		0.1	0.1				0.1
Ffc		0.2	0.1				0.1
Mgh	<1		<1	<1	1	1	
Mfh	<1		<1		<1	<1	

[1] – Mn was measured but not detected (under the detection limit); [2] – below detection limit; [3] – exclusively OH-derived, backward-calculated from OH *mpfu* content assuming lacking H_3O^+ and H_2O molecules in the structure; [4] – backward-calculated from NH_4^+ *mpfu* content; 3 calculated by stoichiometry (filling the *A* site to the occupancy of 1); [5] – by charge balance; [6] – Ama – ammoniojarosite (and hydroniumjarosite), Amj – ammonioalunite (and schlossmacherite), Alu – alunite, Jar – jarosite, Naa – natroalunite, Naj – natrojarosite, Hua – huangite, Caj – "calcio-jarosite" (hypothetical end member), Flc – florencite-(Ce), Ffc – "ferriflorencite-(Ce)" HEM, Mgh – "magnesiohuangite" HEM, Mgj – "magnesioferrihuangite" HEM

Table ST37. Shapiro-Wilk (S-W) normality test results, cerium experiment

	S-W	p-v
Cl	**0.95**	0.75
Na_2O	**0.85**	0.12
K_2O	**0.95**	0.69
MgO	0.70	**0.007**
CaO	0.72	**0.007**
Al_2O_3	**0.85**	0.13
Fe_2O_3	**0.90**	0.30
La_2O_3	**0.98**	0.94
Ce_2O_3	0.74	**0.03**
SiO_2	0.73	**0.007**
TiO_2	0.81	**0.04**
P_2O_5	**0.87**	0.19
SO_3	**0.90**	0.33

p-v – the p-values; meaningful values are given in bold

Table ST38. Element correlation based on Kendall's τ coefficients and uncorrected ρ-values (given in the parentheses), cerium experiment

	Cl	Na_2O	K_2O	MgO	CaO	Al_2O_3	Fe_2O_3	La_2O_3	SiO_2	TiO_2	P_2O_5	SO_3
Cl		**-0.43** (0.18)	0.20 (0.54)	0.20 (0.62)	-0.14 (0.65)	**0.88 (0.006)**	**-0.62 (0.05)**	**-1 (0.01)**	**0.43** (0.18)	**0.49** (0.12)	**-0.62 (0.05)**	0.25 (0.43)
Na_2O	**-0.43** (0.18)		0.20 (0.54)	-0.20 (0.62)	-0.24 (0.45)	**-0.49** (0.12)	0.24 (0.45)	**0.60** (0.14)	-0.24 (0.45)	**-0.49** (0.12)	**0.81 (0.01**	-0.15 (0.64)
K_2O	0.20 (0.54)	0.20 (0.54)		**-0.80 (0.05)**	0.10 (0.76)	0.15 (0.64)	-0.10 (0.76)	**-0.53** (0.20)	-0.29 (0.36)	-0.25 (0.43)	0 (1)	**0.41** (0.20)
MgO	0.20 (0.62)	-0.20 (0.62)	**-0.80 (0.05)**		-0.20 (0.62)	0.11 (0.80)	-0.20 (0.62)	**0.33** (0.60)	**0.60** (0.14)	**0.60** (0.14)	**-0.40** (0.33)	**-0.32** (0.44)
CaO	-0.14 (0.65)	-0.24 (0.45)	0.10 (0.76)	-0.20 (0.62)		-0.29 (0.36)	**0.33** (0.29)	0.20 (0.62)	-0.14 (0.65)	0.20 (0.54)	-0.05 (0.88)	**-0.45** (0.16)
Al_2O_3	**0.88 (0.006)**	**-0.49** (0.12)	0.15 (0.64)	0.11 (0.80)	-0.30 (0.36)		**-0.78 (0.01)**	**-1 (0.01)**	0.29 (0.36)	**0.35** (0.27)	**-0.68 (0.03)**	**0.41** (0.19)
Fe_2O_3	**-0.62 (0.05)**	0.24 (0.45)	-0.10 (0.76)	-0.20 (0.62)	**0.33** (0.29)	**-0.78 (0.01)**		**0.80 (0.05)**	**-0.43** (0.18)	-0.29 (0.36)	**0.43** (0.18)	-0.25 (0.43)
La_2O_3	**-1 (0.01)**	**0.60** (0.14)	**-0.52** (0.20)	**0.33** (0.60)	0.20 (0.62)	**-1 (0.01**	**0.80 (0.05)**		-0.20 (0.62)	-0.11 (0.80)	**0.80 (0.05)**	**-0.45** (0.27)
SiO_2	**0.43** (0.18)	-0.24 (0.45)	**0.30** (0.36)	**0.60** (0.14)	-0.14 (0.65)	0.29 (0.36)	**-0.43** (0.17)	-0.20 (0.62)		**0.68 (0.03)**	-0.24 (0.45)	-0.25 (0.43)
TiO_2	**0.49** (0.12)	**-0.49** (0.12)	-0.25 (0.43)	**0.60** (0.14)	0.20 (0.54)	**0.35** (0.27)	-0.29 (0.36)	-0.11 (0.80)	**0.68 (0.03)**		**-0.49** (0.12)	-0.10 (0.75)
P_2O_5	**-0.62 (0.05)**	**0.81 (0.01)**	0 (1)	**-0.40** (0.33)	-0.05 (0.88)	**-0.68 (0.03)**	**0.43** (0.18)	**0.80 (0.05)**	-0.24 (0.45)	**-0.49** (0.12)		**-0.35** (0.27)
SO_3	0.25 (0.43)	-0.15 (0.64)	**0.41** (0.20)	**-0.32** (0.44)	**-0.45** (0.16)	**0.41** (0.20)	-0.25 (0.43)	**-0.45** (0.27)	-0.25 (0.43)	-0.10 (0.75)	**-0.35** (0.27)	

Strong correlations are given in bold

Table ST39. Results of chemical analyses of AAJ contacting with a solution of $PrCl_3 \cdot 6H_2O$

	1	2	3	4	5	6	7	8	9
					[wt.%]				
P_2O_5[1]	5.19	7.16	6.20	2.67	4.10	3.37	6.08	5.20	6.33
SO_3[2]	19.37	20.07	16.98	14.39	19.62	29.39	20.46	21.15	19.28
SiO_2	1.23	1.57	1.93	1.05	2.42	0.18	bdl	bdl	0.96
TiO_2	0.89	0.97	0.86	0.55	0.85	0.70	1.07	0.89	0.83
Al_2O_3	7.09	9.04	7.18	4.09	8.79	8.61	7.85	8.29	7.21
Fe_2O_3	25.73	26.98	23.77	19.09	21.64	35.47	27.50	26.54	27.39
Pr_2O_3	3.12	2.98	2.68	1.66	2.88	4.05	4.10	3.54	2.82
MgO	bdl	0.10	bdl	bdl	0.09	bdl	bdl	bdl	bdl
CaO	0.29	0.25	0.24	bdl	0.23	0.20	0.23	bdl	0.27
K_2O	bdl	0.02	bdl	bdl	bdl	0.19	bdl	bdl	bdl
Cl	0.67	0.74	0.91	1.04	0.72	0.50	0.51	0.43	0.97
Σ	63.59	69.94	60.80	44.88	61.50	82.77	67.99	66.43	66.20
H_2O[3]	8.08	8.78	7.43	5.51	7.83	11.14	8.85	8.84	8.23
$(NH_4)_2O$[4]	1.20	1.36	1.17	0.89	1.15	1.58	1.28	1.33	1.29
apfu (mpfu), *B* = 3 basis (assuming all Si entering the *T*-site)									
P	0.46	0.57	0.58	0.35	0.38	0.23	0.50	0.43	0.54
S	1.54	1.43	1.42	1.65	1.62	1.77	1.50	1.57	1.46
Si	0.13	0.15	0.21	0.16	0.27	0.01			0.10
Ti	0.07	0.07	0.07	0.06	0.07	0.04	0.08	0.07	0.06
Al	0.88	1.01	0.94	0.74	1.14	0.81	0.90	0.96	0.86
Fe	2.05	1.92	1.99	2.20	1.79	2.14	2.02	1.97	2.08
Pr	0.12	0.10	0.11	0.09	0.12	0.12	0.15	0.13	0.10
Ca	0.03	0.03	0.03		0.03	0.02	0.02		0.03
Mg		0.01			0.02				
K						0.02			
Cl	0.12	0.12	0.17	0.27	0.13	0.07	0.08	0.07	0.17
NH_4[5]	0.85	0.86	0.86	0.91	0.84	0.84	0.83	0.87	0.87
OH[5]	5.69	5.54	5.51	5.63	5.74	5.97	5.76	5.82	5.53
					end members [%]				
Ama[6]	28	31	30	25	36	26	28	32	27
Amj	65	60	63	73	56	68	63	65	66
Alu		<1				1			
Jar		<1				2			
Flp	1	2	2	1	1	1	2	1	1
Ffp	3	3	3	2	2	1	4	3	3
Hua	1	1	1		1	1	1		1
Caj	3	2	2		2	1	2		2
Mgh		1			1				
Mfh		1			1				

[1] – Na and Mn were measured but not detected (under the detection limits); [2] – wt.% of P_2O_5 and SO_3 were backward-calculated from stoichiometry-derived *apfu*(P) and *apfu*(S) due to wrong contents obtained directly from WDS analysis; [3] – exclusively OH-derived, backward-calculated from OH *mpfu* content assuming lacking H_3O^+ and H_2O molecules in the structure; [4] – backward-calculated from NH_4^+ *mpfu* content; 3 calculated by stoichiometry (filling the *A* site to the occupancy of 1); [5] – by charge balance; [6] – Ama – ammoniojarosite (and hydroniumjarosite), Amj – ammonioalunite (and schlossmacherite), Alu – alunite, Jar – jarosite, Naa – natroalunite, Naj – natrojarosite, Hua – huangite, Caj – "calciojarosite" HEM, Mga – "magnesiohuangite" HEM, Mfh – "magnesioferrihuangite" HEM

Table ST40. Shapiro-Wilk (S-W) normality test results, praseodymium experiment

	S-W	p-v
Cl	**0.93**	0.57
CaO	**0.95**	0.73
Al_2O_3	0.74	**0.004**
Fe_2O_3	**0.94**	0.61
Pr_2O_3	**0.88**	0.14
SiO_2	0.82	0.06
TiO_2	**0.89**	0.18
P_2O_5	0.82	**0.04**
SO_3	0.80	0.02

p-v – the p-values; meaningful values are given in bold

Table ST41. Element correlation based on Kendall's τ coefficients and uncorrected ρ-values (given in the parentheses), praseodymium experiment

	Cl	CaO	Al_2O_3	Fe_2O_3	Pr_2O_3	SiO_2	TiO_2	P_2O_5	SO_3
Cl		**0.49** (0.12)	**-0.31** (0.24)	**-0.37** (0.17)	**-0.76 (0.004)**	0.05 (0.88)	**-0.40** (0.13)	-0.11 (0.67)	**-0.59 (0.03)**
CaO	**0.49** (0.12)		**-0.45** (0.16)	-0.15 (0.64)	-0.25 (0.43)	-0.20 (0.57)	0.15 (0.64)	-0.15 (0.64)	**-0.59** (0.06)
Al_2O_3	**-0.31** (0.24)	**-0.45** (0.16)		0.29 (0.28)	**0.34** (0.20)	0.20 (0.54)	0.26 (0.33)	**0.49** (0.06)	**0.51** (0.05)
Fe_2O_3	**-0.37** (0.17)	-0.15 (0.64)	0.29 (0.28)		**0.57 (0.03)**	**-0.52** (0.10)	0.26 (0.33)	**0.61 (0.02)**	0.29 (0.28)
Pr_2O_3	**-0.76 (0.004)**	-0.25 (0.43)	**0.34** (0.20)	**0.57 (0.03)**		-0.24 (0.45)	**0.43** (0.10)	**0.38** (0.16)	**0.57 (0.03)**
SiO_2	0.05 (0.88)	-0.20 (0.57)	0.20 (0.54)	**-0.52** (0.10)	-0.24 (0.45)		**0.39** (0.22)	-0.10 (0.76)	0 (1)
TiO_2	**-0.40** (0.13)	0.15 (0.64)	0.26 (0.33)	0.26 (0.33)	**0.43** (0.10)	**0.39** (0.22)		0.29 (0.27)	0.09 (0.74)
P_2O_5	-0.11 (0.67)	-0.15 (0.64)	**0.49** (0.06)	**0.61 (0.02)**	**0.38** (0.16)	-0.10 (0.76)	0.29 (0.27)		0.14 (0.59)
SO_3	**-0.59 (0.03)**	**-0.59** (0.06)	**0.51** (0.05)	0.29 (0.28)	**0.57 (0.03)**	0 (1)	0.09 (0.74)	0.14 (0.59)	

Strong correlations are given in bold

Table ST42. Results of chemical analyses of AAJ contacting with a solution of $TaCl_5$

	1[1]	2	3	4	5	6	7
			[wt.%]				
SO_3[1]	5.19	11.38	9.59	10.34	8.39	10.29	4.91
P_2O_5	3.54	1.51	1.47	1.69	1.75	1.54	2.11
Ta_2O_5	62.72	70.64	68.85	69.70	73.28	74.44	75.40
SiO_2	1.23	0.48	0.56	0.52	0.48	0.58	0.53
TiO_2	1.16	0.48	0.50	0.49	0.51	0.51	0.62
Al_2O_3	3.00	0.37	0.38	0.56	0.60	0.27	0.41
Fe_2O_3	6.86	4.60	4.83	4.83	5.18	4.67	5.34
CaO	1.57	bdl[2]	0.23	0.52	0.77	0.17	0.90
MgO	0.21	0.11	0.11	0.13	0.13	bdl	0.09
K_2O	0.71	0.11	0.15	0.36	0.35	0.35	0.36
Cl	0.15	0.12	bdl	bdl	bdl	0.28	bdl
Σ	90.89	87.17	89.94	86.82	91.50	91.83	94.22
H_2O[3]	7.86	6.82	6.69	6.87	7.17	7.00	6.95
$(NH_4)_2O$[4]	0.65	1.08	1.02	0.31	0.91	0.80	0.98
apfu (mpfu), *B* = 3 basis (assuming all Si entering the *T*-site), unnormalized							
S	0.44	1.09	0.93	0.99	0.76	0.95	0.43
P	0.34	0.16	0.16	0.18	0.18	0.16	0.21
Ta	1.92	2.46	2.42	2.41	2.40	2.48	2.41
excess Ta_2O_5	0.75	1.23	1.21	1.21	1.20	1.24	1.21
Si	0.14	0.06	0.07	0.07	0.06	0.07	0.06
Ti	0.10	0.05	0.05	0.05	0.05	0.05	0.06
Al	0.40	0.06	0.06	0.08	0.08	0.04	0.06
Fe	0.58	0.44	0.47	0.46	0.47	0.43	0.47
Ca	0.19		0.03	0.07	0.10	0.02	0.11
Mg	0.04	0.02	0.02	0.02	0.02		0.02
K	0.10	0.02	0.02	0.06	0.05	0.06	0.05
Cl	0.03	0.02				0.06	
NH_4[5]	0.49	0.92	0.88	0.26	0.73	0.66	0.77
OH[6]	5.90	5.81	5.78	5.82	5.76	5.73	5.46

[1] – the single analysis corresponding to a possible Ta-exchanged AAJ; [2] – below detection limit; [3] – exclusively OH-derived, backward-calculated from OH *mpfu* content assuming lacking H_3O^+ and H_2O molecules in the structure; [4] – backward-calculated from NH_4^+ *mpfu* content; [5] – calculated by stoichiometry (filling the *A* site to the occupancy of 1); [6] – by charge balance

Table ST43. Element correlation based on Kendall's τ coefficients and uncorrected -values (given in the parentheses), selenium experiment

	SO_3	K_2O	CaO	Fe_2O_3	Na_2O	Ta_2O_5	Al_2O_3	SiO_2	MgO	Cl	TiO_2
SO_3		**-0.51** (0.11)	**-0.69 (0.05)**	**-0.85 (0.007)**	0 (1)	-0.05 (0.87)	-0.25 (0.43)	**-0.49** (0.12)	0 (1)	**-0.59** (0.06)	**-0.72 (0.02)**
K_2O	**-0.51** (0.11)		**0.64** (0.07)	**0.72 (0.02)**	**0.55** (0.08)	-0.10 (0.75)	**0.41** (0.20)	**0.55** (0.08)	**0.36** (0.31)	**0.75 (0.02)**	**0.74 (0.02)**
CaO	**-0.69 (0.05)**	**0.64** (0.07)		**0.97 (0.006)**	-0.07 (0.85)	-0.14 (0.70)	-0.07 (0.85)	**0.73 (0.04)**	**0.32** (0.44)	**0.87 (0.01)**	**0.64** (0.07)
Fe_2O_3	**-0.85 (0.007)**	**0.72 (0.02)**	**0.97 (0.006)**		0.20 (0.54)	-0.10 (0.75)	0.25 (0.43)	**0.68 (0.03)**	0.21 (0.55)	**0.78 (0.01)**	**0.77 (0.02)**
Na_2O	0 (1)	**0.55** (0.08)	-0.07 (0.85)	0.20 (0.53)		-0.10 (0.76)	0.20 (0.54)	**0.33** (0.20)	**0.41** (0.24)	0.24 (0.45)	0.25 (0.43)
Ta_2O_5	-0.05 (0.87)	-0.10 (0.74)	-0.14 (0.70)	-0.10 (0.75)	-0.10 (0.76)		-0.25 (0.43)	**-0.39** (0.22)	**-0.50** (0.16)	0.10 (0.76)	0.15 (0.63)
Al_2O_3	-0.25 (0.43)	**0.41** (0.20)	-0.07 (0.85)	0.25 (0.43)	0.20 (0.54)	-0.25 (0.43)		-0.10 (0.76)	0.07 (0.84)	0.20 (0.54)	**0.52** (0.11)
SiO_2	**-0.49** (0.12)	**0.55** (0.08)	**0.73 (0.04)**	**0.68 (0.03)**	**0.33** (0.29)	**-0.39** (0.22)	-0.10 (0.76)		**0.55** (0.12)	**0.52** (0.10)	**0.45** (0.16)
MgO	0 (1)	**0.36** (0.310	**0.32** (0.43)	0.21 (0.55)	**0.41** (0.24)	**-0.50** (0.16)	0.07 (0.84)	**0.55** (0.12)		**0.41** (0.24)	0.21 (0.55)
Cl	**-0.59** (0.06)	**0.76 (0.02)**	**0.87 (0.01)**	**0.78 (0.01)**	0.24 (0.45)	0.10 (0.76)	0.20 (0.54)	**0.52** (0.10)	**0.41** (0.24)		**0.75 (0.02)**
TiO_2	**-0.72 (0.02)**	**0.74 (0.02)**	**0.64** (0.07)	**0.77 (0.02)**	0.25 (0.43)	0.15 (0.63)	**0.51** (0.11)	**0.45** (0.16)	0.21 (0.55)	**0.75 (0.02)**	

Strong correlations are given in bold

Table ST44. Shapiro-Wilk (S-W) normality test results, tantalum experiment

	S-W	p-v
SO_3	**0.81**	**0.05**
K_2O	**0.87**	0.19
CaO	**0.95**	0.76
Fe_2O_3	0.80	**0.04**
Na_2O	**0.92**	0.44
Ta_2O_5	**0.93**	0.58
Al_2O_3	0.65	**0.001**
SiO_2	0.77	**0.02**
MgO	**0.88**	0.27
Cl	0.76	**0.02**
P_2O_5	**0.93**	0.48
TiO_2	0.65	**0.001**

p-v – the p-values; meaningful values are given in bold

APPENDIX FIGURES

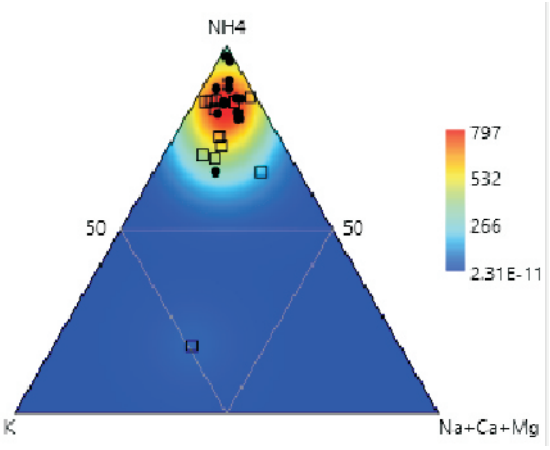

Fig. SF1. Ternary *A*-site heat

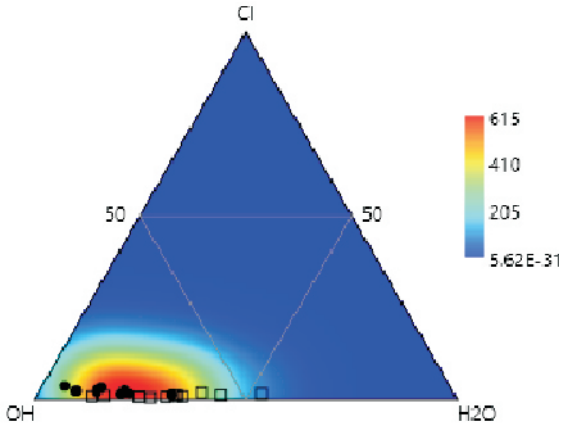

Fig. SF2. Ternary *X*-site heat

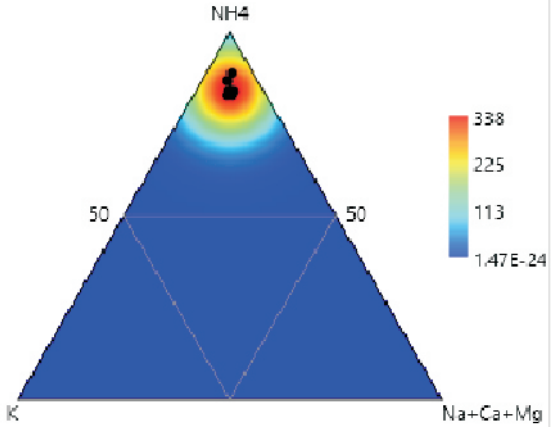

Fig. SF3. AAJ-Li ternary heat

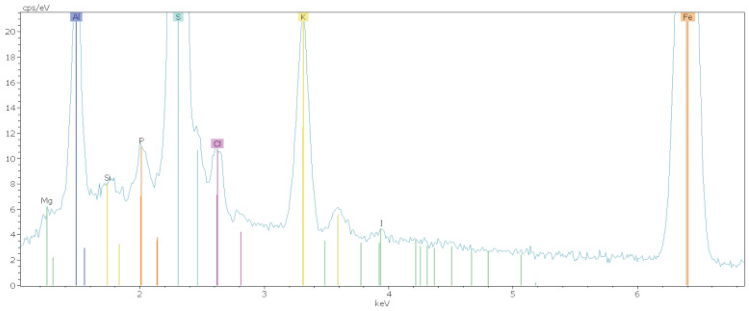

Fig. SF4. KI - EDS

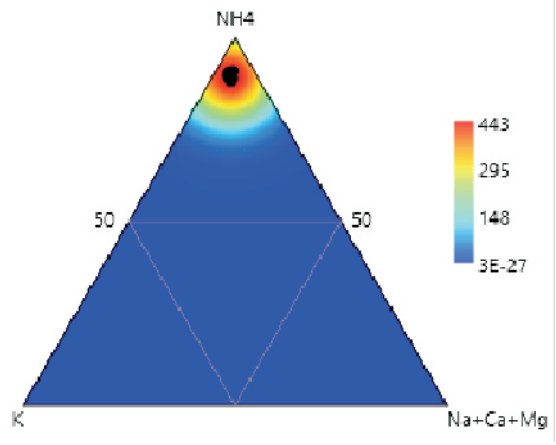

Fig SF5. AAJ-KI triplot heat

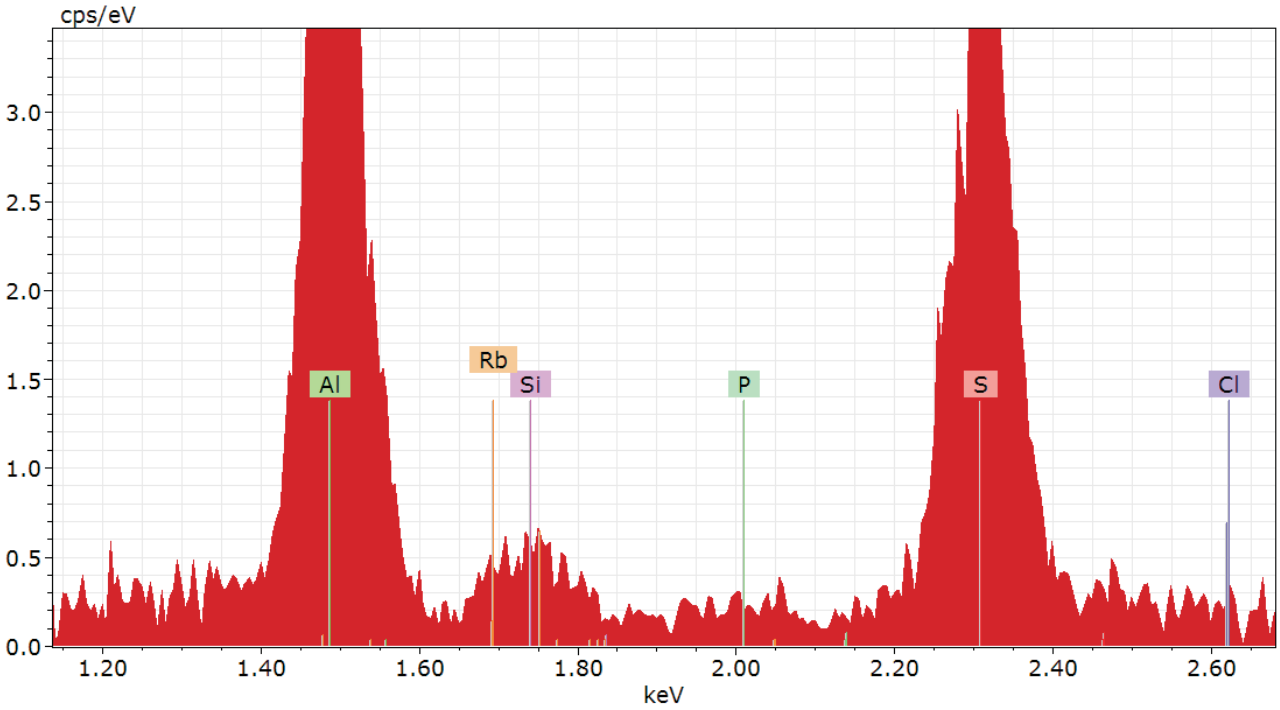

Fig. SF6. Rb - EDS

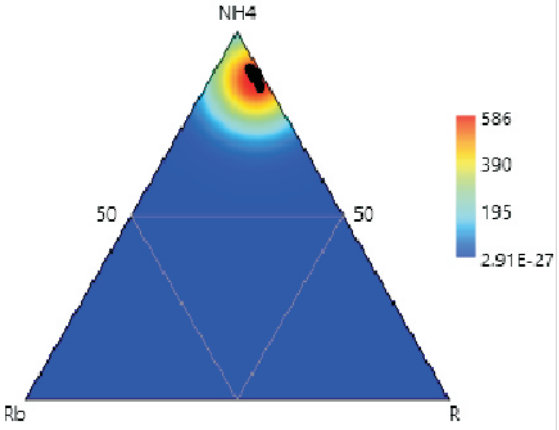

Fig. SF7. AAJ-Rb ternary heat

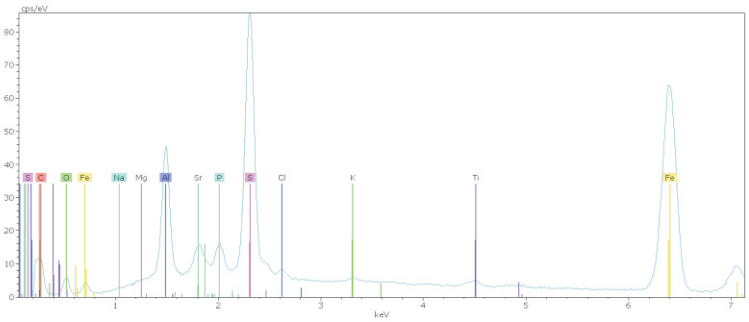

Fig. SF8. Cs - EDS

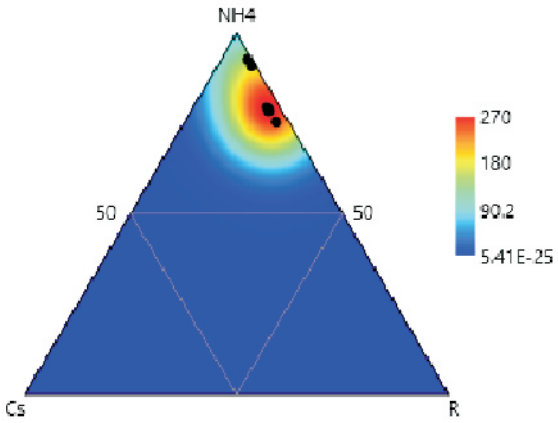

Fig. SF9. AAJ-Cs ternary heat

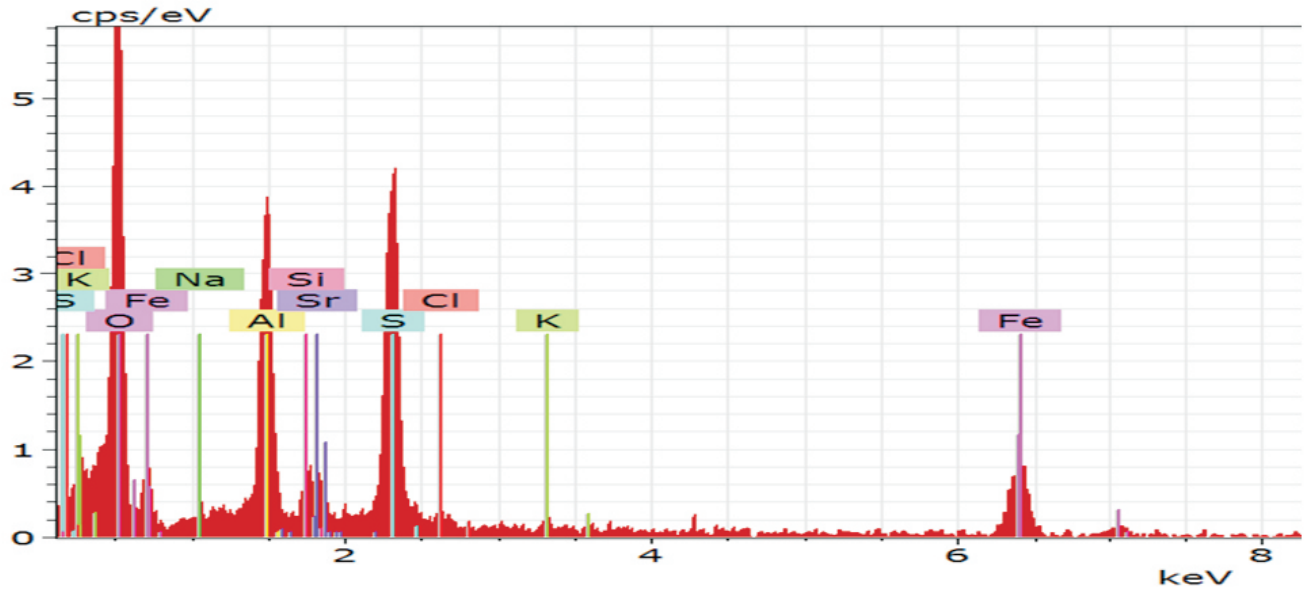

Fig. SF10. Sr-EDS

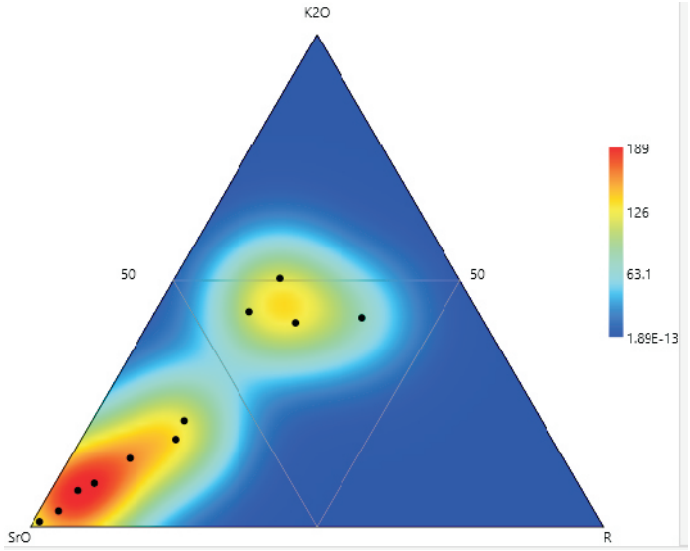

Fig. SF11. AAJ-Sr ternary heat

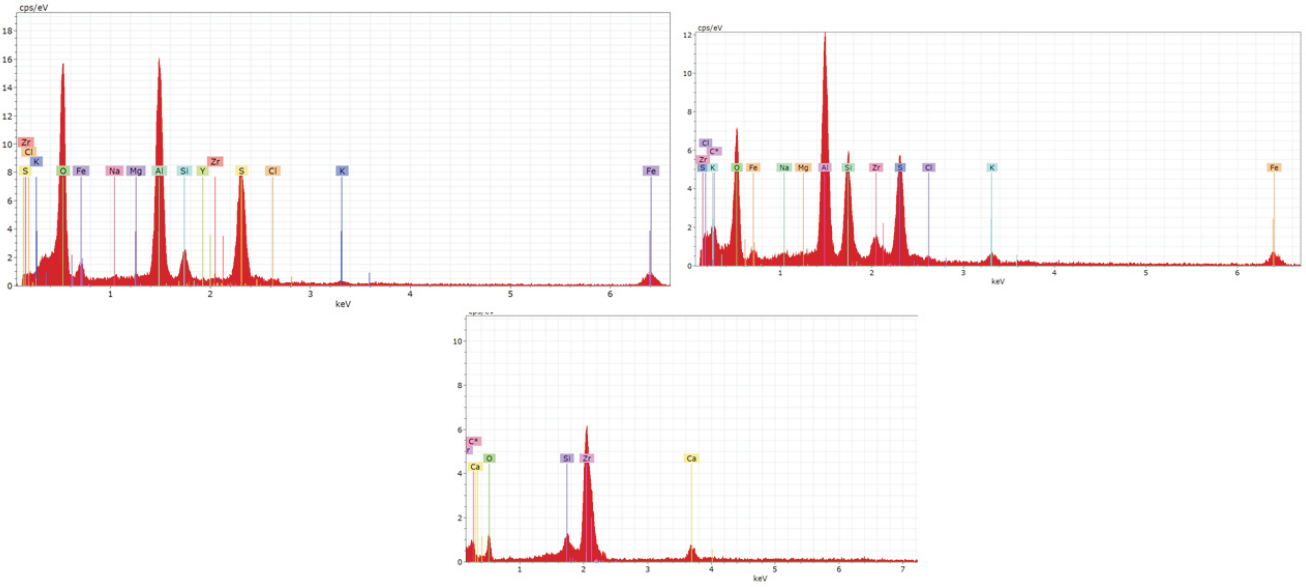

Fig. SF12. Zr - EDS

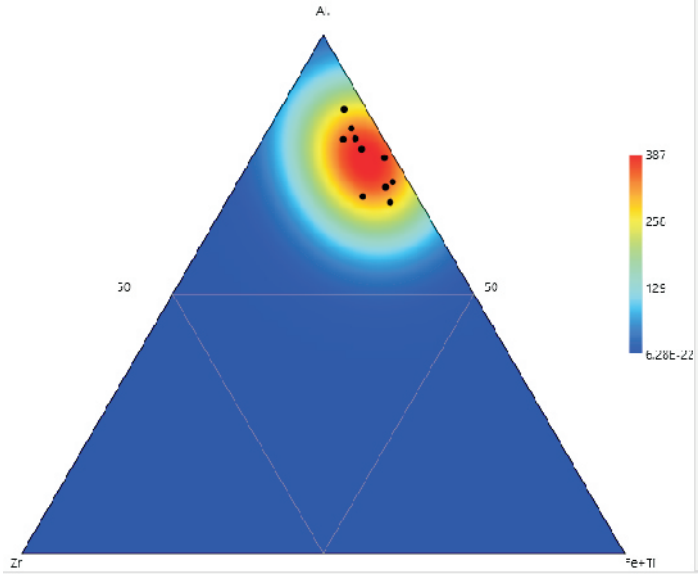

Fig. SF13. AAJ-Zr B-site tern heat

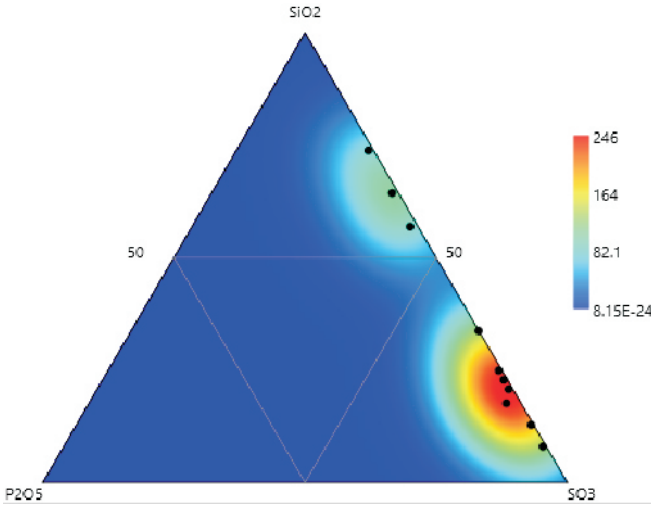

Fig. SF14. AAJ-Zr triplot T-site

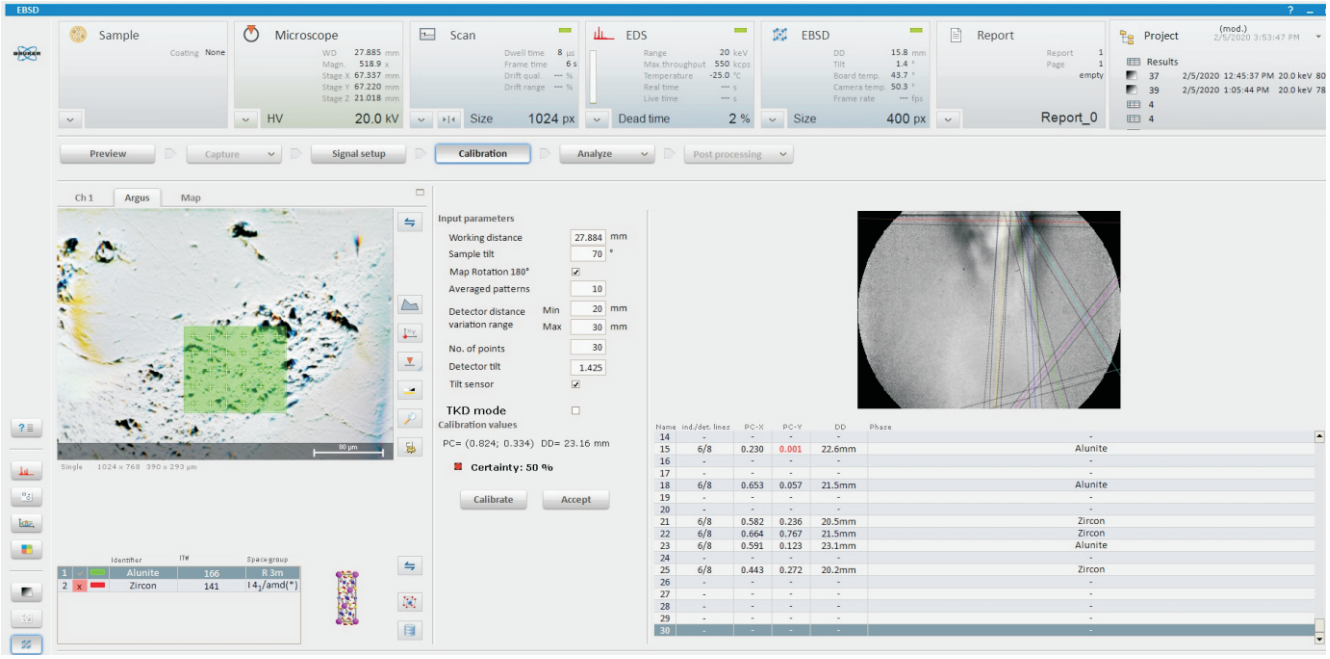

Fig. SF15. AAJ-Zr EBSD

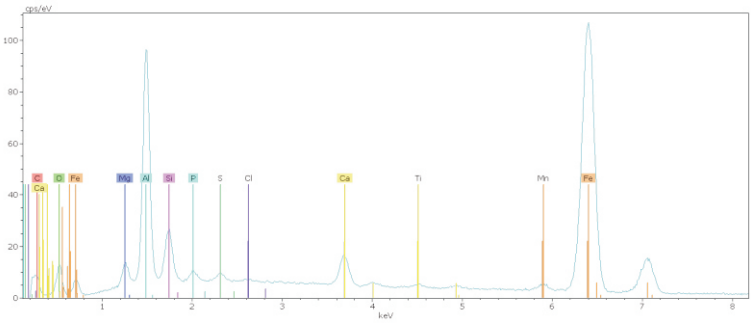

Fig. SF16. Mn-EDS

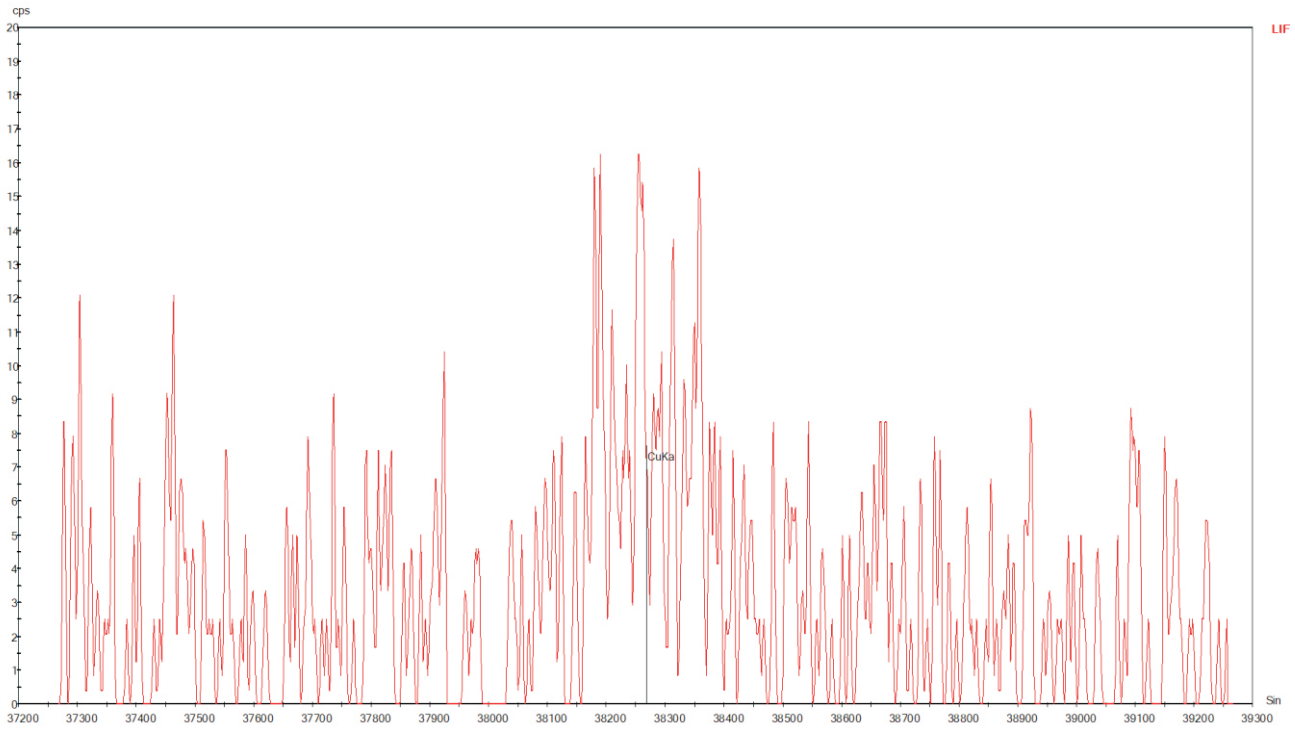

Fig. SF17. Cu-EDS

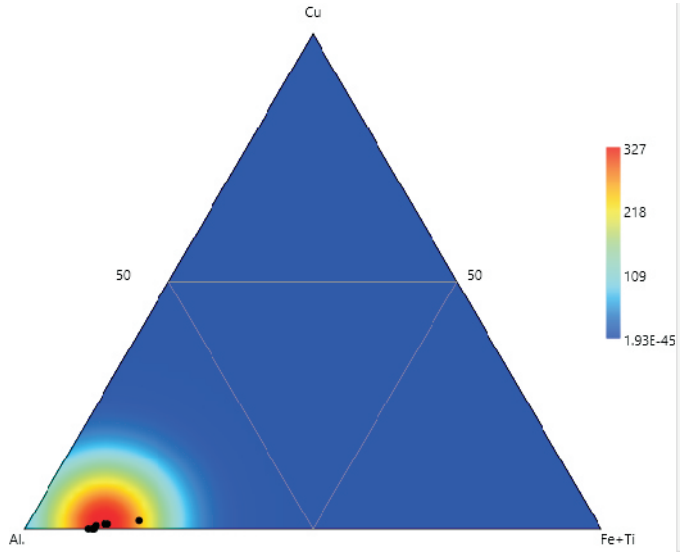

Fig. SF18. AAJ-Cu B-site tern heat

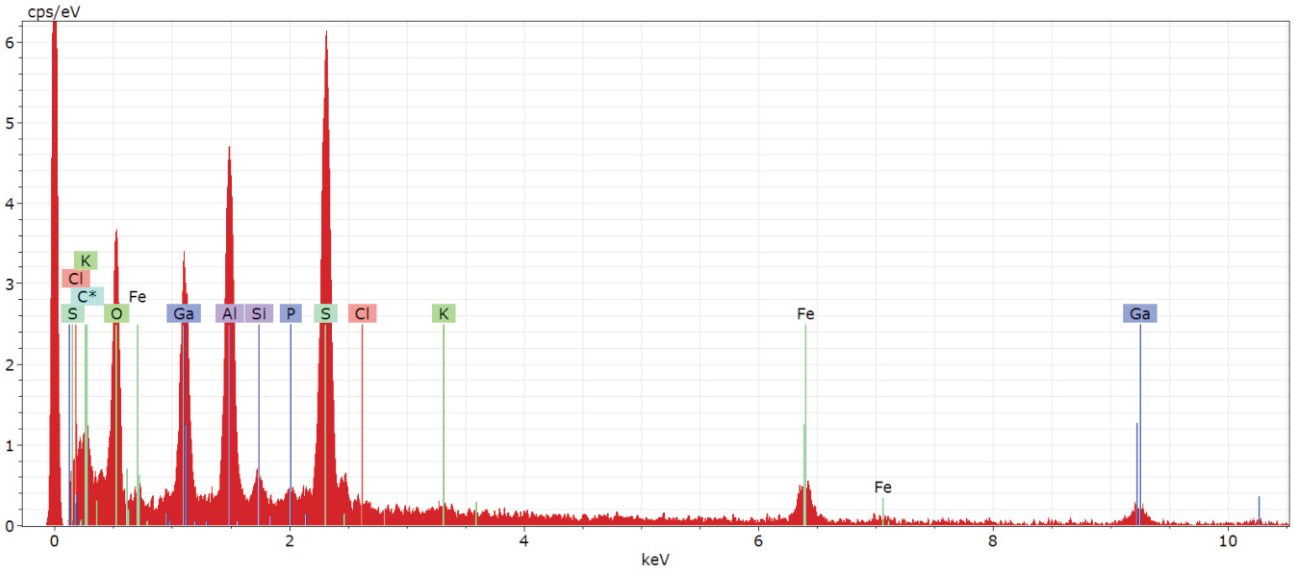

Fig. SF19. Ga - EDS

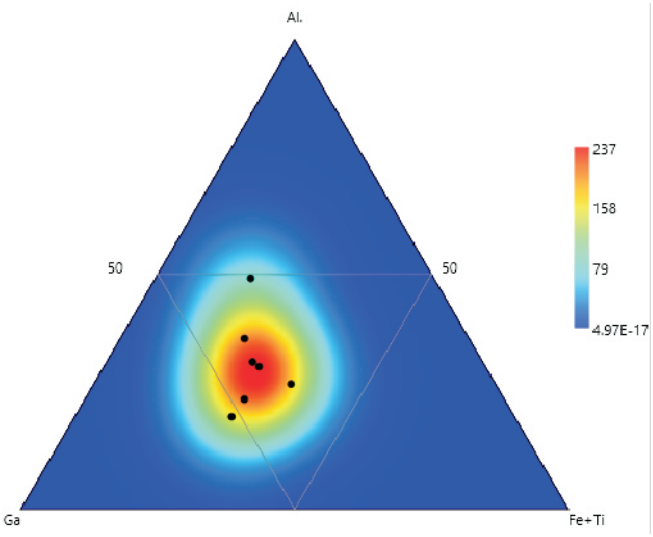

Fig. SF20. AAJ-Ga B-site ternary heat

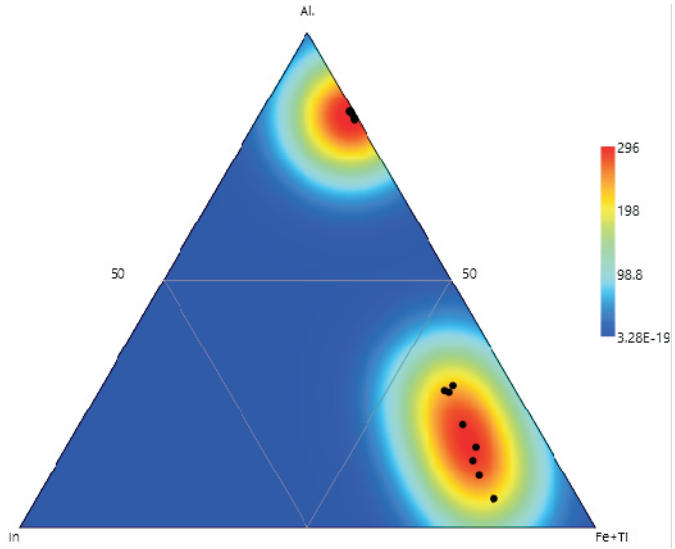

Fig. SF22. AAJ-In B-site tern heat

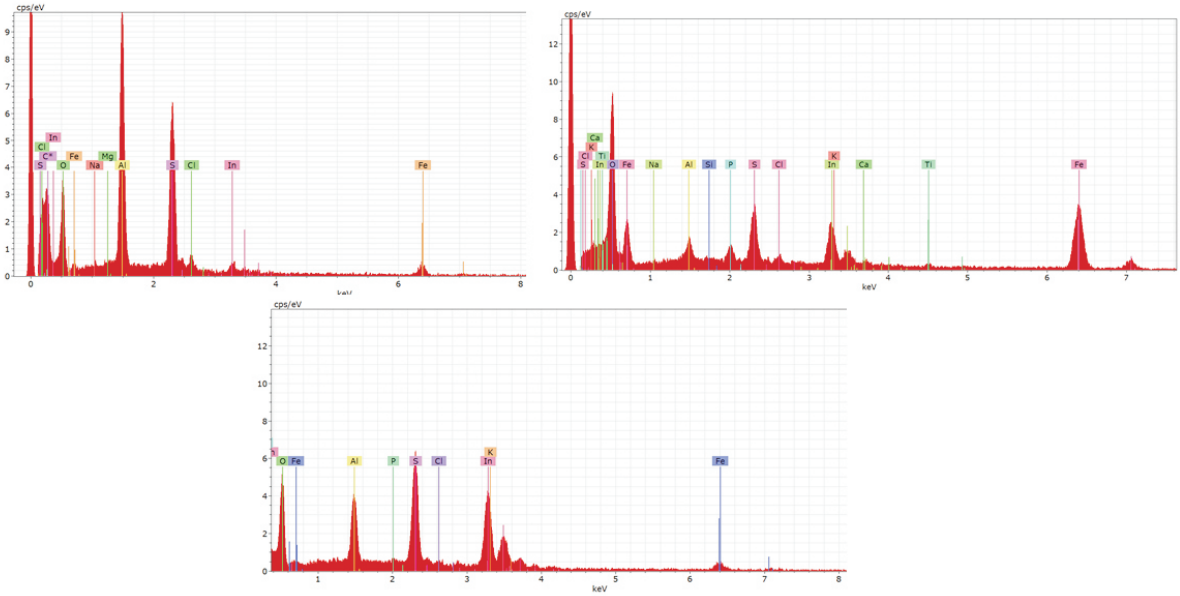

Fig. SF21. In - EDS

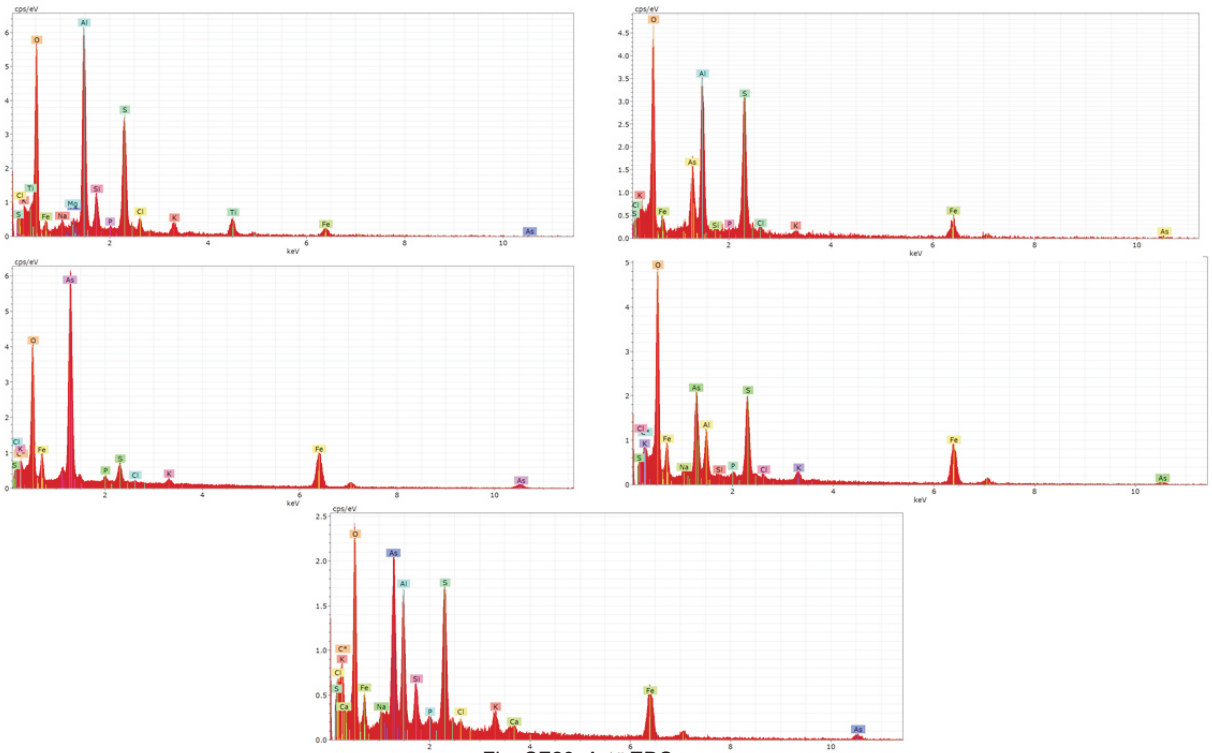

Fig. SF23. As - EDS

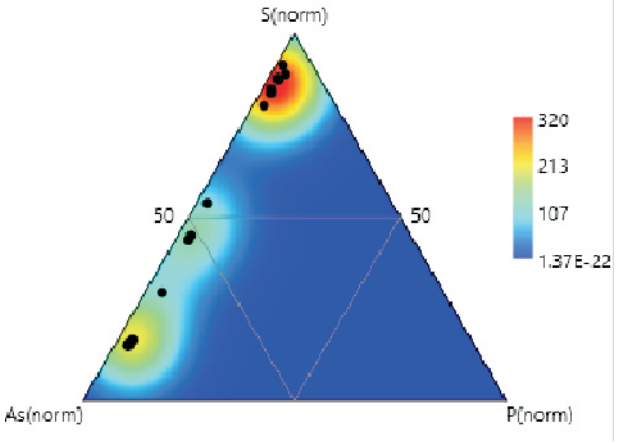

Fig. SF24. AAJ_As_T-site tern heat

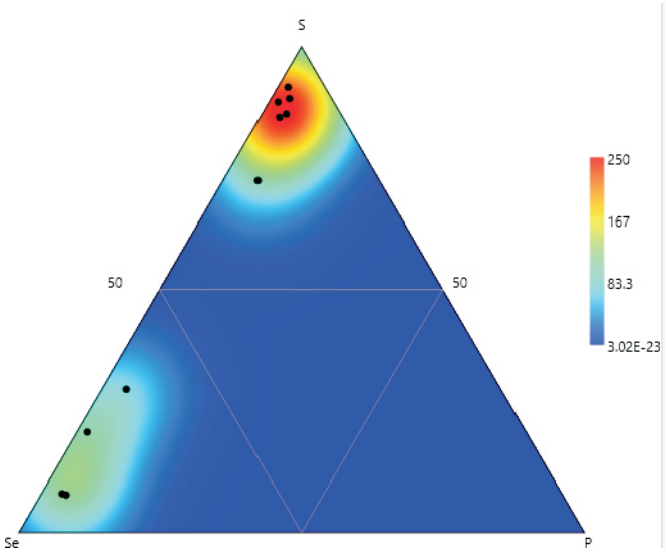

Fig. SF26. AAJ-Se tern heat apfu Se-S-P

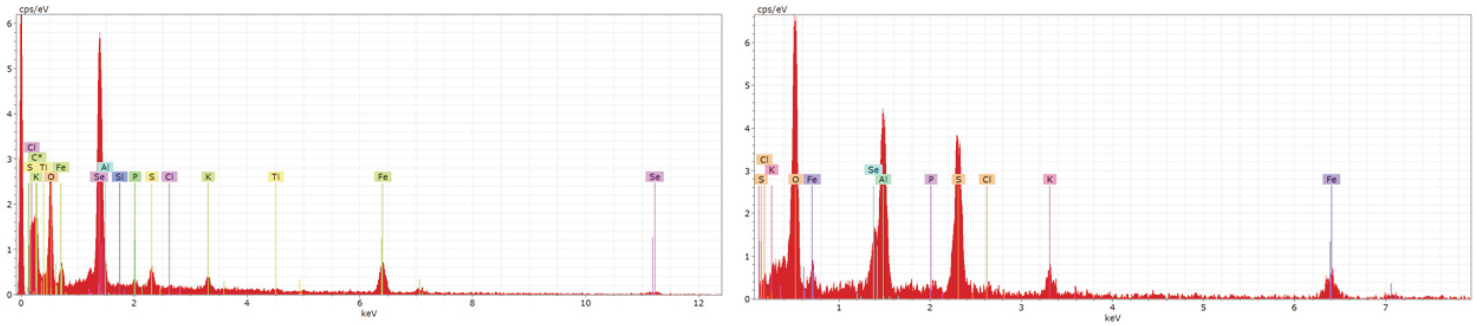

Fig. SF25. Se - EDS

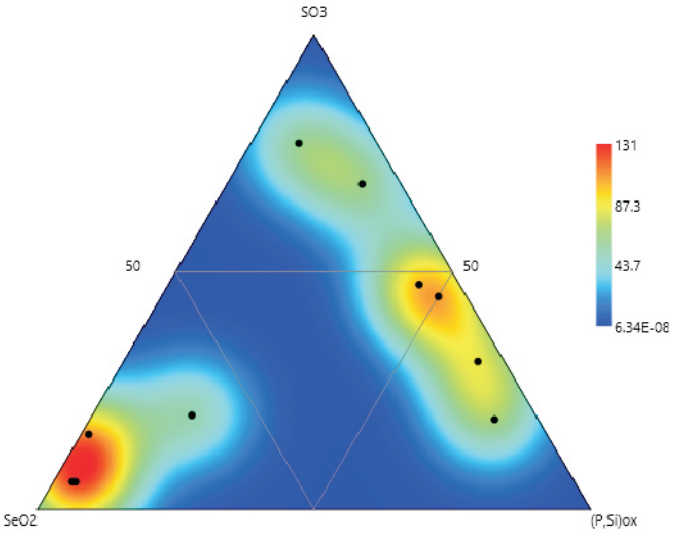

Fig. SF27. AAJ-Se tern heat ox

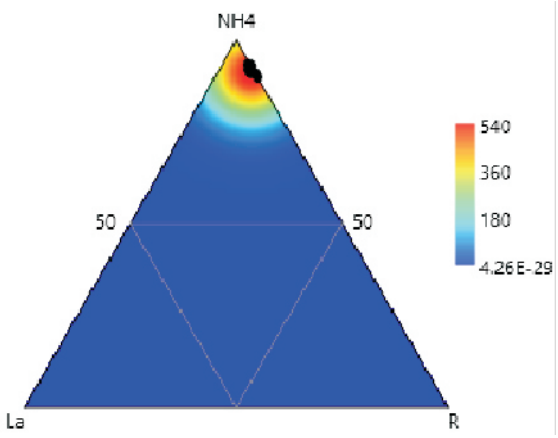

Fig. SF29. AAJ-La A-site tern heat

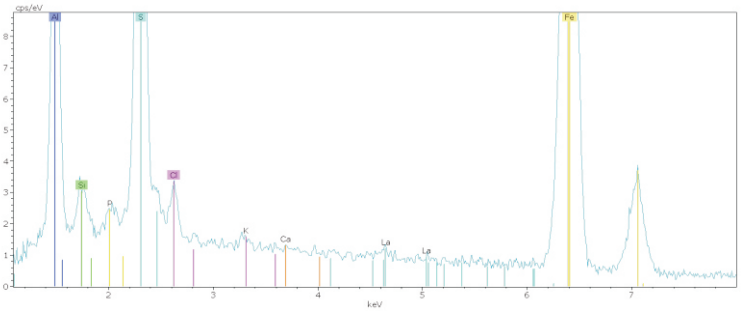

Fig. SF28. La - EDS

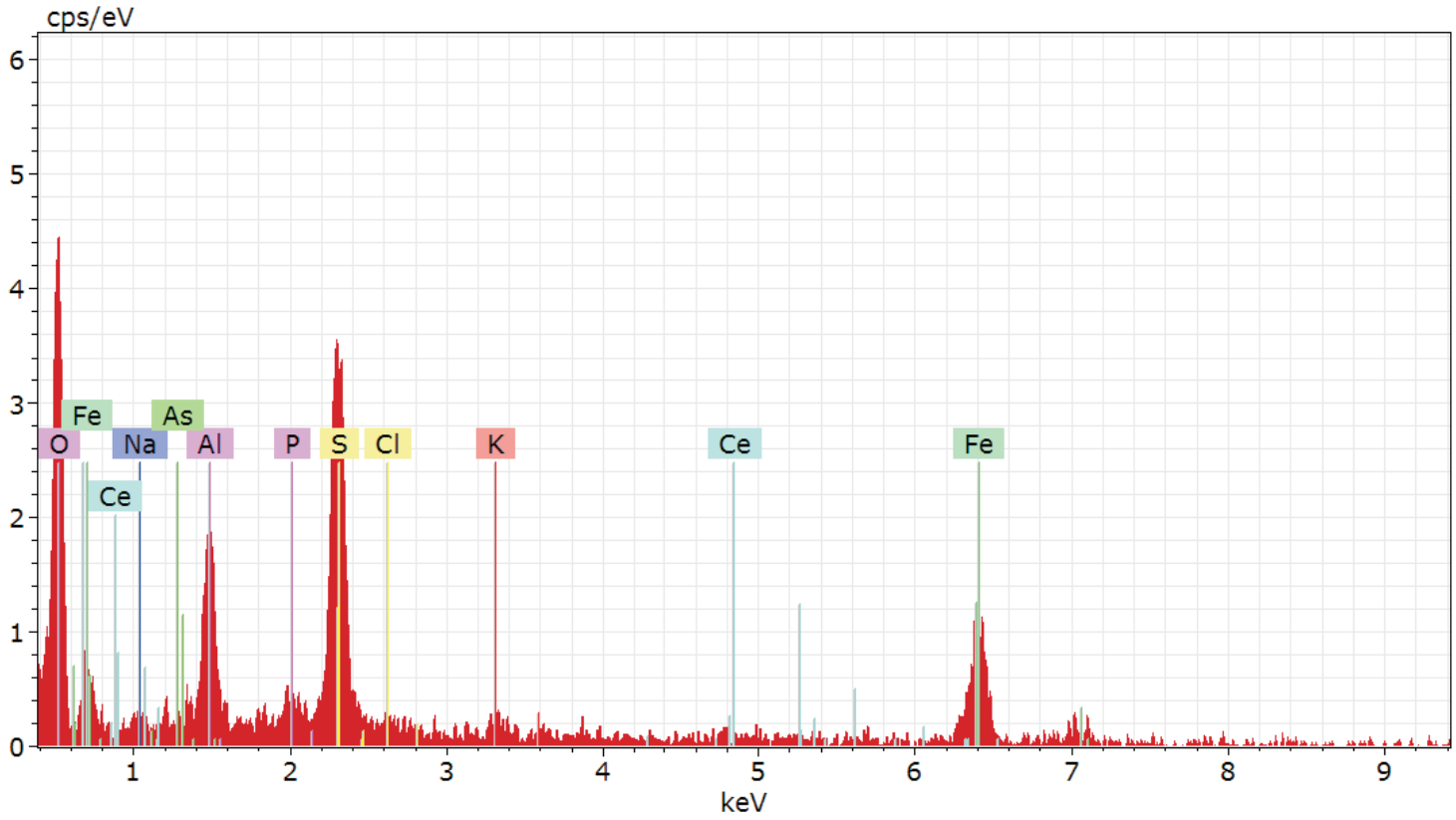

Fig. SF30. Ce - EDS

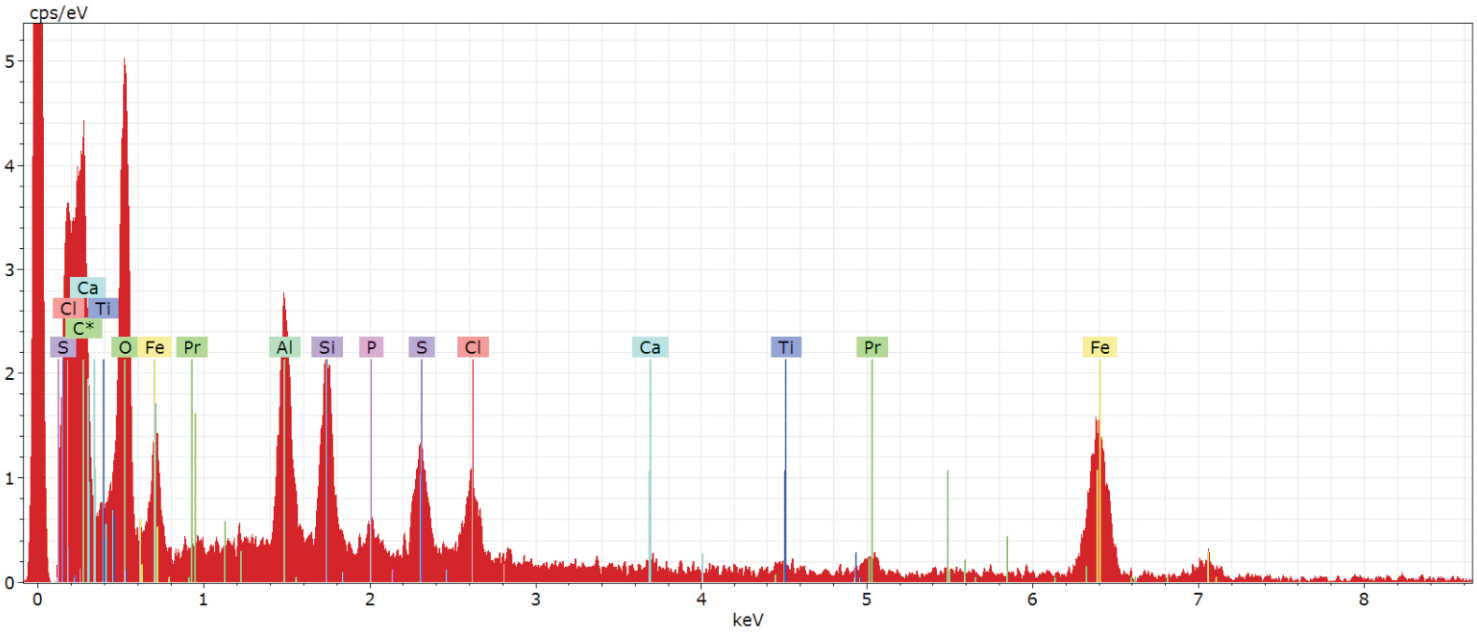

Fig. SF31. Pr - EDS

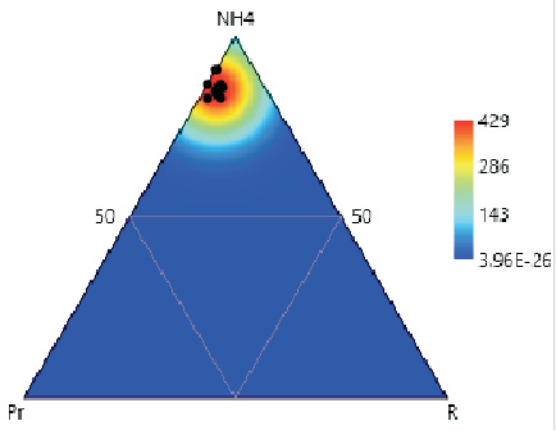

Fig. SF32. AAJ-Pr triplot heat

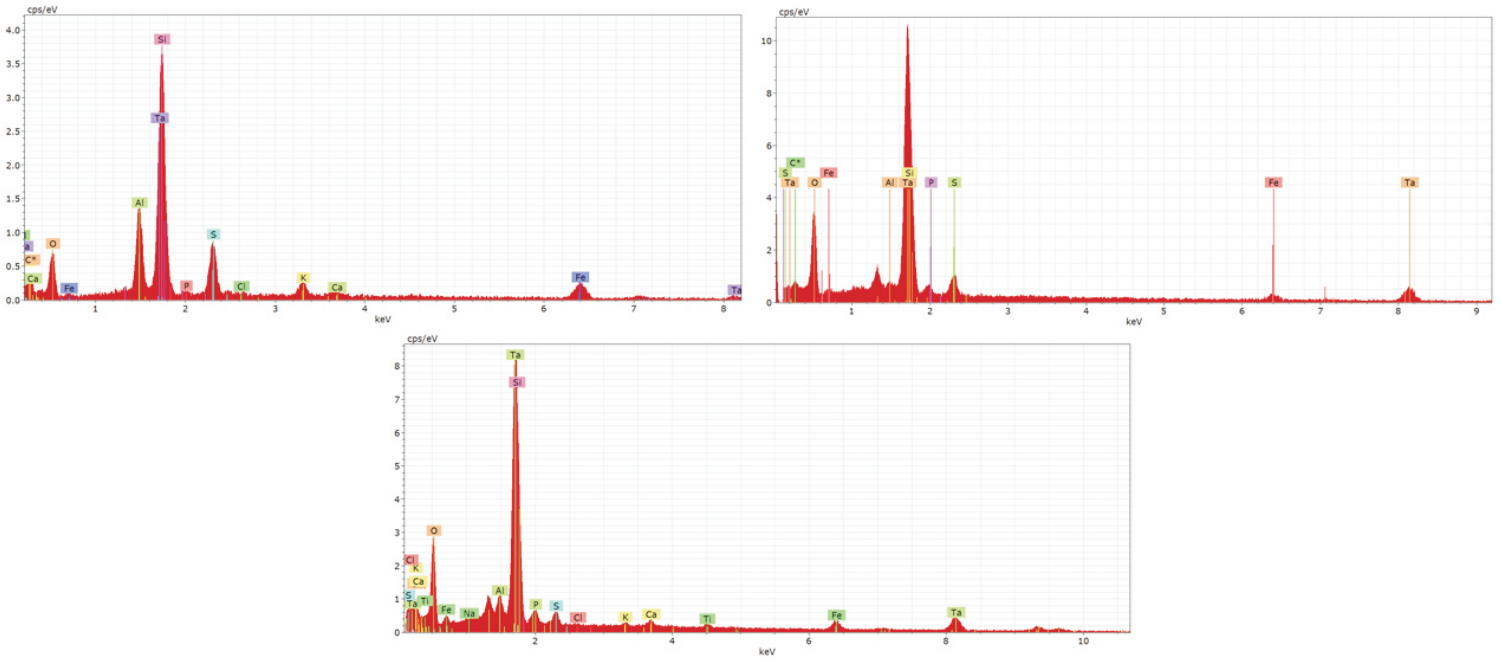

Fig. SF33. Ta - EDS